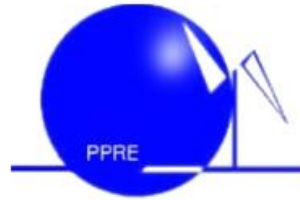


# **Master Thesis**

“Determination of the required Power Response of Inverters to provide fast Frequency Support in Power Systems with low Synchronous Inertia”

In the Postgraduate Programme

Renewable Energy



Department of Physics

Faculty of Mathematics & Science

Carl von Ossietzky University

Oldenburg / F.R. Germany

Day of Examination: September 27<sup>th</sup> 2019

Student: Alejandro Rubio

Registration number: 4565447

Academic Supervisor: Prof. Dr. Carsten Agert

Second Supervisor: Dr. Stefan Geißendörfer



This work is dedicated to my beloved parents, José Rubio and Alejandrina Rodríguez, who taught me the most important lessons in life, supported me and encouraged me through the path that brought me here.



## **Abstract**

---

Decommissioning of conventional power plants and the installation of inverter-based renewable energy technologies decreases overall power system inertia. This reduction in system inertia has an impact in the power system frequency response when an imbalance between generation and load occurs, increasing the rate of change of frequency (RoCoF) of the system. In a future scenario where renewables are predominant in power systems and due to the natural variability of the resource, imbalances of 40 percent or more are prompt to happen. When a system is islanded or operates as such and combined with low inertia, it may lead to frequency collapse. This expected high values of RoCoF shorten the response time needed before load shedding or generation curtailment take place and a subsequent possible black out occurs. Through the simulation of two scenarios with different primary reserve response, the requirements for the fleet of connected inverters was determined in terms of activation time and total power to be provided in order to avoid load shedding. This activation time was determined to be the time at which frequency would reach the load shedding value, known as critical time. With such value and knowing the time required for the synchronous reserve to deploy the imbalance power, a simple expression based on nullifying RoCoF at the critical time was obtained for the required inverter based fast power reserve. It was obtained that full activation time for inverter fast power reserve with penetration above 80% of inverter based generation would need to be between 50-500 ms for imbalances up to 40%; meaning that current frequency measurement techniques and renewable deployment times would not ensure system stability under the foreseen future possible power system conditions. A power ramp in the order of 300% the load per second is necessary for fast power reserve to maintain frequency within the allowed limits.



# Table of Contents

---

List of Figures.....	i
List of Tables .....	iii
Abbreviations .....	iv
1    Introduction.....	1
2    Theory .....	3
2.1    Conventional Frequency Control and Stability .....	3
2.2    Primary Reserve Characteristics.....	4
2.3    Frequency Control with Distributed Energy Resources.....	5
2.4    Frequency Measurement time and RE deployment time. ....	7
2.5    Load Balancing and Fast Power Reserve .....	8
3    Methodology.....	10
3.1    Determination of Inverter based Fast Power Reserve.....	11
3.2    Cases for Assessing Inverter based Fast Power Reserve .....	14
3.3    Simplified IEEE 9 Bus Model.....	16
3.4    Extended IEEE 9 Bus Model.....	22
3.5    European Island Model .....	27
4    Simulation of the Study Cases .....	32
4.1    Simplified IEEE 9 bus Model .....	32
4.2    Extended IEEE 9 bus model.....	43
4.3    European Island Case.....	47
5    Analysis of the Simulation Results .....	53
5.1    Analysis of Critical Time .....	53
5.2    Analysis of Synthetic Inertia and Fast Power Reserve .....	55
5.3    Synchronizing effect, lack of damping torque and implications. ....	60
6    Conclusions.....	63
7    Outlook.....	65
8    References .....	66
9    Appendix I: Synchronous machine parameters and models .....	68
IEEE simplified model.....	68
Simscape IEEE model: Governor and Exciter parameters .....	69
10    Appendix II: SIMULINK models .....	71
IEEE simplified model.....	71

11	Appendix III: Nadir time.....	73
	IEEE 9 bus simplified model .....	73
	IEEE Extended model .....	74
	European model .....	75

# List of Figures

---

Figure 2-1: Frequency control in power systems [2] .....	4
Figure 2-2: Step response for steam and hydro governor controllers. Amplitude of mechanical speed output signal depicted in Y axis; as a result of a step input signal.....	5
Figure 2-3: Sorted hourly residual load plot. In blue residual load for a 25% of renewables and in red for a 60% of renewable .....	8
Figure 3-1: Frequency response of a typical power system subjected to a severe negative power unbalance.....	11
Figure 3-2: Expected power systeem frequency response with the addition of Inverter Based Fast Power Reserve. ....	12
Figure 3-3: Comparisson of assumed power reserve deployment and typical real response. ....	13
Figure 3-4: Assumed primary power reserve and IBFPR. ....	13
Figure 3-5: WSCC or IEEE 9 bus model used for stability studies. ....	16
Figure 3-6: Single machine representation of the IEEE 9 bus model. ....	16
Figure 3-7: Step response of Governor model for different values of acceleration time constant. Amplitude of speed response depicted in Y axis. ....	17
Figure 3-8: Kinetic energy stored in generator rotating masses as function of generator capacity. A linear relation is exhibited between the machine capacity and its store kinetic energy . ....	18
Figure 3-9: Simplified IEEE model with IBFPR implementation. ....	19
Figure 3-10: Implementation of synthetic inertia in the simplified IEEE model. ....	20
Figure 3-11: Synthetic inertia control model where $T_{wt}$ is the filter constant, $H_{wt}$ is the turbine's inertia constant, $P_{wt}$ is the nominal wind capacity (MW) and $K_i$ is a gain constant. Frequency input in pu and system output is power in MW.....	20
Figure 3-12: Synthetic inertia and IBFPR implementation. ....	22
Figure 3-13: IEEE extended model with IBFPR implementation. ....	22
Figure 3-14:Model implemented to calculate the required current to meet the specified power rate from measured voltage signal shown in Figure 3-15.....	24
Figure 3-15: Controlled current sources acting as grid following inverters. Signals $I_a$ and $I_b$ comes from model in figure 3-14; similarly signals $V_{ab}$ and $V_{bc}$ go to the same model. ....	25
Figure 3-16: Simplified European power system. ....	27
Figure 3-17: Comparisson between the modeled reference scenario by ENTSOE and the adjusted model. Power loss of 3GW, load of 150 GW (2%), self-regulation of 2%/Hz and acceleration time constant of 10 s. ....	28
Figure 3-18: Primary reserve deployment time of the interconnected European system .....	29
Figure 3-19: Comparisson between system step response before the PID tunning (blue) and the desired step response of the system (purple). ....	30
Figure 3-20: Comparisson between the actual response (blue) and the desired step response of the system (purple); after PID tuning.....	30
Figure 3-21: European model with IBFPR and Synthetic Inertia. ....	31
Figure 4-1: Critical time as function of acceleration time constant and load imbalance.....	32
Figure 4-2: Critical time for specific system acceleration time constants.....	33
Figure 4-3: Critical time fit as function of RoCoF.....	33
Figure 4-4: Frequency nadir without auxiliary frequency support from IBG.....	34
Figure 4-5: Inverter based fast power response ramp .....	35
Figure 4-6: IBFPR ramp for specific shares of non-synchronous generation .....	35

Figure 4-7: Frequency nadir with IBFPR implemented. Dotted lines indicate share of inverter based generation .....	36
Figure 4-8: Frequency response assuming no UFLS implementation. Comparison of responses with and without IBFPR .....	36
Figure 4-9: Frequency nadir only with implementation of synthetic inertia; having a 40% of contribution of wind power the total IBG. ....	37
Figure 4-10: Frequency nadir only with the implementation of synthetic inertia; having an 80% of contribution of wind power the total IBG. ....	38
Figure 4-11: Frequency response for a penetration of 80% IBG and an imbalance of 10% when synthetic inertia is applied to the system.....	38
Figure 4-12: Frequency response for a penetration of 80% IBG and an imbalance of 15% when synthetic inertia is applied to the system. ....	39
Figure 4-13: Power response for 80% IBG and imbalance of 15% when synthetic inertia is provided by the 80% of the total IBG.....	39
Figure 4-14: Frequency nadir with IBFPR delayed 100 ms. ....	40
Figure 4-15: Frequency nadir with IBFPR delayed 200 ms. ....	41
Figure 4-16: Critical imbalances as function of delay in IBFPR activation. ....	41
Figure 4-17: Symmetry in critical time for over and under-frequency events.....	42
Figure 4-18: Critical time for SIMSCAPE IEEE model. ....	43
Figure 4-19: Critical time for specific penetrations levels of IBG for SIMSCAPE IEEE model....	43
Figure 4-20: Critical time as function of RoCoF. ....	44
Figure 4-21: Frequency nadir with no additional frequency support.....	45
Figure 4-22: Frequency nadir with the implementation of IBFPR. ....	45
Figure 4-23: Frequency response with an accel. time constant of 2 s (85% IBG) for different levels of imbalance. IBFPR is implemented. ....	46
Figure 4-24: Comparison of critical times for over and under-frequency cases.....	46
Figure 4-25: Critical time in an electric island in the European power system. ....	47
Figure 4-26: Critical time for specific penetrations of IBG.....	47
Figure 4-27: Critical time fit as function of RoCoF.....	48
Figure 4-28: Frequency nadir without IBFPR. ....	48
Figure 4-29: IBFPR ramp response in GW/s.....	49
Figure 4-30: Nadir frequency with IBFPR support; UFLS inside the marked area.....	50
Figure 4-31: Frequency nadir. 80% of IBG is considered to provide synthetic inertia.....	50
Figure 4-32: Frequency nadir when IBFPR has a delay of 100 ms. ....	51
Figure 4-33: Frequency nadir when IBFPR has a delay of 200 ms. ....	51
Figure 4-34: Comparison of critical times for over and under-frequency cases.....	52
Figure 5-1: Critical time for all scenarios at 80% IBG penetration. ....	54
Figure 5-2: Synthetic Inertia power response characteristics of the simplified IEEE model. ....	56
Figure 5-3: Frequency response with 20% synthetic inertia.....	56
Figure 5-4: Power ramp slope with 80% of IBG penetration. ....	58
Figure 5-5: Fast power reserve at 80% of IBG. ....	59
Figure 5-6: Oscillatory effect in rotor speeds in the Extended IEEE model with 85% IBG and 35% load unbalance and IBFPR support.....	61
Figure 5-7: Oscillatory behavior from SIMSCAPE IEEE model with 95% IBG and 2% unbalance. No IBFPR is provided. ....	61
Figure 5-8: Oscillatory behavior from SIMSCAPE IEEE model with 95% IBG and 2% unbalance. IBFPR is provided .....	62
Figure 9-1: General purpose governor model.....	68

Figure 9-2: General settings of steam turbine model .....	69
Figure 9-3: Exciter settings for Generator 1 .....	69
Figure 9-4: Exciter settings for Generator 3 .....	70
Figure 9-5: Exciter settings for Generator 2 .....	70
Figure 10-1: Synthetic inertia block diagram .....	71
Figure 10-2: Complete simplified model, including SI and IBFPR .....	71
Figure 10-3: IBFPR block control block diagram .....	72
Figure 11-1: Relation between nadir time and accel. constant .....	73
Figure 11-2: Relation between nadir time, accel. constant and imbalance .....	74
Figure 11-3: Relation between nadir time and accel. constant in the European grid representation.	75

## List of Tables

---

Table 2-1: Activation times for fast power reserve of non-synchronous technologies .....	7
Table 3-1: Constants for implementation of synthetic inertia. ....	21
<i>Table 3-2: System steady state-initial conditions</i> .....	24
Table 5-1: Critical times for European case in seconds. ....	55
Table 5-2: Fast power reserve in per unit <sup>2</sup> for European case .....	60
Table 9-1: Common governor parameters.....	68
Table 11-1: Nadir time for simplified IEEE model .....	73
<i>Table 11-2: Nadir time as function of imbalance and accel. constant.</i> .....	74
Table 11-3: Nadir time for European model.....	75

## **Abbreviations**

---

AGC: Automatic Generation Control

DER: Distributed Energy Resources

ENTSOE: European Network of Transmission System Operators for Electricity

FPR: Fast Power Reserve

HVDC: High Voltage Direct Current

IEEE: Institute of Electric and Electronic Engineers

IBFPR: Inverter based Fast Power Reserve

IBG: Inverter Based Generation

PID: Proportional Integral Derivative (controller)

PV: Photovoltaic

RoCoF: Rate of Change of Frequency

SI: Synthetic Inertia

UFLS: Under Frequency Load Shedding.

WSCC: Western System Coordinated Council

# 1 Introduction

---

As part of the international efforts set to counteract global warming, the deployment of renewable energies in the electric sector has been considered an energetic priority as a measure to reduce CO<sub>2</sub> emissions. This objective is also reflected in the regulatory energy policies and plans of some countries. For instance, in Germany the transformation of the electricity sector through renewables, known as “*Energiewende*”, contemplates to achieve a share in electricity consumption from renewables of 80 percent [3]. As part of it, the renewable energy act, “*Erneuerbare Energien Gesetz*”, regulates the expansion of renewables and convectional generation decommissioning.

Even though power systems have grown in size and complexity, frequency control has been always performed through power balancing between generation and demand due to synchronous generator characteristics. The variation of load during a given period of time is followed by a change on the prime mover power of the synchronous generator. When an imbalance occurs, the excess or lack of power is injected to or released from the kinetic energy in the rotor. Therefore in synchronous grids, the magnitude of the rate of change of frequency (RoCoF) during an imbalance is inversely proportional to the system's inertia.

Decommissioning of convectional generating power plants and its replacement with inverter-based renewables power plants has as an effect a reduction of system inertia and consequently increasing values of RoCoF. The relevance of system inertia is to avoid rapid changes in frequency as load-generation imbalance occurs; in this way enough time is given to the activation of primary power reserve to recover balanced stable conditions. Therefore the need of new frequency control strategies is evident in this context; where inverter-based generation has a significant share in the grid. Due to the expected higher values of RoCoF, load shedding caused by low frequency and generation curtailment due to over-frequency may occur faster than nowadays grid configuration. Hence, the participation of non-synchronous generation in providing frequency support ancillary service is a key factor in achieving high integration of renewables without jeopardizing power system reliability.

So far, some ancillary services have been included in inverter's capabilities; inverter based generation from PV has been employed to contribute to voltage regulation by meanings of providing reactive power into the grid at cost of some active power. Similar approaches have been implemented for over frequency limitations, by curtailment implementation and ramping limitation of inverters when system frequency approaches an upper limit allowed by local codes [4, 5]. In the same sense, new techniques have been developed in order to enable inverter based generation, such as PV and Wind, to also participate in frequency support for under-frequency cases. The most common techniques try to emulate the droop power-frequency characteristic of the synchronous machine by leaving some power headroom during normal operation, so when a system frequency sag occurs, the inverter is able to push part or the total available power headroom to counteract the frequency drop [6].

Hence renewable sources are not any longer operating at its maximum power point, therefore these methods also have some economic constraints. Another approach to limit the frequency drop during the seconds after the event leading to a frequency decay, is to mimic the inertial response of synchronous machines. Since PV systems do not count with rotating masses, this approach is only achievable with wind turbines. Due to the decoupling of wind turbines from the grid dynamics, modified control strategies in the power electronics allows the controller to extract part of the stored kinetic energy in the rotating masses of the wind turbine [6].

In this investigation the conditions, which should be fulfilled by inverters in highly penetrated grids by non-synchronous generation, to provide an inverter based fast power reserve (IBFPR) are investigated. Then the required triggering time and power response to avoid under-frequency load shedding (UFLS) in such kind of islanded grids are estimated. Over-frequency phenomenon is treated with the same approach as the under-frequency case. The alternative of synthetic inertia is evaluated to see how effective it is under some assumed future scenario conditions. With the consideration of two cases, a benchmark taken as a micro-grid and an electric island in the European scale; a methodology to determine the requirements of the fleet of inverters to offer frequency support is developed. The subsequent chapters will be covering the following content: Chapter 2 corresponds to the literature related to power system operation and primary reserve. Here an overview to the aspects behind the operation of typical power systems is presented, as well as how frequency is established and controlled. Additionally, the influence and contribution from inverter based generators is noted. Chapter 3 presents the methodology to estimate the power rate needed to avoid transient frequency instability. The developed method and expression for power rate are then evaluated in two cases: A micro-grid with fast primary reserve response and an electric island in a European scale with relative slow primary reserve response. A detailed demonstration of parameter setting and assumptions is presented as well. The simulation results of the implemented method in each scenario is then shown in Chapter 4; critical times, frequency nadir and power responses are obtained. A detailed discussion and analysis of the main features and trends observed in the results section, is then followed in Chapter 5. The main conclusions and areas for future work are outlined in Chapters 6 and 7 respectively.

## 2 Theory

---

No matter the size or composition of the power system, a reliable and proper designed power system should fulfill some fundamental requirements [7]:

- The power system must have the capability of meeting the changing required load throughout time.
- Reduce costs and environmental impact.
- Ensure power quality and system stability (Voltage, frequency and level of reliability)

In conventional power systems, power balancing and frequency regulation is establish through the control of synchronous machines power output. Although power systems capacities have increases along with their complexity for control and study, frequency control is implemented in the same way in any conventional grid.

### 2.1 Conventional Frequency Control and Stability

The balance between generation and load must be maintained so rotor speed and electric frequency are kept constant as described by the swing equation [7, 8]. In order to achieve the before cited system conditions, a number of control devices and strategies must be implemented. Such controls must allow the system to remain in operation after small or severe events (change in loads, loss of generation units, faults...) maintaining frequency and voltage excursions under certain levels during transient conditions until steady conditions are reached.

**Equation 2-1** represents the so called swing equation, where  $f_0$  is the nominal system frequency,  $P_{mech}$  is the mechanical power from prime mover,  $P_{elec}$  is the electrical power demand,  $H$  is machine inertia constant and  $S_B$  is nominal power of the machine [7].

*Equation 2-1*

$$\frac{df}{dt} = \frac{(P_{mech} - P_{elec}) * f_0}{2 * H * S_B}$$

Power balancing in synchronous generating units is performed by the governor of the prime mover coupled to the shaft of the generator.

As depicted in **Figure 2-1**; conventional frequency control is comprised by three stages [9]:

- Inertia response: Subsequent to a power unbalance, power is subtracted or injected to the rotating mass of the rotor, creating a deaccelerating or accelerating torque in the shaft. This torque will decrease or increases rotor speed and frequency. The change

## Primary Reserve Characteristics

in frequency will be given by the amount of energy stored in the rotating masses (proportional to its inertia).

- Primary reserve: In a multi-machine system, all synchronous units contribute according to its capacity and droop characteristic. After the imbalance, the response time depends on governor control time. Once steady conditions are reached, an offset from the nominal frequency will remain as a consequence of the droop characteristics of the governors.
- Secondary reserve or Automatic Generation Control (AGC): This is coordinated from a central command (Transmission System Operator). Nominal frequency is restored from the deviation resulted from primary reserve implementation. This reserve do not necessarily comprises all connected generating units.

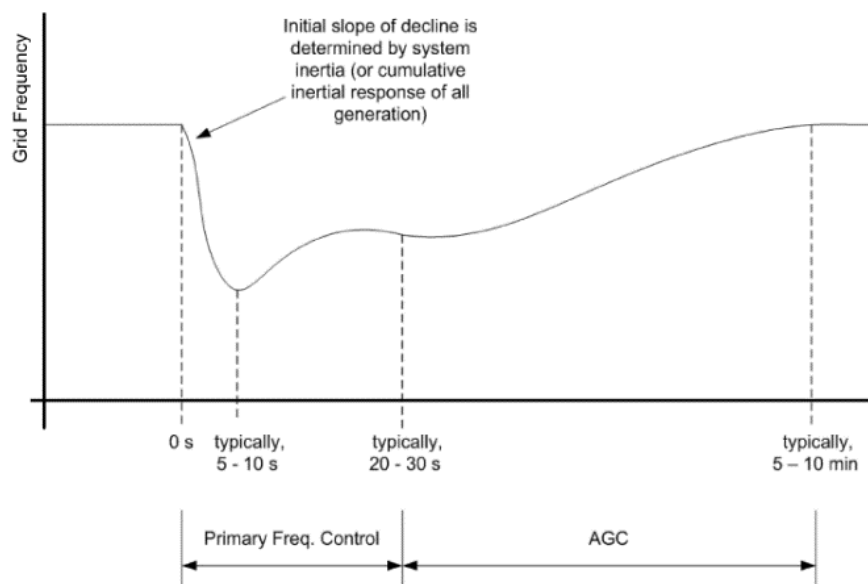
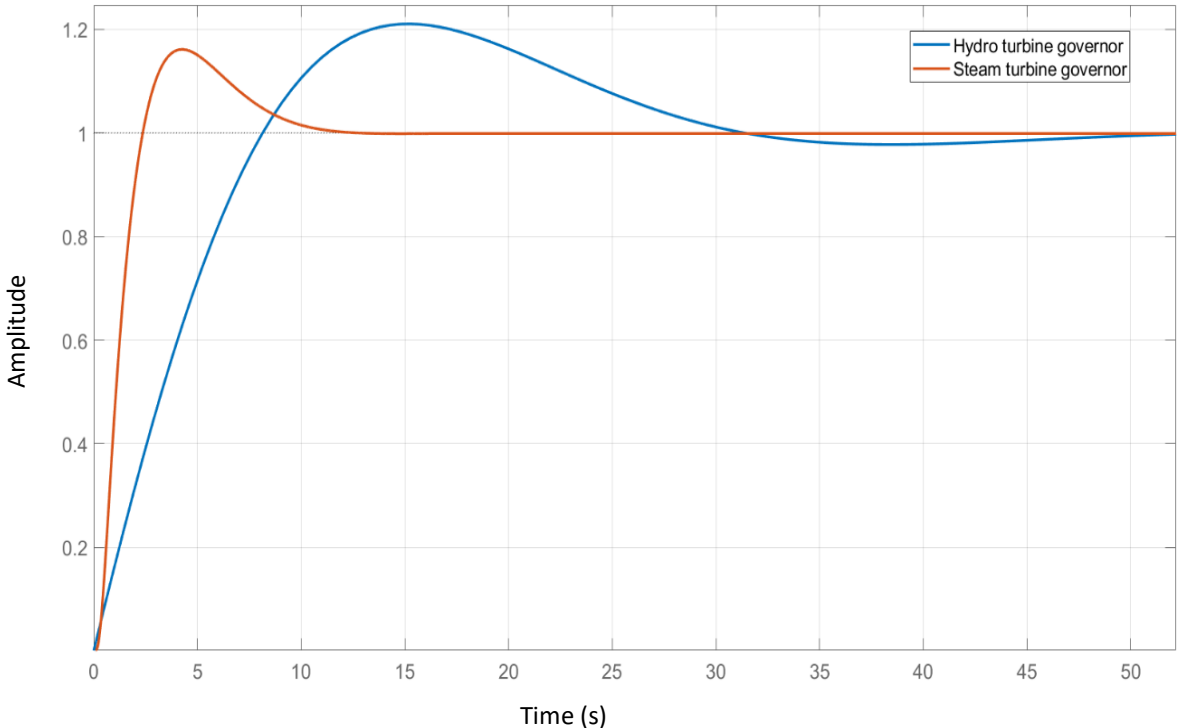


Figure 2-1: Frequency control in power systems [2]

## 2.2 Primary Reserve Characteristics

Primary reserve requirements are different for each region or country. In Europe, ENTSOE establishes that the primary reserve must be equal to the size of the two biggest nuclear power plants. In this sense, a realistic scenario is considered. A bigger generation loss seems to be very unlikely. Commonly, primary reserve has a delay of a couple of seconds before it activates (2-5 s). As previously pointed out, during this time, inertial response from the rotating masses take care of slowing down frequency drop. In the European case, it is expected that the primary reserve is deployed completely in 30 seconds. This time is a common reference for primary reserve deployment [1]

The characteristics of primary reserve are a combined response of the spinning generators online at the moment of a power imbalance. Each generator may present very different power response to changes in frequency [10, 11]. When single turbine-governor characteristics are considered a variety of responses could be achieved depending on governor model, settings and time constants. **Figure 2-2** shows the different governor controller step response, depending on the type of turbine selected [8]. Detailed governor model and time constants are shown in **Appendix I**.



*Figure 2-2: Step response for steam and hydro governor controllers. Amplitude of mechanical speed output signal depicted in Y axis; as a result of a step input signal.*

When both models are compared, it can be noticed the faster response from the steam governor over the hydro governor. Even though steam turbines are less efficient when they are ramping power, it is shown that they can offer certain flexibility and fast governor response [12]. On the other hand, hydro turbines have a slower response than conventional units [11]. Whenever single governor response is considered in this thesis, the selected governor type is steam turbine governor in order to be compared with the assumed slower primary reserve.

### 2.3 Frequency Control with Distributed Energy Resources

Distributed Energy Resources (DER) in power system are mainly comprised by renewable energy resources. Currently one of the challenges in the implementation of DER as frequency control support is the lack of inertia response from them. As it was previously pointed out, inertia response is the first natural measure against the change in frequency when an imbalance occurs. In the case of PV systems, the generation of power is given by the photoelectric effect and no rotating masses are involved, having no inertia.

Additionally, given the inherent variability of renewable resources and technology characteristics (Asynchronous generation in variable speed wind turbines and DC power generation in PV), such technologies need the implementation of power converters which transform the unsuitable power output from the DER generators into suitable power to be injected into the grid. The power converter to be connected between the generator and the grid is in all cases an inverter; since it will convert the DC output of PV into AC synchronized power. In the case of variable speed wind turbines, the AC power with variable frequency is first converted to DC by rectifiers and then it is converted from DC to AC synchronized power output. This AC-DC-AC transition inhibits the wind turbine to react to grid disturbances. In general, it could be stated that the inertia of a power system is a measurement of its robustness, which means the higher the system inertia, the lower the rate of change of frequency (RoCoF) for a given system imbalance.

Since the most prevailing inverter technology in grid connected DER is the grid-following type; frequency and voltage from the system are followed by the inverter, acting as a current source that operates at maximum power point, decoupling in this way the DER power production from the grid dynamics and disabling the participation of renewables in power balancing and frequency regulation.

It is expected that grids with high penetration of DER to have a lower system inertia, leading to higher values of RoCoF. This high value of RoCoF can provoke big frequency excursions, having as possible consequence load shedding or even total system black out [1, 6]. Frequency is maintained in power system under very strict limits because sustained values out of the nominal range can cause severe mechanical damages in turbines and deterioration due to thermal effects and saturation in generators and transformers.

As synchronous machines installed capacity diminishes, not only the inertia of the system is reduced but also the contribution of synchronizing torque during disturbances. This can create small signal stability as well as frequency stability problems [13].

Several novel approaches may be found in the literature for implementation of renewables in frequency regulation and inertia contribution. The main inertia control strategies are synthetic inertia and fast reserve power [6].

- Synthetic inertia: This control strategy applies only to wind turbines. This approach attempts to extract the kinetic energy from the rotating blades of the wind turbine when a disturbance occurs. Typically the control loop releases the kinetic energy based on the RoCoF and frequency deviation.
- Fast reserve power: In contrast to synthetic inertia, fast reserve power injects a constant amount of power during a certain amount of time through the control of rotor speed set point.

For frequency regulation, techniques such de-loading and droop control have been studied:

- De-loading: Wind turbines and PV plants typically operate at their maximum power point. That means obtaining the most of power from the primary resource (wind or solar irradiation), therefore when lack of generation occurs they cannot contribute to primary reserve for frequency regulation. In this approach the generators do not

Frequency Measurement time and RE deployment time.

- operate at their maximum power point but at a lower than maximum in order to allow the generator to operate at maximum when more power is required by the load.
- Droop control: Similarly to droop governors in synchronous machines, the control loop in wind turbines emulates the power-frequency dependency, allowing the turbine to react to changes in frequency with change in power output.

## 2.4 Frequency Measurement time and RE deployment time.

The current capabilities of non-synchronous technologies for fast power reserve are summarized in **Table 2-1**, additionally to such metrics, 100 ms for RoCoF measurement is noted [14].

*Table 2-1: Activation times for fast power reserve of non-synchronous technologies [14].*

Technology	Full Fast Frequency response (ms)
Wind turbine-Synthetic inertia	~500
Lithium batteries	10-20
Flow batteries	10-20
Lead-acid batteries	40
Flywheels	<4
Super capacitor	10-20
Solar PV	100-200
HVDC	50-500

Precise and fast frequency measurement along with fast full power deployment are a requisite for fast power reserve. Hence, depending on the application and required activation times, each of the options presented in **Table 2-1** could represent an option for fulfilling such needs.. Promising technologies due to the expected reduction of prices in future and their very short activation time are storage technologies. For example, Flywheels have very short time for activation, high power capacity but really low energy storage capacity, therefore it could discharge high amounts of power during a few seconds [15]. Lithium ion batteries are expected to drop their cost by 54-61% in 2030. Additionally, lithium ion batteries offer a good power and energy capacity, which make them suitable for ancillary services [15]. PV and wind are the predominant renewables, therefore they represent a great opportunity for integration of fast power reserve. In any case, each type of technology has an activation time faster by far than conventional synchronous machines, the application of any will depend on prices and system needs.

## 2.5 Load Balancing and Fast Power Reserve

Currently in Germany, plant commitment of renewable energy plants have a priority in the power market for dispatch due to its zero marginal cost for generation. This has an effect in market auctions and also technical implications [12]. Balancing of the residual load is provided by conventional units, so curtailment of renewable energy resources is the last preferred option for power balancing [16]. Experience from power plants in Germany and Denmark have shown that certain flexibility can be obtained from conventional power. This added flexibility enables conventional generation to provide the service of power balancing of the residual load instead of performing as base generation [12].

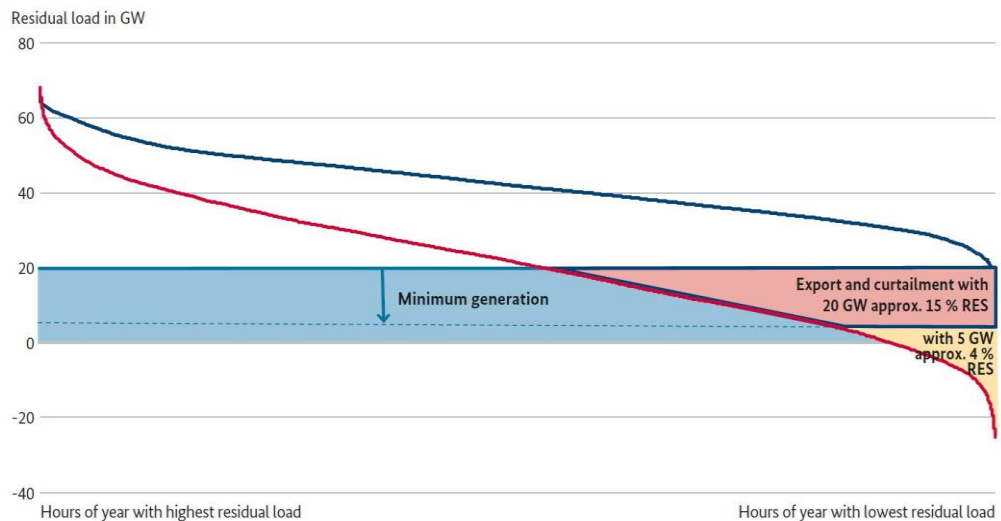


**Figure 2-3: Sorted hourly residual load plot. In blue residual load for a 25% of renewables and in red for a 60% of renewable [17]**

As shown in **Figure 2-3**, when the penetration of renewable energy increases, the residual load decreases accordingly. In future scenarios negative values of residual load are expected, being energy storage and power to X some balancing alternatives instead of curtailment.

As an immediate result of an imbalance between generation and load the system frequency starts deviating from its rated value. The range of 49.8 Hz and 50.2, in Continental Europe, should be maintained by reserves after a power imbalance. This frequency range corresponds to the ordinary operation range. The primary reserve for the interconnected system is able to withstand a power imbalance of 3 GW (2%) when the system has a total load of 150 GW [1].

At an European level, the dimensioning reference case scenario of power loss of 3 GW has been found adequate even with high penetration of renewables [1, 16]. Nevertheless, there will be still many hours with positive residual load and due to the decommissioning of conventional power plants [16, 17]; their diminished capacity to provide balancing power services at such low inertia levels will have to be compensated by balancing services coming from renewables/storage. Additionally to the uncertainty of conventional generation availability in the German power system, is also not clear whether instantaneus reserve

services from abroad would be available and if transmission capacities will be enough for such [16].

If an imbalance out of this range occurs, load shedding can not be avoided. When the global security of the system is endangered or/and under-frequency load shedding is activated the system is in the emergency state. If the frequency exceeds the range of 47.5 Hz or 51.5 Hz, a system blackout can hardly be avoided [1]. Consequently the system will reach the so-called blackout state and will have to be restored. Before black out, the system tries to recover balance by load shedding and generation curtailment. Load shedding starts at 49 Hz rejecting partial loads as frequency decreases. On the other hand, curtailment thresholds between 50.2 and 50.5 have been studied by ENTSOE for overfrequency scenarios [1]. In this thesis, a deviation of  $\pm 1$  Hz is used as threshold before load shedding and curtailment starts. Hence, to keep frequency within such threshold; the investigated critical time and power response, correspond to the maximum allowed activation time for fast power reserve in order to inject power from renewables or storage in case of under-frequency; or to extract power from the grid to be stored or converter in another energy form in the case of over-frequency.

Fast power reserve must be understood as a mean for balancing generation and load at any moment and at any point of the system. Therefore under normal interconnected operation or in a split scenario resulting in electric islands, fast power reserve should avoid or minimize load shedding when a lack of generation is the problem, by injecting power from deloaded renewables power sources or from energy storage. Furthermore when surplus of power is available as result of system split or even under normal operation conditions, fast power reserve (negative) should be able to provide the meanings for minimizing or avoid curtailment and system shut down as result of over-frequency.

Although the focus of this investigation was centered in the positive power injection to avoid under frequency load shedding; as it will be demonstrated in the result section, the required fast power reserve and critical times can be also understood as negative reserve for over-frequency cases too.

### 3 Methodology

---

As it was explained in chapter 2, the transitory frequency response of the system and therefore its stable and reliable operation after a perturbation, depends on the inherent characteristics of the power system (system inertia) and the counteraction measurements engaged automatically by the system (primary reserve). As the share of inverter based generation increases, the more sensible to instability the power system becomes. In this sense the added inverter based fast power reserve (IBFPR) must be capable of maintaining transitory frequency value within the allowed limits.

Two terms commonly found in the literature of power system stability will be used along this section:

- Inertia constant  $H$ : It has units of seconds (s) and it is the ratio of the kinetic energy stored in the rotating masses of the generators ( $E_k$  in MWs) and its nominal capacity ( $S_{nom}$  in MVA).
- Acceleration time constant  $T_a$ : It also has the units of seconds (s) but this is the ratio of double the kinetic energy (MWs) and generators nominal power output ( $P_{nom}$  in MW).

Acceleration time constant is a measure of the robustness before disturbances of the system. It could be interpreted as the required time to remove the kinetic energy from the rotating masses of the generators connected in a grid, at the rate of the supplied power load. Hence the higher the time constant, the higher the kinetic energy available. Nowadays Europe's acceleration constant is around 14 seconds [1]. As the share of synchronous generations decreases, this constant decreases proportionally.

With  $f$  as frequency,  $f_0$  as nominal frequency and  $\Delta P$  as power imbalance the swing equation can be expressed as follows:

*Equation 3-1*

$$\frac{df}{dt} = \frac{\Delta P * f_0}{2 * H * S_{nom}} = \frac{\Delta P * f_0}{T_a * P_{nom}} = \frac{\Delta P * f_0}{2 * E_k}$$

To describe the penetration of inverter based generation into the grid, these terms can be related to the overall power system. Even though the inertia constant  $H$  is most commonly used in the literature, the term of system acceleration time constant  $T_a$  is used instead when the penetration of non-synchronous generation in a power system is evaluated (ENTSOE 2016); this due to the fact it relates the load real power term (MW).

In this section the steps and methods applied in order to calculate the required Inverter Based Fast Power Reserve (IBFPR) to maintain frequency stability are presented.

### 3.1 Determination of Inverter based Fast Power Reserve

**Figure 3-1** depicts the typical frequency response when a negative power imbalance occurs in a power system. If the imbalance is high enough or the system inertia is too low, the initial RoCoF can lead to frequency excursions below the UFLS value. The value of RoCoF is brought to zero normally by the action of the primary reserve; equalizing the power imbalance assuming no load frequency dependency. At this time the minimum value of frequency (frequency nadir) is reached as well.

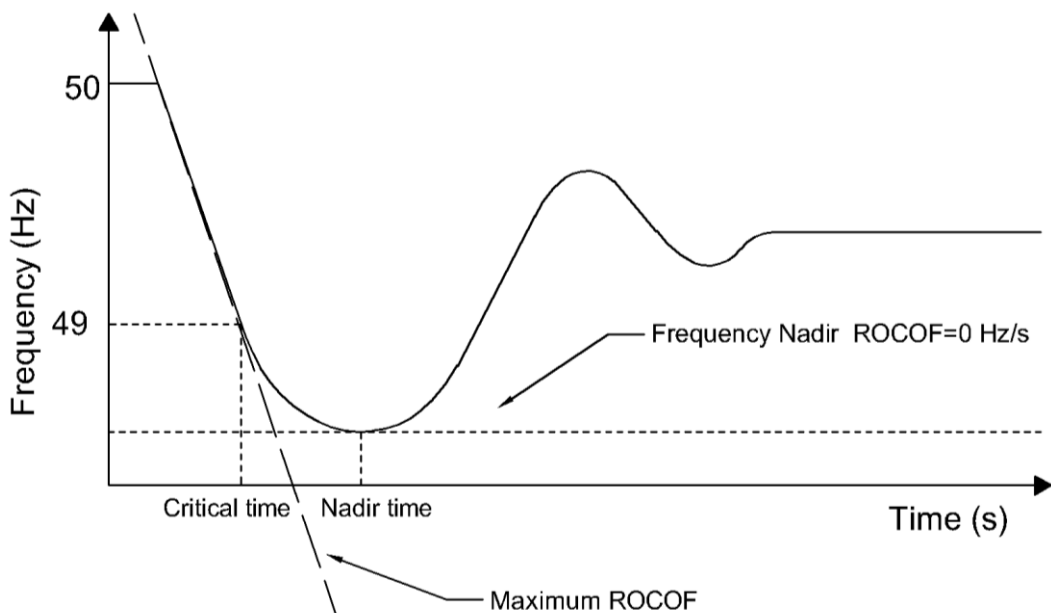


*Figure 3-1: Frequency response of a typical power system subjected to a severe negative power unbalance.*

When it is assumed that no load is rejected at UFLS frequency, the frequency continues dropping below 49 Hz. The time at which the system frequency equals the UFLS value is called in this thesis as critical time. This is the maximum available time for the inverter based reserve to deploy the required power to the system.

## Determination of Inverter based Fast Power Reserve

In the critical condition that would lead to load shedding, it is expected from the IBFPR to at least counteract the ROCOF at the critical time, as illustrated in **Figure 3-2**.

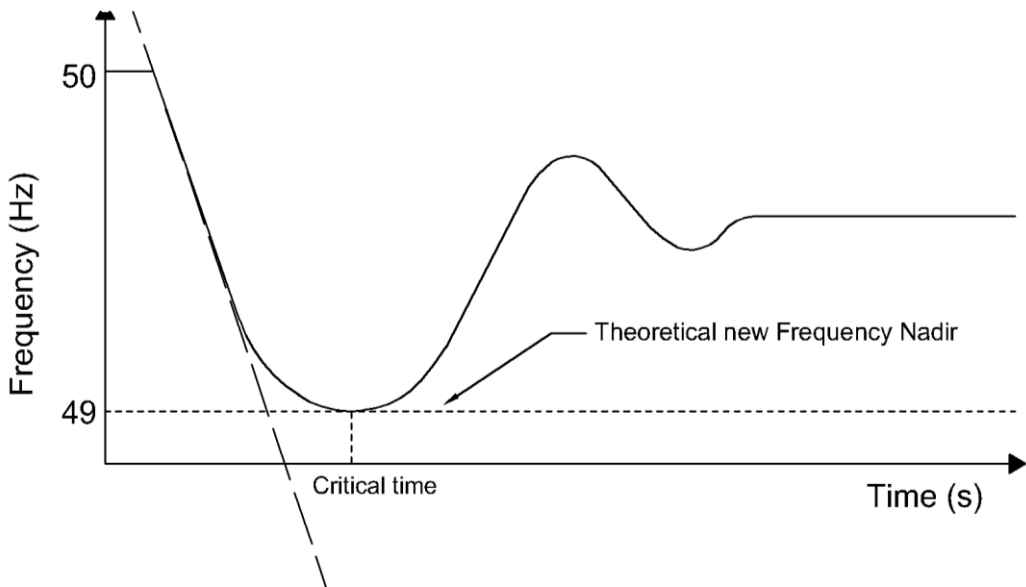


*Figure 3-2: Expected power system frequency response with the addition of Inverter Based Fast Power Reserve.*

Recalling **Equation 3-1**; it is necessary that the machine's accelerating power (power imbalance) become zero at the critical time.

*Equation 3-1*

$$P_a(t_{cr}) = P_{mech} - P_{elec} + P_{IBFPR} = 0$$

Where  $P_a$  is accelerating power,  $P_{mech}$  is mechanical power,  $P_{elec}$  is electrical power (load),  $t_{cr}$  is the critical time and  $P_{IBFPR}$  is inverter based fast power reserve.

Typical primary power reserve response follows the indicated behavior shown in **Figure 3-**. Conventional turbine governor response is frequency dependent and may not respond linearly. For the estimation of IBFPR it was assumed a linear power deployment over time until the critical time. Inspecting **Equation 3-1**; it can be notice that only the power imbalance determines the rate of change in frequency in the system along with the kinetic energy stored in the rotating masses of the generators. For this reason the analysis is focused on the change on mechanical power after the event, ignoring the electrical load and mechanical power in the stable operation before the perturbation.

From the assumption of a linear mechanical deployment given from the synchronous machines governors, the rate of change in mechanical power, after a power imbalance  $\Delta P$ , is given by  $\Delta P/t_{nadir}$ , where  $t_{nadir}$  represents the time at which the frequency nadir occurs. Given the power balance **Equation 3-1** at the critical time,  $t_{cr}$ ; the IBFPR response must be equal to  $P_{elec} - P_{mech}$ , being  $P_{elec}$  equal to  $\Delta P$ . **Figure 3-** illustrates the behavior of both responses together. The sum of both at critical time counteracts power imbalance.

## Determination of Inverter based Fast Power Reserve

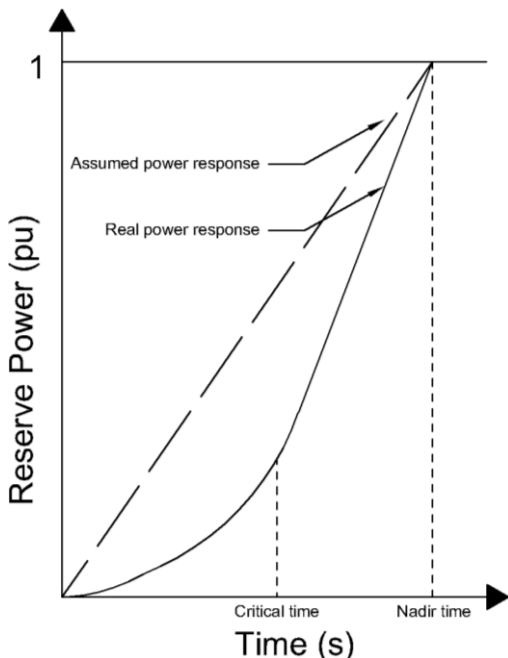


Figure 3-3: Comparisson of assumed power reserve deployment and typical real response.

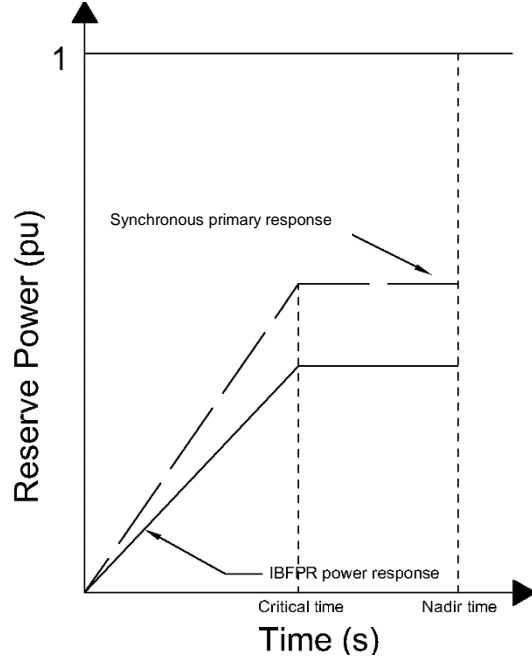


Figure 3-4: Assumed primary power reserve and IBFPR.

Substituting  $P_{mech}$  by  $\Delta P * t_{cr} / t_{nadir}$  and  $P_{elec}$  by  $\Delta P$  in **Equation 3-1**, the following expression is obtained for the  $P_{IBFPR}$  at time  $t_{cr}$ .

**Equation 3-2**

$$P_{IBFPR}(t_{cr}) = \Delta P * \left(1 - \frac{t_{cr}}{t_{nadir}}\right)$$

It is assumed that  $P_{IBFPR}$  remains with a constant power output after  $t_{cr}$  long enough to stabilize the system frequency. The result of the previous equation represents the slope of the power output since the inception of the incident until the critical time, which with the implementation of IBFPR, it will be not any longer critical but rather it will be the new desired frequency nadir time.

**Equation 3-3: IBFPR before critical time.**

$$P_{IBFPR}(t) = \frac{\Delta P}{t_{cr}} * \left(1 - \frac{t_{cr}}{t_{nadir}}\right) * t$$

The positive value of **Equation 3-3** represents the injection of fast power response from renewables or storage to counteract frequency drop below of the load shedding frequency setting of 1 Hz below nominal. Nevertheless when there is an over-frequency phenomenon with surplus in generation, the negative value of **Equation 3-3** can be taken as the power rate required to limit over-frequency to no more than 1 Hz above nominal. Similarly, critical times would apply for upper and down frequency thresholds.

According to the obtained expression; it can be realized that the desired power response from the inverters depends exclusively on parameters which cannot be directly measured from the grid connection point. In a real situation the values of  $\Delta P$ ,  $t_{nadir}$  and  $t_{cr}$  cannot be known in advance, representing this factors a challenge in the implementation of this ideal power response. Those values are dependent on the grid characteristics; depending on the primary conventional reserve deployment time and the overall system inertia [18]. Thus two main cases are considered for the remaining analysis with the intent of covering a wider range of systems with different characteristics.

### 3.2 Cases for Assessing Inverter based Fast Power Reserve

As presented in the previous section, the values of critical time and frequency nadir time depend on the system imbalance and primary reserve deployment time. In chapter 2 it was illustrated the different governor response for different primary reserve type. To be able to assess the influence of the grid size and the primary reserve characteristics, two main cases are considered. In all cases is assumed that the initial steady frequency is the nominal 50 Hz.

- Small scale grid scenario: For the evaluation of this case; typical governor data is considered in a well-known and studied benchmark grid topology as the WSCC model, also known as the IEEE 9 bus model. Synchronous reserve deployment time in the order of  $\sim 3$  s due to governor response [7, 11]
- Large scale grid scenario: The European island scale all synchronous machines are modeled and simplified as one single machine, provided with the characteristic expected from the overall system. Synchronous primary reserve deployment in the order of  $\sim 30$  s [1, 19]

## Scenario Summary

### Small Scale Grid Scenario

Implementation of individual governor response to generators.

Case A-Simplified Model: One machine, one load and no losses representation to the IEEE 9 bus model.

- Determination of critical time.
- Determination of IBFPR and impact of SI and frequency measurement delay in frequency response.

Case B-Extended Model: All the power system components (transmission lines, transformers, excitors and governors of the three generators) and its dynamic characteristics are considered in the IEEE 9 bus model.

- Determination of critical time.
- Influence of the full dynamic grid model.

### Large Scale Grid Scenario

Case-Split operation: Analysis with imbalances up to 40% with variation of primary power reserve deployment in 30 s in an islanded system. Island frequency response is assumed to be the same that the European response analyzed by ENTSOE.

- Determination of critical time.
- Determination of IBFPR and impact of SI and frequency measurement delay.

### 3.3 Simplified IEEE 9 Bus Model

Microgrids can operate connected to the bulk transmission/distribution system or stand alone. In any case, it is assumed that imbalances could occur due to internal faults when island configuration is considered or islanding from the external system results from a contingency while a considerable amount of power load of the microgrid was being ‘imported’ or ‘exported’. For the study of power systems and the increasing interest in stability analysis in micro-grids, the IEEE benchmarks represent a widely used option, based on some real data. This is also the case of the IEEE 9 bus model or WSCC (Western System Coordinated Council). The IEEE 9 bus model is a representation of the former western interconnected power system of North America of 1967. For stability and reliability studies, this system has been employed in many publications as study case [20], which allows the comparison of results. **Figure 3-3** illustrates grid’s configuration.

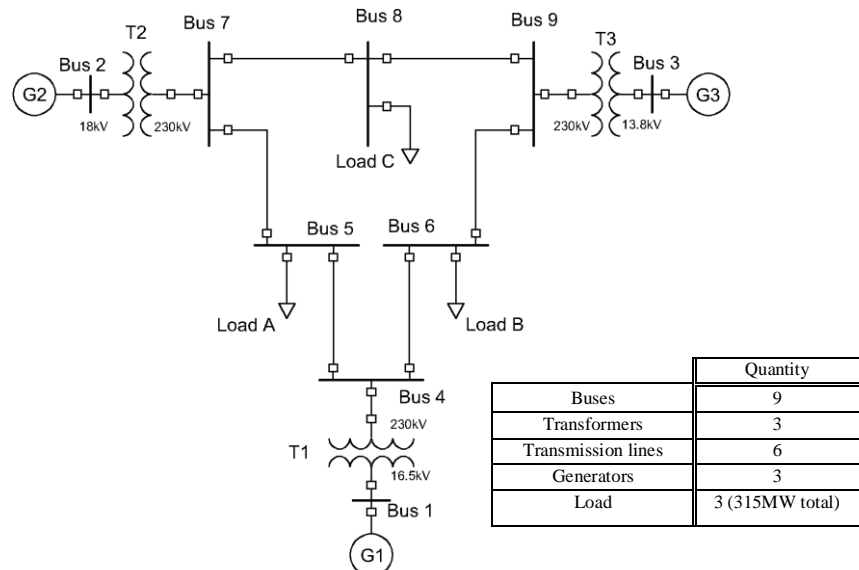


**Figure 3-3:** WSCC or IEEE 9 bus model used for stability studies.

As a first step to evaluate the impact of inverter based generation and power imbalances in the grid, the whole system is simplified as one single generating unit; neglecting all losses in the system (Transformers, transmission lines and generators) with the assumption that the mechanical output of the prime mover is the same than the electrical power output at generator terminals. A schematic representation of such system is presented in **Figure 3-4**.

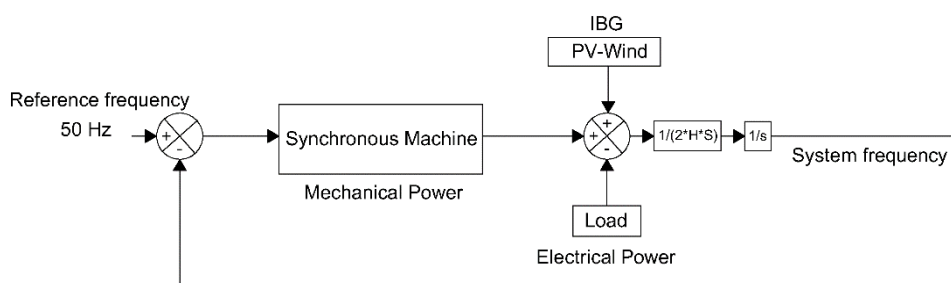


**Figure 3-4:** Single machine representation of the IEEE 9 bus model.

**Figure 3-4** is the block representation of the swing equation, it only differs in the fact that a source representing the inverter based generation has been included. This power source output would typically remain constant during an imbalance. The mechanical power is represented by the output of a steam turbine governor model, which is used to represent the synchronous machine [8]. The addition of the former sources represents the total generation. When steady state conditions are met, the accelerating power resulting from the subtraction of the load from the total generation is zero. When equilibrium is lost, the accelerating power is multiplied by the transfer function  $1/(2*H*S)$ , where  $H$  is the machine's inertia constant and  $S$  is the machine's power rating. From **Equation 2-1** this product equals the derivative of frequency, therefore an integrator block, denoted by  $1/s$  is added to obtain the frequency response [7, 21, 22]. A feedback loop is added and an error signal obtained from the reference frequency so the synchronous machine can react as frequency deviates from nominal. The step response of the governor model under a three different penetration of non-synchronous generation is presented in **Figure 3-5**. From that, rise time is between 1.14-3.24 s.

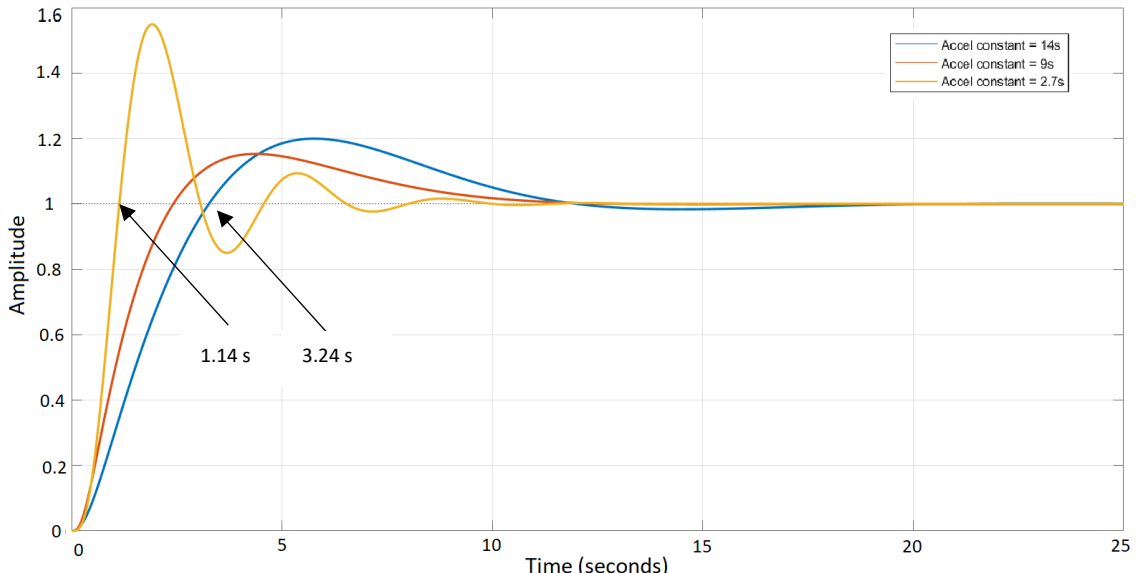


*Figure 3-5: Step response of Governor model for different values of acceleration time constant. Amplitude of speed response depicted in Y axis.*

The values of kinetic energy and time constants of a synchronous machines of 835 MVA were selected to represent the synchronous response, with the load of 315 MW the system acceleration time constant is 14 s [8], which is approximately today's Europe acceleration constant [1]. This is the base scenario, assuming 100% synchronous generation. To evaluate the impact of the penetration of inverter based generation; the values of lower capacity generators were selected [8], assuming the compensation of the remaining power by a constant power source representing the inverter based generation, decreasing in this manner the total system acceleration time constant, thus the kinetic energy of the generator. Up to this point, neither synthetic inertia nor frequency support from renewables is considered.

Inverter based power output remains constant before, during and after the perturbation. Therefore the system imbalance is covered only by the synchronous equivalent machine.

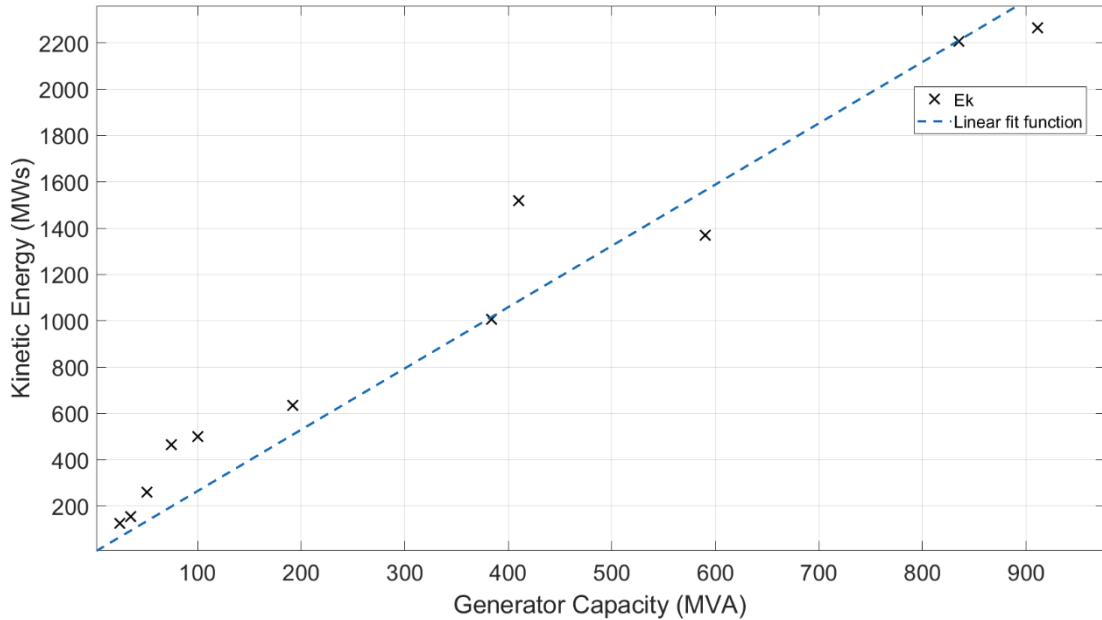


Figure 3-6: Kinetic energy stored in generator rotating masses as function of generator capacity. A linear relation is exhibited between the machine capacity and its store kinetic energy .

Even though load imbalances up to 40% were simulated in each inertia scenario, the power capacity limit of the generators was disregarded for estimation of the critical time. The negative imbalance was simulated by increasing the system load by the corresponding factor. A block diagram representing the system in the given conditions was designed in MATLAB-SIMULINK. With the help of a MATLAB code several simulations were run and the critical and nadir times acquired for each scenario. With the calculated times, the IBFPR to avoid load shedding under each scenario was calculated as given by **Equation 3-3** and it is shown in the Results section.

All the acquired values of critical time, as result from the simulations, are then related with the system RoCoF, so a regression can be performed and link the critical time with system RoCoF.

For the system conditions and the employment of the fitting tool provided by MATLAB, an expression is obtained for critical time as a function of RoCoF.

As it will be detailed shown in the result section, for unstable conditions the maximum critical time is 2.7 seconds. Therefore critical time must be lower or equal to that value; calculating in this way that the minimum RoCoF for activation as 0.6143 Hz/s, when the fitting equation obtained from the regression is used.

### Implementation of IBFPR in the IEEE 9 bus model

In order to test the values found of power response from the inverters, these are implemented through a simple SIMULINK algorithm which estimates the power imbalance and critical time based on the measurement of the RoCoF, when system inertia it is known. Based on those estimated values, the algorithm provides the power ramp before the calculated critical time is reached and maintained constant power output after this time.

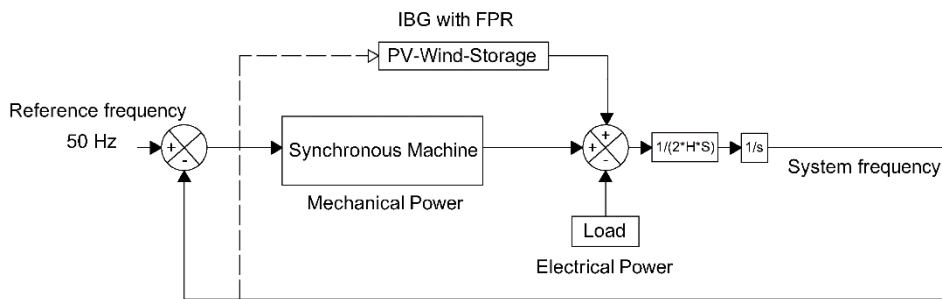


Figure 3-7: Simplified IEEE model with IBFPR implementation.

The algorithm works in a simple way:

1. It measures the system RoCoF.
2. If the value exceeds  $0.6143 \text{ Hz/s}$  the IBFPR is activated.
3. According to the measured value of RoCoF and available system inertia, a ramp power response is injected into the system during a time equal to the calculated critical time according to **Equation 3-3**. Critical time calculated from fit.
4. When the calculated critical time is reached, the IBFPR must stop ramping power and keep a steady value until frequency is restored to an acceptable value as per **Equation 3-2**.

The block diagram is provided in **Appendix II**.

### Synthetic Inertia in the IEEE 9 bus model

Synthetic inertia was explained in chapter 2 as one of the new techniques that manufacturers and researchers are considering to tackle with the low inertia problem in power systems [23, 24]. Frequency support through synthetic inertia was considered with the following assumptions [6, 25]:

1. Power output from synthetic inertia is limited to 10% of wind turbine nominal power.
2. Due to mechanical and thermal stresses, the additional power can be delivered only for a maximum time of 10 s.
3. It's assumed that all wind turbines operate at its maximum power output. The value of 1.5 MW was selected for such purpose.
4. In order to avoid wind turbine stall, the removed kinetic energy from the blades (injected to the grid in electrical form) it is limited to half [26].

## Simplified IEEE 9 Bus Model

To be able to extract energy from the rotating blades of the wind turbine, an adequate control system is needed. From the expression of power as the derivative of energy and the kinetic energy stored in the blades, the rate of energy extracted from the wind turbine can be obtained, considering that rotational speed changes in time.

$$P = \frac{dE_k}{dt} ; E_k = \frac{J_{wt} * w^2}{2}$$

$$P = \frac{J_{wt}}{2} * \frac{dw^2}{dt}$$

$$J_{wtc} = \frac{2 * H_{wt} * S_{wtc}}{w^2}$$

**Equation 3-4**

$$P_{pu}(t) = 2 * H_{wt} * w_{pu}(t) * \frac{dw_{pu}(t)}{dt}$$

Where  $E_k$  is kinetic energy,  $H_{wt}$  is the turbine inertia constant,  $w$  the rotational speed,  $S_{wtc}$  is turbine's nominal power and  $J_{wt}$  the turbine inertia.

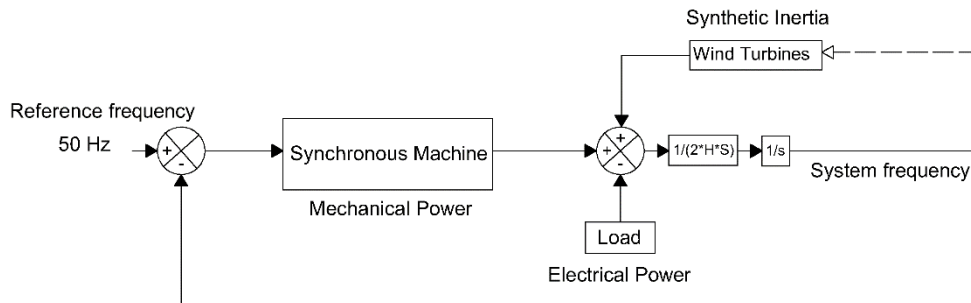


**Figure 3-8: Implementation of synthetic inertia in the simplified IEEE model.**

**Equation 3-4** represents the rate of change of kinetic energy extracted from the rotating masses of the wind turbine in per unit. The implementation of such equation in SIMULINK is shown in **Figure 3-9**. Additionally, a gain block  $K_i$  was added in order to inject more power

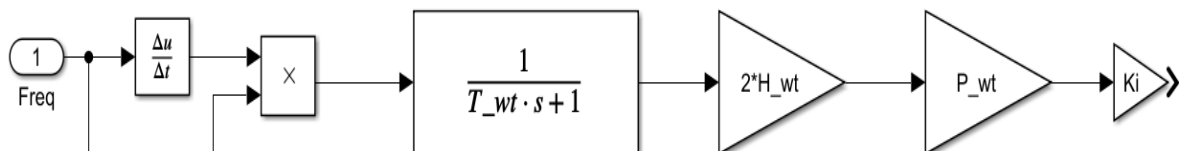


**Figure 3-9: Synthetic inertia control model where  $T_{wt}$  is the filter constant,  $H_{wt}$  is the turbine's inertia constant,  $P_{wt}$  is the nominal wind capacity (MW) and  $K_i$  is a gain constant. Frequency input in pu and system output is power in MW.**

from the very beginning of the power imbalance. A filter at the signal entrance was added in order to suppress non desired oscillations on the system [24, 25].

Typical values for inertia constant of wind turbines are not openly available from the manufacturers to the public. Hence an approximate value was calculated with the utilization of an equation which relates nominal power and inertia constant for wind turbines [27].

**Equation 3-5: Wind turbine inertia constant as function of the nominal power in MW.**

$$H_{wt} \cong 1.87 * P_{nwt}^{0.0597}$$

For a wind turbine with nominal power output of 1.5 MW the value of  $H$  corresponds to 4.37 s, which is in an acceptable range [28].

It is assumed that all the wind turbines, when operating, are delivering their nominal power output. A nominal rotational speed of 18 rev/min was considered [28]. To avoid the wind turbine to stall, only a reduction of 5 rev/min it is allowed by the implementation of the control system. This change of rotational speed equals a change of 3 MWs reduction on kinetic energy out of a total of 6 MWs.

**Table 3-1: Constants for implementation of synthetic inertia.**

T <sub>wt</sub>	H <sub>wt</sub>	P <sub>wt</sub>	K <sub>i</sub>
-	s	MW	-
1	4.37	1.5*n <sub>wt</sub> <sup>1</sup>	10

### Synthetic Inertia and IBFPR in the IEEE 9 bus model

In this model the contribution to system frequency stability of both models operating together is evaluated as shown in **Figure 3-10**. Similar to **Figure 3-4**, accelerating power determines de change in frequency. In this case, the sources IBFPR and Synthetic inertia will change their output to counteract the imbalance according to the change in frequency in the system. No additional modification or adjustment was performed to the IBFPR or the synthetic inertia model.

Procuring to estimate frequency measuring time influence, an intentional delay was introduced to the IBPR and the SI response. This delay emulates the required time for frequency measurement, filtering and signal processing. A delay transport block was added in the power response. Depending on the technique and precision desired, the time for acquiring frequency reading may differ considerably, however, for the purpose of this research the time of 100 ms with was taken as the fastest measurement reading time [14].

---

<sup>1</sup> n<sub>wt</sub> refers to the number of wind turbines with synthetic inertia control.

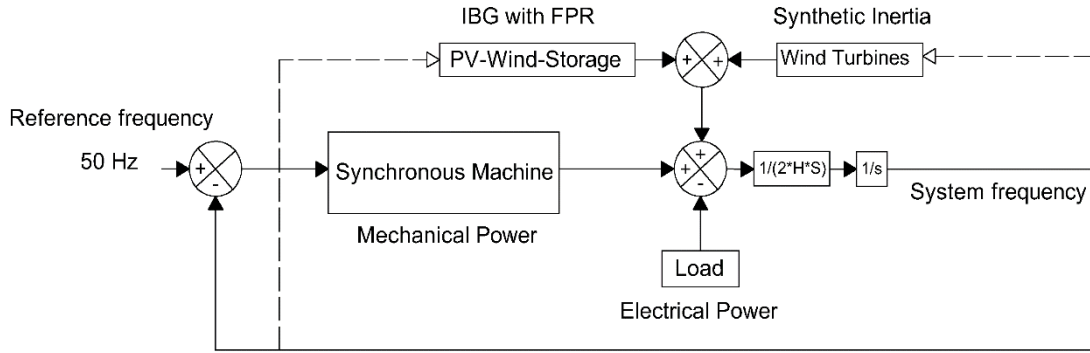


*Figure 3-10: Synthetic inertia and IBFPR implementation.*

### 3.4 Extended IEEE 9 Bus Model

It was previously stated that in the first approach, only the total load was considered in the simulations as well as the synchronous generation represented by one single machine and no system losses. Since it is desired to compare the results of the system with such simplifications against some model that takes into account the whole system components, losses and dynamics; An extended representation of the IEEE 9 bus model was implemented in SIMULINK [20]. In this representation, simulations for different values of system inertia and load imbalance were performed, similarly as it was done with the simplified representation of the model. **Figure 3-11** shows the extended IEEE 9 bus grid architecture with IBG added.

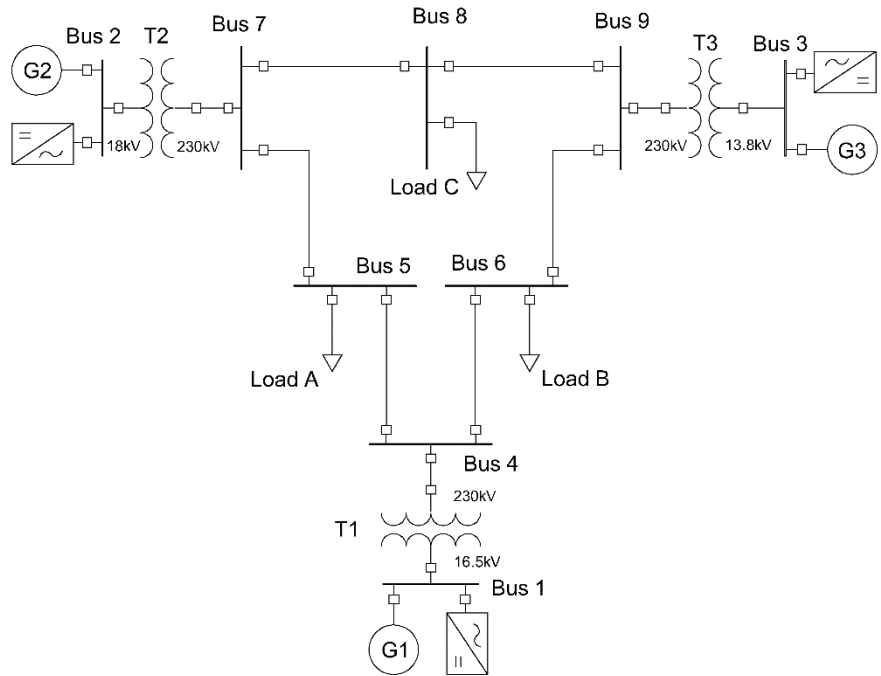


*Figure 3-11: IEEE extended model with IBFPR implementation.*

In order to evaluate the validity of the equation describing the IBFPR needed to avoid ULFS, the Extended model was modified with the insertion of ideal controlled power sources blocks, which were set up to inject power into the grid accordingly to the simulated scenario. Therefore, no means of frequency measurement were included and only IBFPR was assessed.

### **System settings for stability study**

Since it is desired to compare the complete representation of the IEEE 9 bus model against the simplified model representation; it is assumed in the same manner that the total acceleration time constant of the system equals 14 s, similarly as in the block representation. Hence the same kinetic energy should be distributed among the three generators rotating masses in the extended model as in the simplified representation. From **Equation 3-6** for system acceleration time constant, it can be easily calculated that the system kinetic energy with 14 s (100% synchronous generation) is 2205 MWs.

*Equation 3-6*

$$T_{sys} = \frac{2 * E_k}{P_{LOAD}}$$

Due to the fact that inverter based generation reduces the system kinetic energy; for different levels of inverter based generation, the generators nominal capacities ( $S$ , MVA) values were kept constant and the inertia constant ( $H$ , s) of each machine multiplied by the synchronous share factor ( $f_{ss}$ ). Total system kinetic energy is the summation of all units together. In this way, the synchronous generators in the initial state of equilibrium represent both power sources, inverter based plus synchronous.

*Equation 3-7*

$$E_k = 2 * (H * f_{ss}) * S$$

### **Prime mover and governor**

The type of prime mover selected was conventional steam turbines and its governor system. Governor model and generator exciter were selected from SIMSCAPE library for specialized power systems.

The block contains a complete tandem-compound steam prime mover, including a speed governing system, a four-stage steam turbine, and a shaft with up to four masses. The speed governing system consists of a proportional regulator, a speed relay, and a servomotor controlling the gate opening. The steam turbine has four stages, each modeled by a first-order transfer function. The first stage represents the steam chest while the three other stages represent either reheaters or crossover piping. The boiler is not modeled and boiler pressure is constant at 1.0 pu. Additionally, an exciter system was added to the machines, the parameters of such blocks as well as turbine constants are presented in **Appendix I**.

In order to start the simulations in steady state, a load flow calculation of the grid must be carried out with the objective of calculate the initial conditions for the exciter and prime mover models.

**Table 3-2** summarizes the main values for setting system initial conditions; acquired from the power flow tool provided by SIMSCAPE.

**Table 3-2: System steady state-initial conditions**

Bus number	Bus type	Voltage	Power	Reactive Power
		Per unit	MW	MVAr
1	Slack	1.04 $\angle 0^\circ$	72.2	25.64
2	PV	1.025 $\angle 9.83^\circ$	163	8
3	PV	1.025 $\angle 4.63^\circ$	85	-9.41
5	PQ	0.9949 $\angle -4.42^\circ$	125	50
6	PQ	1.01211 $\angle -4.16^\circ$	90	30
8	PQ	1.0172 $\angle 0.17^\circ$	100	35

### IBFPR representation

Similarly as it was done in the simplified block model, a subsystem is implemented in the extended model in order to represent the IBFPR and analyze the system behavior with the addition of this power. To do so, the IBFPR was modeled as controlled current sources; such controlled sources inject active power according to the load imbalance and system inertia simulated. Continuous voltage measurement is required in order to determine the amount of current needed to supply the requested power. **Figure 3-12** depicts the schematics of the IBFPR control.

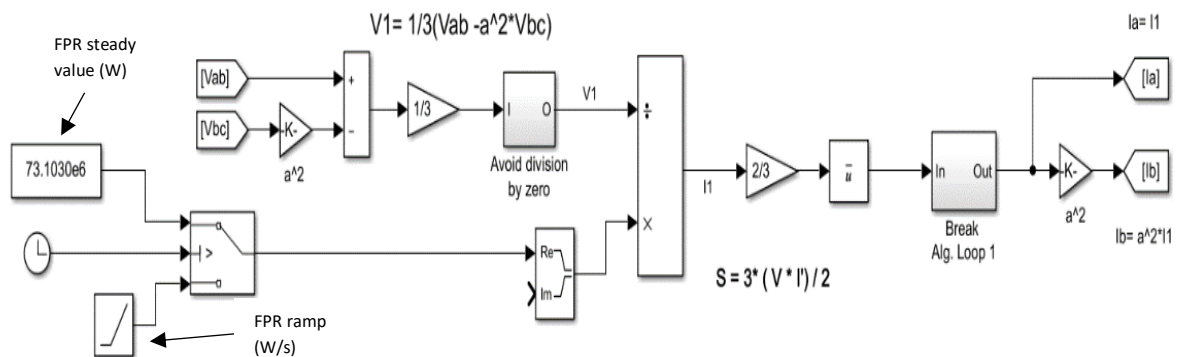


**Figure 3-12:** Model implemented to calculate the required current to meet the specified power rate from measured voltage signal shown in Figure 3-13.

It can be noticed from **Figure 3-13** that the IBFPR is composed of 2 current sources, 2 voltage readers (complex measurement), two resistance and 3 connecting ports.

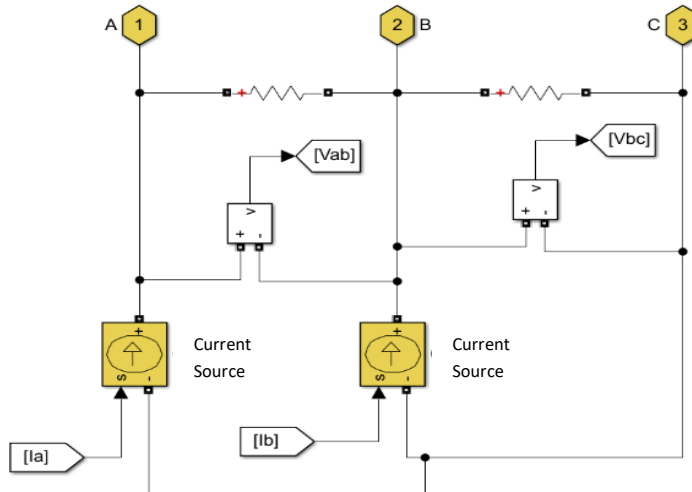


*Figure 3-13: Controlled current sources acting as grid following inverters. Signals  $I_a$  and  $I_b$  comes from model in figure 3-14; similarly signals  $V_{ab}$  and  $V_{bc}$  go to the same model.*

The IBFPR will have symmetrical and balanced characteristics. Due to this reason, the magnitude and angle of the current phasor will be obtained from the positive sequence of the measured voltage, since unsymmetrical line voltages may be present on the system.

Given a symmetrical IBFPR; only two current sources are needed because the addition of balanced currents in a three phase system equals 0. Hence, leg c will be fed with the negative of the sum of both sources.

$$I_a + I_b + I_c = 0$$

$$I_c = -I_a - I_b$$

The ports are connected at the medium voltage side of the system (generator's side). The resistance must have a high value (negligible current flowing through); this is a requirement for the implementation of SIMSCAPE current sources.

**Figure 3-12** shows the block diagram implemented to obtain the positive symmetrical component of line voltage and the positive sequence of current that will be provided by the subsystem to meet to needed power from the ramp input depending on the voltage readings. From the definition of complex power and voltage symmetrical components in three phase systems, the positive sequence component of phase voltage and line current are obtained. The positive sequence component of complex power is equal to the complex balanced power [21]:

*Equation 3-8*

$$S_{3\omega}^I = 3 * V_{LN}^I * \overline{(I_L^I)}$$

This equation is valid for RMS values of voltage and current; nevertheless the measured voltage values and the sought current values are given in peak values, the equation for power and current become:

*Equation 3-9*

$$S_{3\omega}^I = \frac{3 * V_{LNpeak}^I * \overline{(I_{Lpeak}^I)}}{2}$$

*Equation 3-10*

$$I_{Lpeak}^I = \sqrt{\frac{2 * S_{3\omega}^I}{3 * V_{LNpeak}^I}}$$

With the help of the **a** operator ( $-0.5+j\sqrt{3}$  or  $1\angle 120^\circ$ ) the values of the positive sequence component of phase voltage can be obtained.

$$\text{From } V_a + V_b + V_c = 0 \text{ and } V_a^I = (1/3) * (V_a + aV_b + a^2V_c)$$

$$V_a^I = (1/3) * (V_a + aV_b - a^2V_b - a^2)$$

$$V_a^I = (1/3) * \{V_a * (1 - a^2) + aV_b * (1 - a)\}$$

Since  $V_{an}^I = \frac{V_a^I}{\sqrt{3} \angle 30^\circ}$ ,  $\sqrt{3} \angle 30^\circ = (1 - a^2)$  and  $\sqrt{3} \angle -30^\circ = (1 - a)$  then after some algebraic manipulation the expression for  $V_{an}^I$  becomes:

*Equation 3-11*

$$V_{an}^I = (1/3) * (V_a - a^2V_b)$$

With the obtained expressions for the positive sequence of phase voltage and complex power, the needed current to supply the IBFPR related to the measured voltages can be implemented. The ramping function will last until the critical time is reached, afterwards, the IBFPR output will remain constant.

### 3.5 European Island Model

Under normal operation ENTSOE has reported values of RoCoF in the range of 5-10 mHz/s for power outages of 1 GW in the current interconnected power system. If an imbalance event of more than 3 GW occurs with depleted primary reserve, extraordinary values of frequency and RoCoF might be reached. After serious disturbances the Continental European Power System has experienced RoCoF between 100 mHz/s and 1 Hz/s. Imbalances of 20% or more along with RoCoF greater than 1 Hz/s have been determined by experience to be critical [1].

ENTSOE has determined that under the case of the reference scenario (The loss of 3 GW generation with 150 GW load and 2%/Hz self-regulation) in the interconnected operation, the influence of inverter based generation, and therefore the reduction of system inertia would not jeopardize system stability. Due to the expected increase of non-synchronous generation in the future, international power trade and renewables variability; ENTSOE estates in its future split reference scenario that the power system must be capable of withstanding imbalances greater than 40% with RoCoF of 2 Hz/s or higher. Under these circumstances the resulting islands must avoid load shedding. Hence, only the split scenario is considered for further analysis.

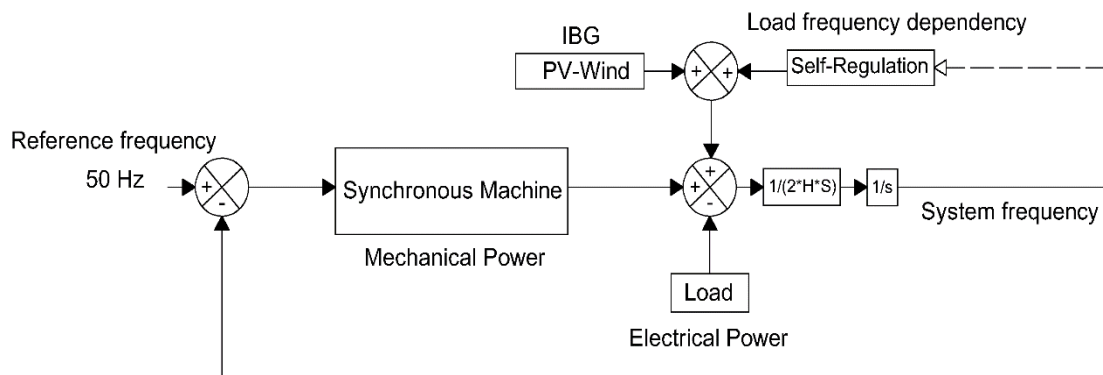


*Figure 3-14: Simplified European power system.*

When considering the system blackout of November 4<sup>th</sup> 2006, in which four electric islands resulted from the European system split; system blackout due to under frequency was experienced in the so known western area. This island, at the moment of split, had approximately a load of 190 GW (27% more than the low load ENTSOE scenario) [29]. For its comparable ‘size’ and the uncertainty of knowing beforehand the resulting islands after a major contingency, the selected load for simulation was the same as the ENTSOE reference scenario as well as the primary reserve deployment time.

To simulate the behavior of the resulting island in the European split scenario; a simplified approach was selected. Similarly as it was done with the simplified block model for the IEEE 9 bus model, in the equivalent European representation all the synchronous generation will be represented by a single machine, which will provide governor response when a

perturbation takes place. Additional to the synchronous response, a load response of 2% was added to the model, which means that for every Hertz reduced or augmented, the load will reduce or increase by a 2% [1].

**Figure 3-15** depicts the results of ENTSOE for the interconnected reference scenario frequency response model. It is intended that the implemented model for the island would perform in a similar way like the ENTSOE model for the same conditions [1].

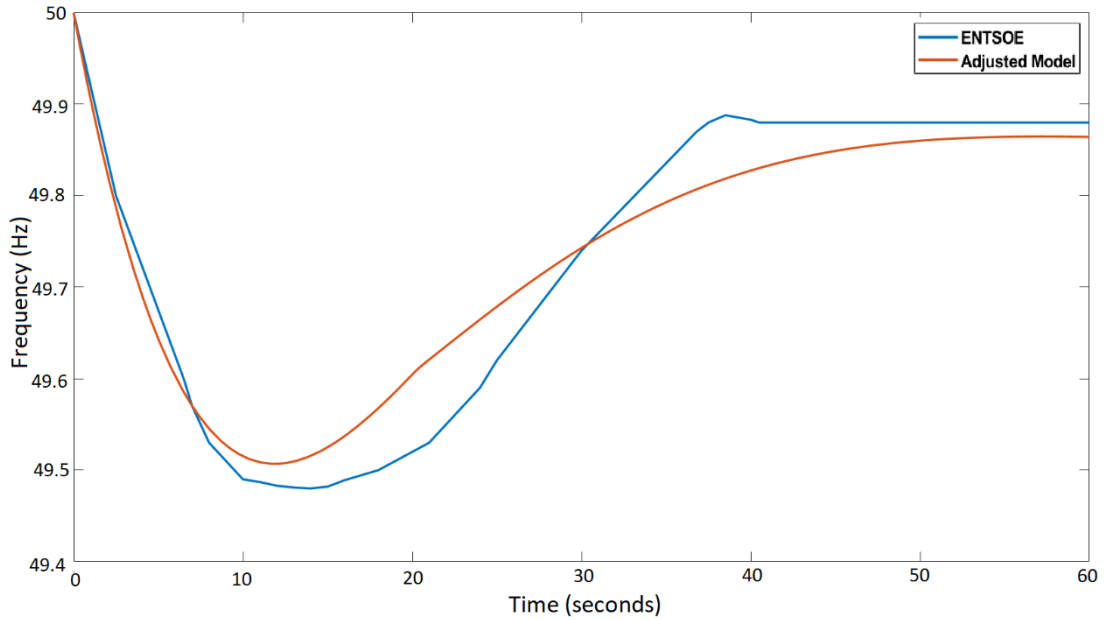


*Figure 3-15: Comparisson between the modeled reference scenario by ENTSOE and the adjusted model. Power loss of 3GW, load of 150 GW (2%), self-regulation of 2%/Hz and acceleration time constant of 10 s.*

To fit the behavior of the system to the modeled by ENTSOE, a PID controller was added in the SIMULINK micro-grid model to the steam turbine governor; this was done with the intention of adjusting the time response of the primary reserve as much as possible to the desired one. With the PID approach, the primary power reserve can be easily tuned with the assistance of the Control System Tuner App available in MATLAB. The period of time of utmost interest for analysis is from the inception of the power imbalance and the nadir time. Therefore, the system must perform as similar as possible in this region compared to the ENTSOE reference, whereas after the nadir time, the disparity between responses can be neglected. In the European scale the reserves must be completely deployed within 30 s after the occurrence of the disturbance.

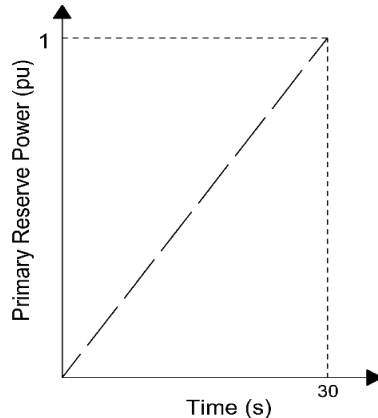


*Figure 3-16: Primary reserve deployment time of the interconnected European system*

### System parameters

A power system of  $n$  number of synchronous machines is assumed; having each of them a capacity  $S$  in MVA, a nominal power  $P_n$  in MW and a nominal power factor.

Assuming that each machine operates at a de-load factor  $dl$  of  $P_{nom}$ ; with an acceleration constant equal to  $T_{nom}$  then the number of machines  $n$ , for the synchronous load  $P_{load\_sync}$  is:

*Equation 3-12*

$$n = \frac{P_{load\_sync}}{P_{nom} * dl}$$

Then the time acceleration constant of the system  $T_{sys}$  can be obtained as follows:

$$T_{sys} = \frac{\sum_i^n P_i * T_i}{P_{LOAD}}$$

$$T_{sys} = \frac{n P_{nom} * T_i}{P_{LOAD}}$$

$$T_{sys} = \frac{P_{load\_sync} * T_{nom}}{P_{LOAD} * dl}$$

*Equation 3-13*

$$T_{sys} = \frac{Sync\ share * T_{nom}}{dl}$$

In this sense the base system time acceleration constant (synchronous share 100%) is calculated from the values of  $T_{nom}=10$  s [1, 8], synchronous share  $Sync\_share=1$ , and a de-load factor  $dl=0.8$  having as a result  $T_{sys}=12.5$  s

## European Island Model

The values of the PID controller and the step response characteristics of the model are set in order to have a step response with 2% overshoot and a time constant of 8 seconds [22]. Step response before and after PID tuning can be observed in **Figure 3-** and **Figure 3-**.

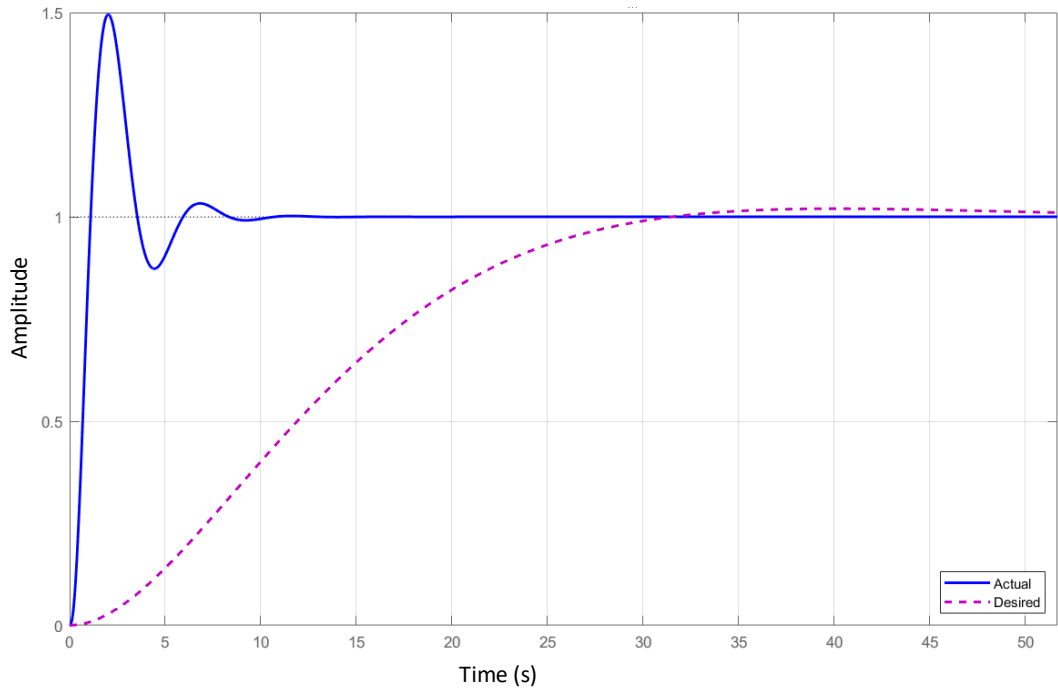


**Figure 3-19:** Comparisson between system step response before the PID tunning (blue) and the desired step response of the system (purple).

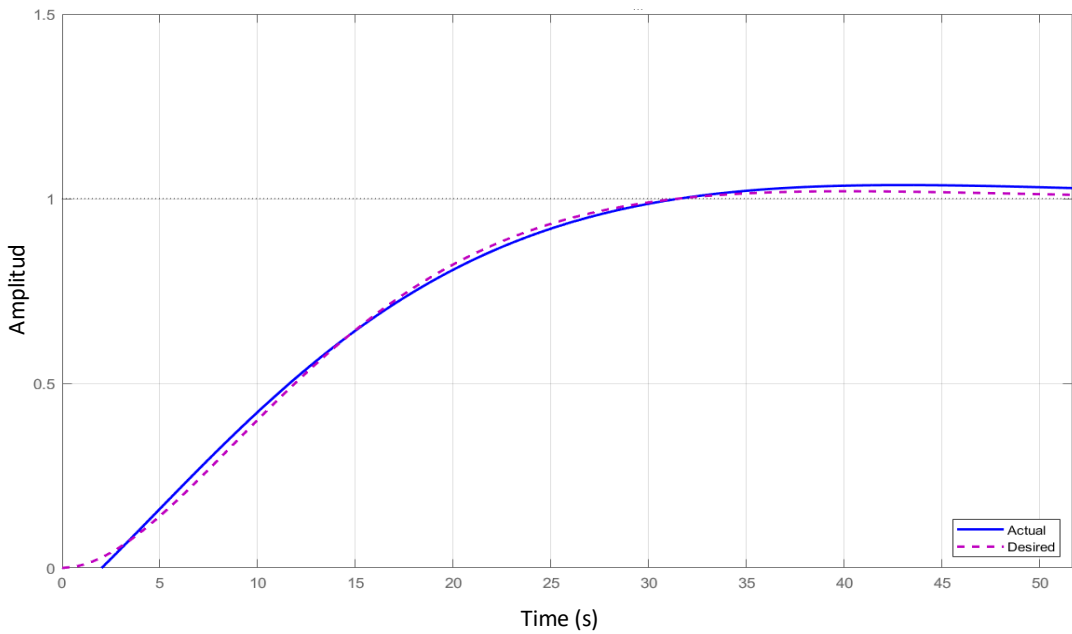


**Figure 3-20:** Comparisson between the actual response (blue) and the desired step response of the system (purple); after PID tuning.

Considering only the swing equation, as done in the model, it can be demonstrated that the RoCoF and therefore the frequency response of the system is only dependent on the percentage of load imbalance and the system acceleration time constant.

From the definition of RoCoF as  $\frac{df}{dt} = \frac{\Delta P * f_0}{2 * E_k}$  and  $T_{sys} = \frac{2 * E_k}{P_{LOAD}}$ :

$$\frac{df}{dt} = \frac{\Delta P * f_0}{P_{LOAD} * T_{sys}}$$

*Equation 3-14*

$$\frac{df}{dt} = \frac{\Delta P_{pu} * f_0}{T_{sys}}$$

In **Equation 3-14**, the value of  $\Delta P_{pu}$  is the normalized value of power imbalance having as base power the value of load  $P_{LOAD}$ . As shown in the equation, when only the swing equation is considered, the frequency response is only dependent on system acceleration constant and the relative value of imbalance. This relative value of imbalance varies during time, depending on load response to change on frequency and the response of primary reserve of the system.

### IBFPR and Synthetic Inertia implementation.

Likewise in the simplified IEEE model, inverter based fast power reserve and synthetic inertia influence are analyzed when they are incorporated into the European grid representation. The needed IBFPR is obtained after the calculation of the critical and nadir time for each of the inertia scenarios is performed. When synthetic inertia is analyzed, the same model considered in the simplified model applies for the European scale model as well.

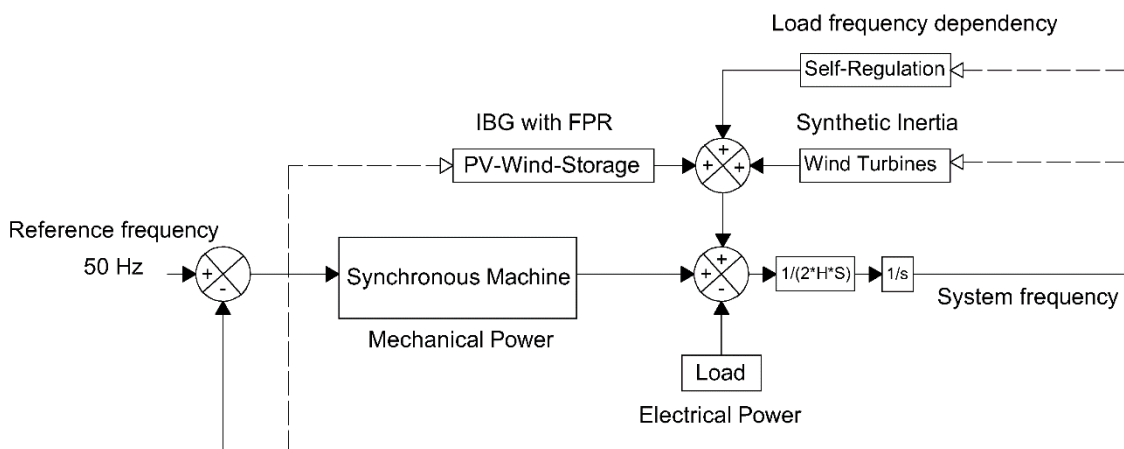


*Figure 3-17: European model with IBFPR and Synthetic Inertia.*

## 4 Simulation of the Study Cases

---

In this section the main results of the cases described in the former section are presented. The results are presented by subsections according to the specific cases:

### 4.1 Simplified IEEE 9 bus Model

#### Determination of critical time

The simplified block representation of the IEEE 9 bus model presented in chapter 3 was used to determine the critical times; for which the inverter based generation must supply the ramping power in order to avoid frequency instability. **Figure 4-1** depicts the range of critical time depending on the combination of system inertia (Acceleration time constant) and power imbalance. It is well to note that the absolute values of RoCoF and power imbalance where considered.

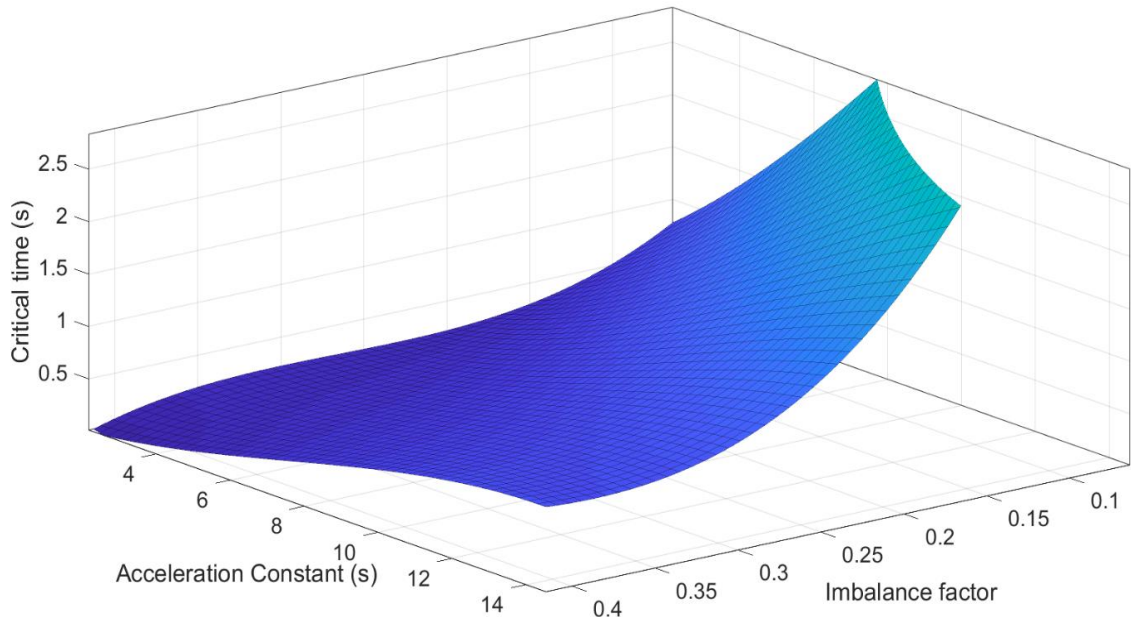


*Figure 4-1: Critical time as function of acceleration time constant and load imbalance.*

For a better observation of the results; the critical times for specific system acceleration time constants are presented in **Figure 4-2**.

## Simplified IEEE 9 bus Model

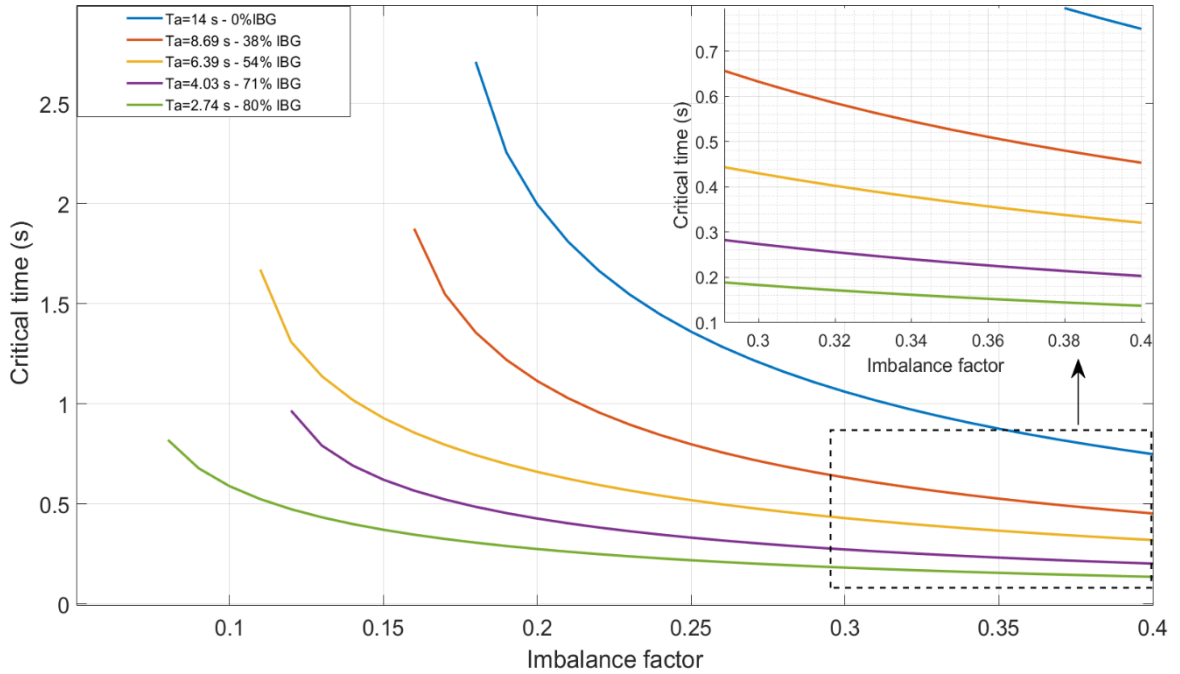


**Figure 4-2: Critical time for specific system acceleration time constants**

It can be noticed that in a very adverse case scenario; which corresponds to a penetration of inverter based generation of 80% (system acceleration constant of 2.74 s), the UFLS starts with an imbalance of 8% of the load. In this specific case, the critical time to deploy the inverter based fast reserve is 0.82 seconds whereas for an imbalance of 40% the available time is 0.14 seconds. With the results obtained from the simulations of the simplified block model, a regression was performed to relate the critical time and RoCoF. The form of the obtained curve is a rational function.

**Figure 4-3** shows the fit for critical time as function of RoCoF. It is noticed how the fit improves as RoCoF increases for all the simulated inertia scenarios.

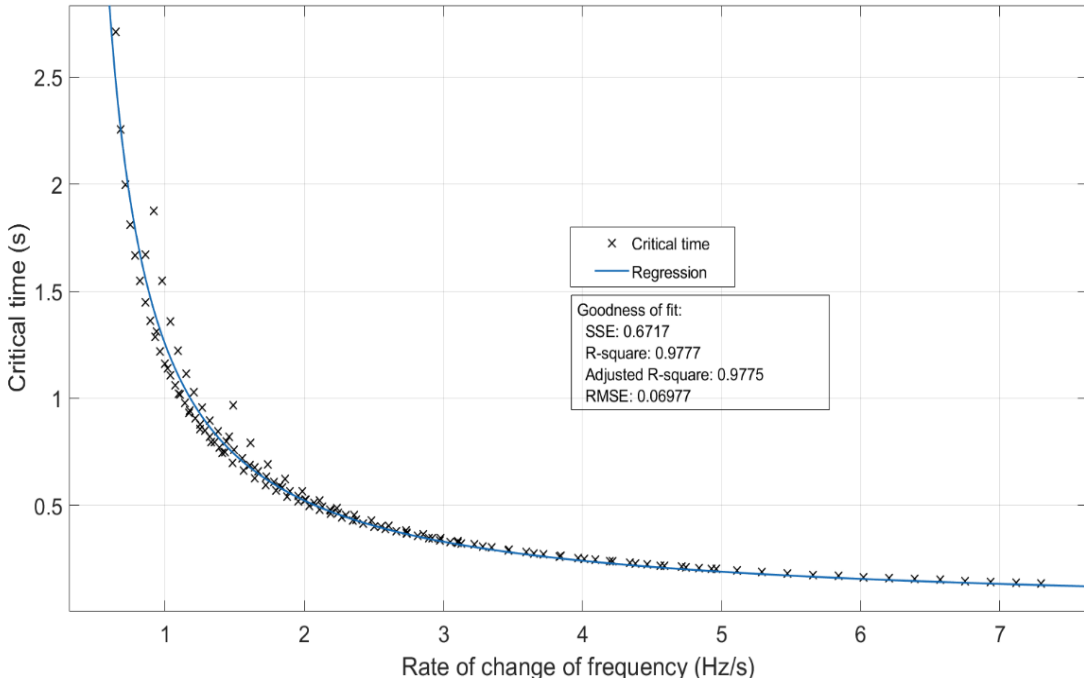


**Figure 4-3: Critical time fit as function of RoCoF**

## Simplified IEEE 9 bus Model

Thus the critical time in seconds as function of RoCoF is described in this model by the following equation:

$$t_{cr}(t) = \frac{0.8991}{RoCoF - 0.2824} \text{ (seconds)}$$

The frequency nadir when no support is given for inverter based generators is presented in **Figure 4-4**.

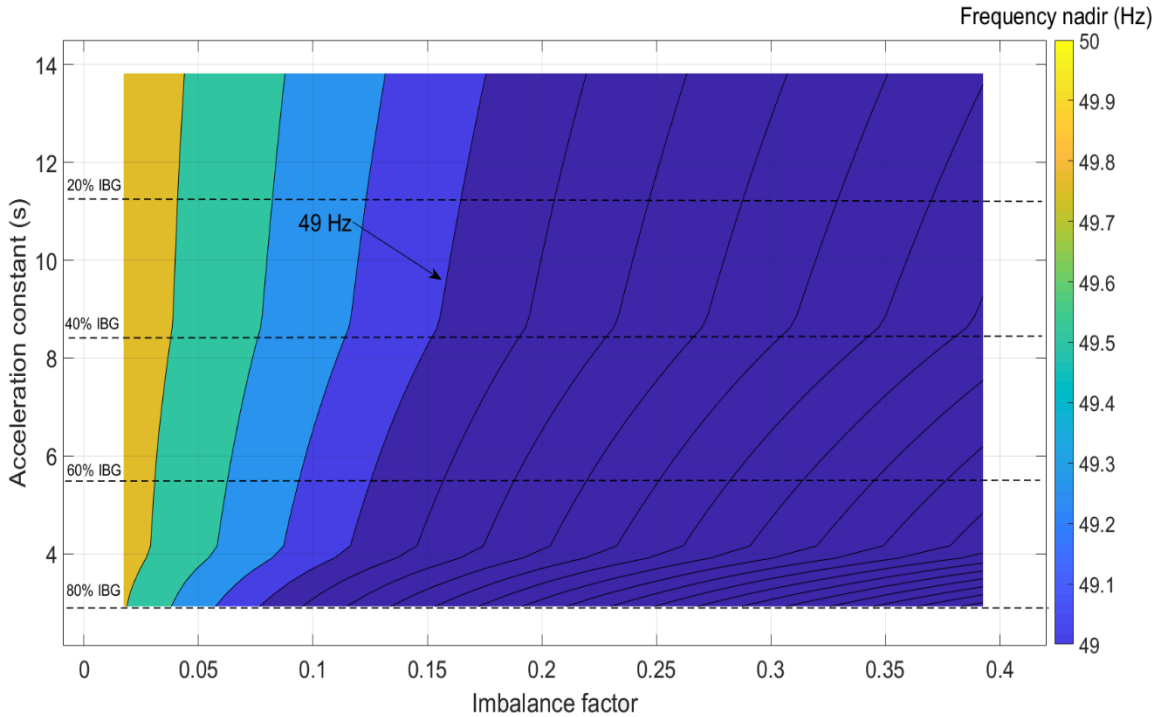


*Figure 4-4: Frequency nadir without auxiliary frequency support from IBG.*

By inspection of **Figure 4-4** it can be noticed that for acceleration constants lower than 6 seconds, frequency nadir lower than 49 Hz would be reached with power imbalances starting at ~10%. It is observed how the frequency nadir drops down to 45 Hz for a combination of high IBG and high load imbalance.

### Applying IBFPR to the model

With the implementation of **Equation 3-2**; the values of power response from the inception of the disturbance until the critical time are presented in **Figure 4-5** as function of the imbalance and system acceleration constant.

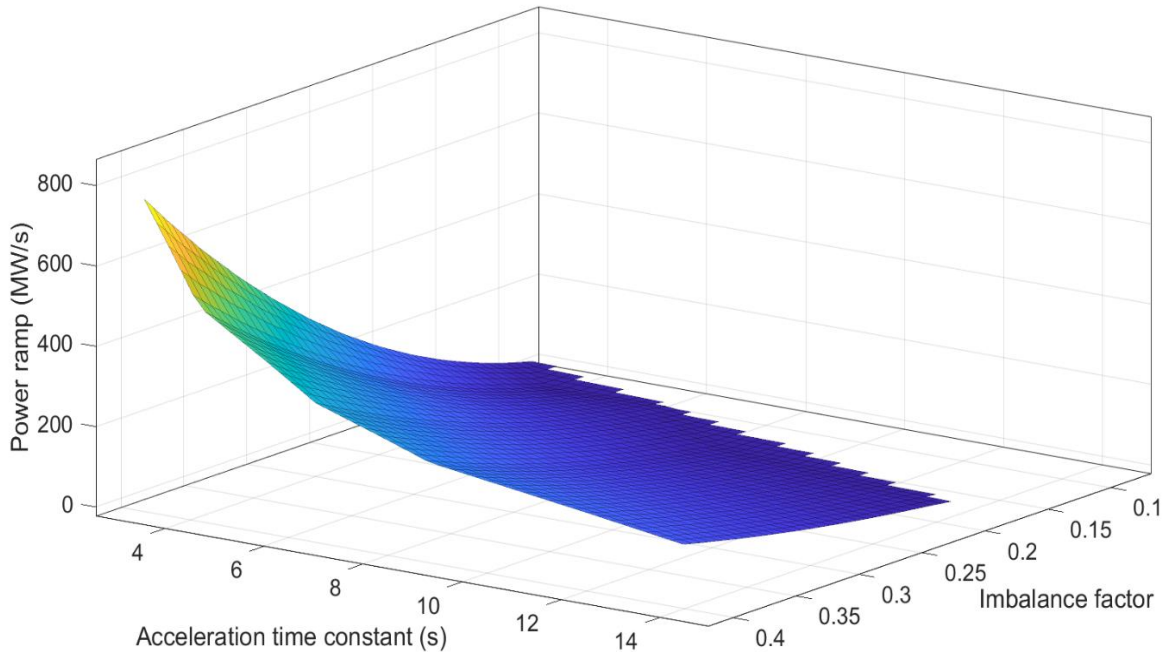


*Figure 4-5: Inverter based fast power response ramp*

Similarly as it was presented with the critical time, the power ramp is presented in **Figure 4-6** for specific system acceleration constants.

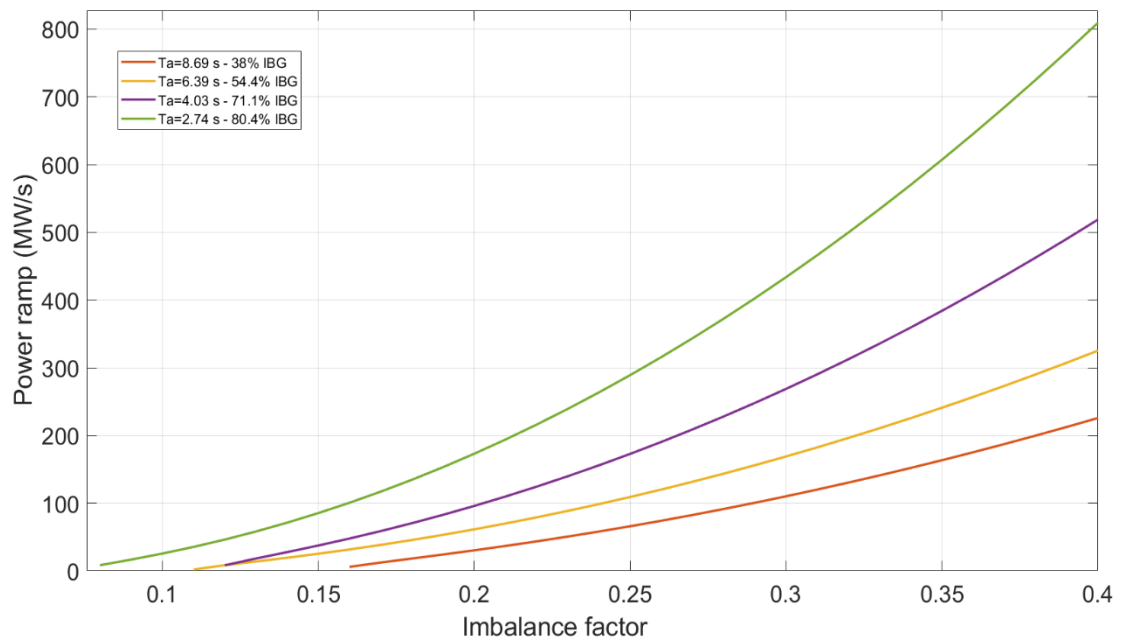


*Figure 4-6: IBFPR ramp for specific shares of non-synchronous generation*

## Simplified IEEE 9 bus Model

It can be noticed that for an 80% penetration of non-synchronous generation, a power ramp of 8.5 and 809.35 MW/s are needed to avoid UFLS for imbalances of 8 and 40% respectively.

Applying the resulting ramping power responses to the system an overall improvement is observable. As shown in **Figure 4-7**; the frequency nadir of the system aided by the inverter based fast power reserve barely reach 49.1 Hz.

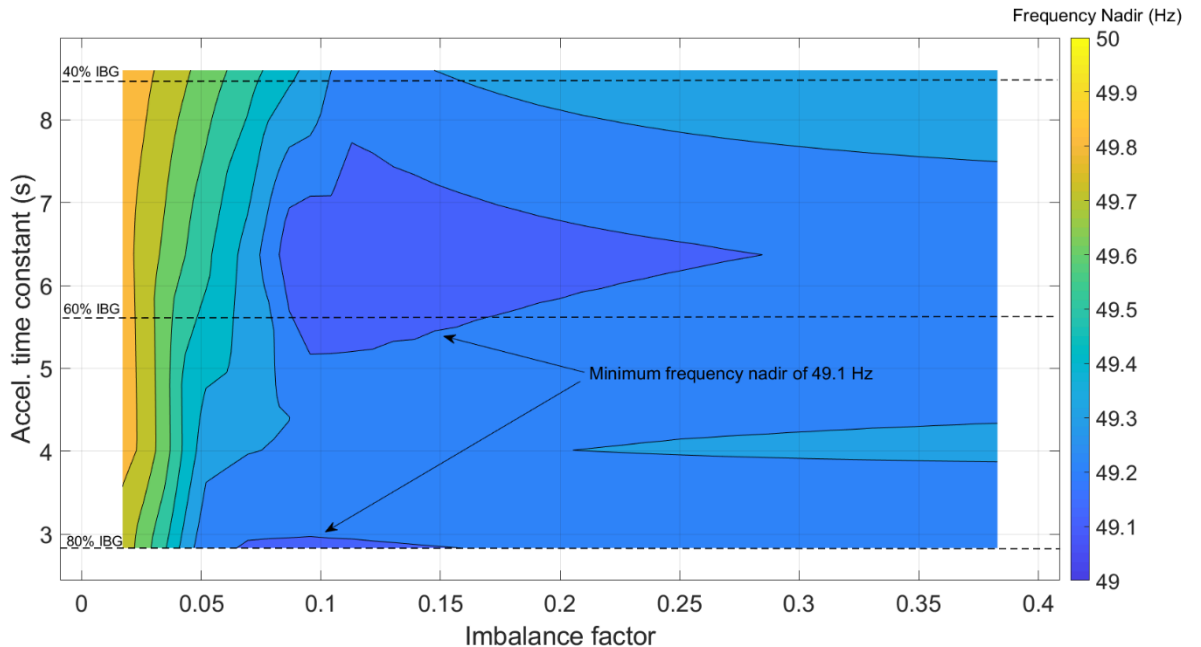


**Figure 4-7: Frequency nadir with IBFPR implemented. Dotted lines indicate share of inverter based generation**

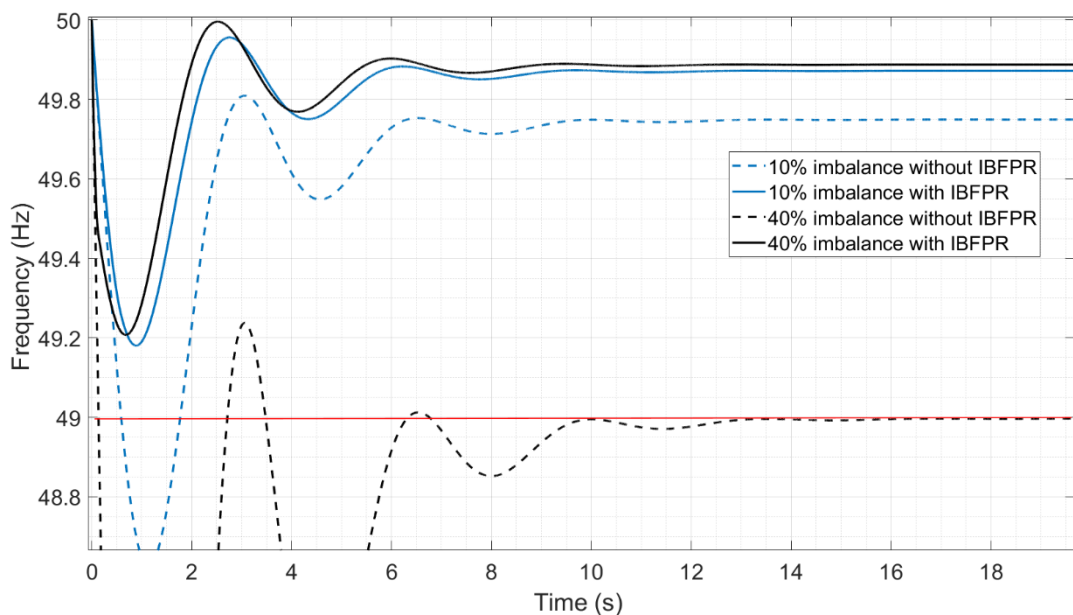


**Figure 4-8: Frequency response assuming no UFLS implementation. Comparison of responses with and without IBFPR**

### Applying only Synthetic Inertia to the System

When the power response of the system is performed solely by the synchronous machines and the decoupled wind turbines are controlled in such a way; that some of the kinetic energy stored in the rotating masses can be extracted when a frequency event takes place, the following frequency nadir characteristic is achieved.

Since inverter based generation is considered to be comprised by wind and PV technologies; the share between wind and PV was considered, in figures **Figure 4-7** and **Figure 4-8** the cases where wind comprises 40 and 80% of the non-synchronous generation were explored, assuming that the total amount of units count with synthetic inertia controls.

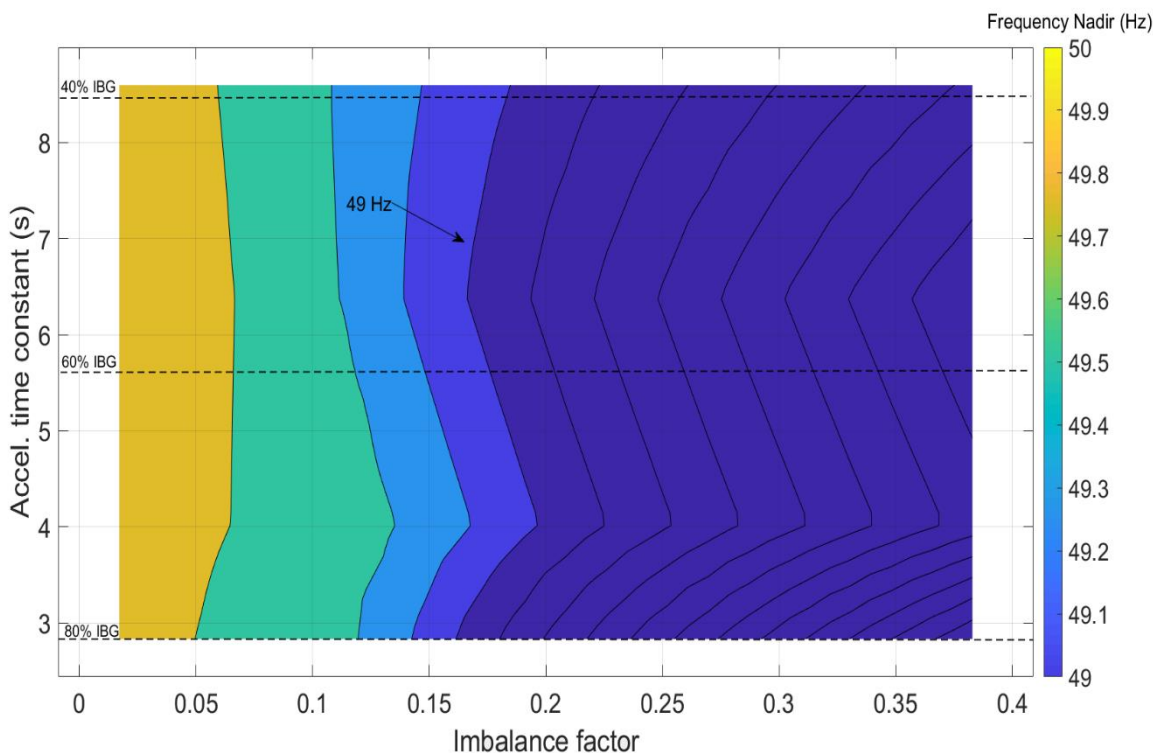


**Figure 4-7:** Frequency nadir only with implementation of synthetic inertia; having a 40% of contribution of wind power the total IBG.

For wind power contributions of 40 and 80% of the total inverter based generation, frequency nadir can reach 46 and 46.5 Hz respectively; when the worst imbalance is considered. In any case, UFLS is not avoided for all combination of variables (imbalance and acceleration constant). It can also be observed that frequency nadir under 49 Hz are reached for imbalances bigger than 15% combined with system acceleration constant lower than 8 seconds.

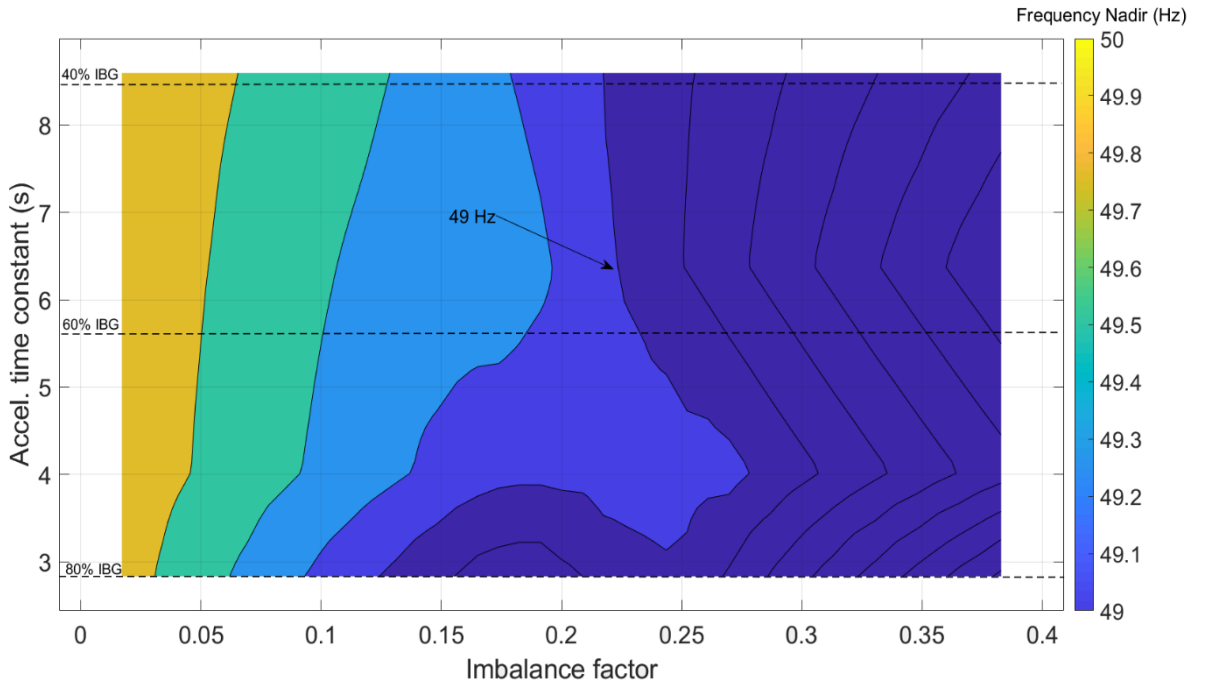


**Figure 4-8:** Frequency nadir only with the implementation of synthetic inertia; having an 80% of contribution of wind power the total IBG.

**Figure 4-9** and **Figure 4-10** show the frequency response of the system with an acceleration time constant of 2.73 seconds (80% non-synchronous generation) for different load imbalances.

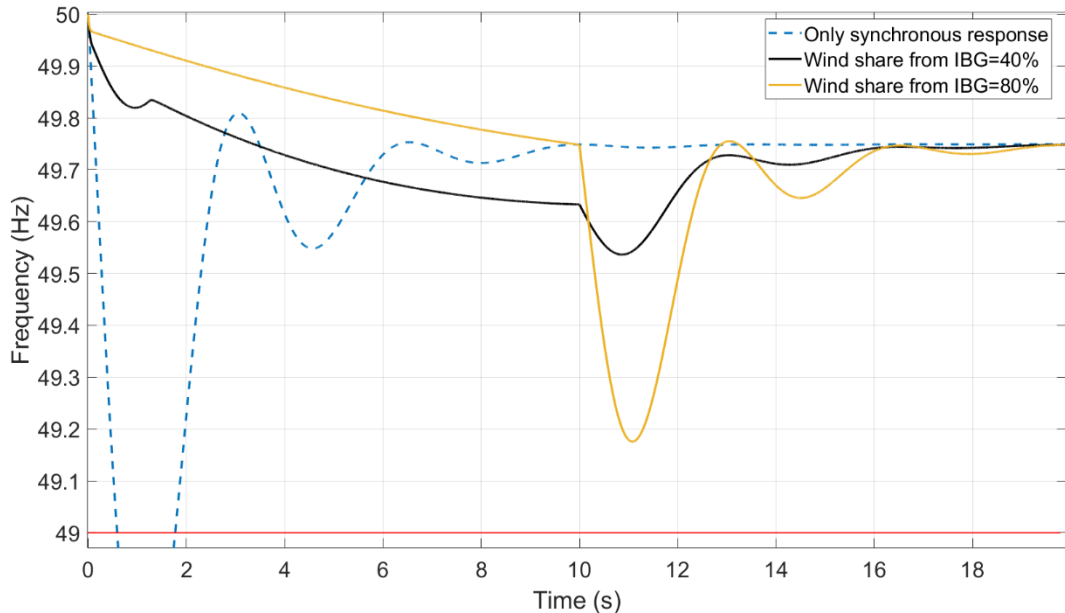


**Figure 4-9:** Frequency response for a penetration of 80% IBG and an imbalance of 10% when synthetic inertia is applied to the system

In **Figure 4-9** it can be observed how the frequency drops below 49 Hz with a 10% of imbalance, when no IBFPR or synthetic inertia is used as frequency support strategy. In the same figure, the frequency responses for different levels of synthetic inertia are presented.

It is noticed the improvement in the response with the implementation of synthetic inertia with each contribution of wind energy to the non-synchronous generation. UFLS is avoided for every share of synthetic inertia, assuming that primary reserve takes place after SI.

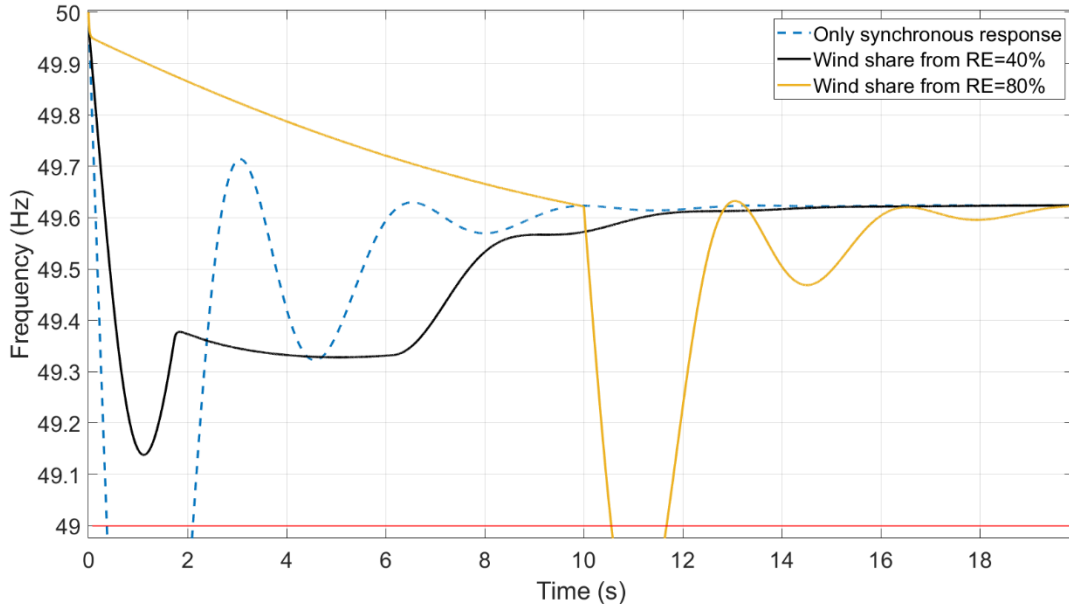


**Figure 4-10:** Frequency response for a penetration of 80% IBG and an imbalance of 15% when synthetic inertia is applied to the system.

As the imbalance increases, the effectiveness of the synthetic inertia decreases, depending on the contribution of wind power to the inverter based generation. **Figure 4-10** shows how a contribution of wind power of 40% from the inverter based generation is capable of avoiding UFLS. Nevertheless the share of 80% begins with a low rate of frequency decrement, the frequency suddenly drops below 49 Hz. This is due to the high amount of synthetic inertial power when compared to the load imbalance. This situation leads to UFLS after the 10 s

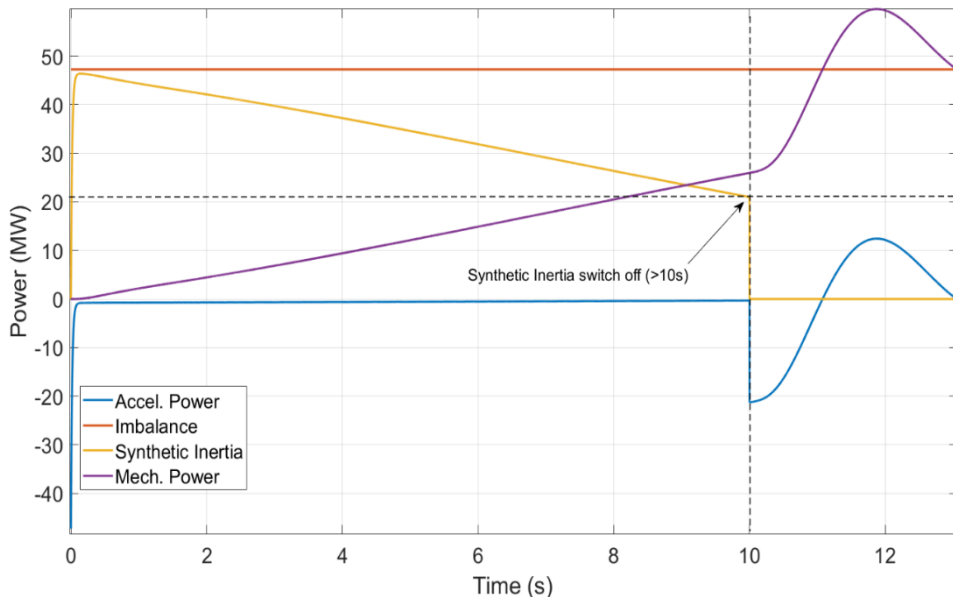


**Figure 4-11:** Power response for 80% IBG and imbalance of 15% when synthetic inertia is provided by the 80% of the total IBG

because frequency has been sustained during that time by the synthetic inertial power. Since 10 seconds is the assumed time limit for exceeding nominal turbine power rate; the synthetic inertial power, which has a big contribution to counteract the power imbalance, is switched off as depicted in **Figure 4-11**. On the other hand, when a higher imbalance occurs and the synthetic inertial response is saturated, due to the limitation of 10% of rated power, the mechanical power increases at 10 seconds, having a less severe impact the switching off of the inertial response.

### Influence of frequency measurement time delay

It was pointed out in chapter 2 the relevance of frequency time measurement in the frequency support response from inverter based generation. The expression obtained for power ramp in chapter 3 did not considered any delay, therefore, the application of the same power ramps to the same combination of acceleration time constant and imbalance was simulated but with an intentional delay added in order to emulate the required time for frequency measurement. **Figure 4-12** and **Figure 4-13** present the results for the frequency nadir when a delay of 100 ms and 200 ms is introduced to the system.

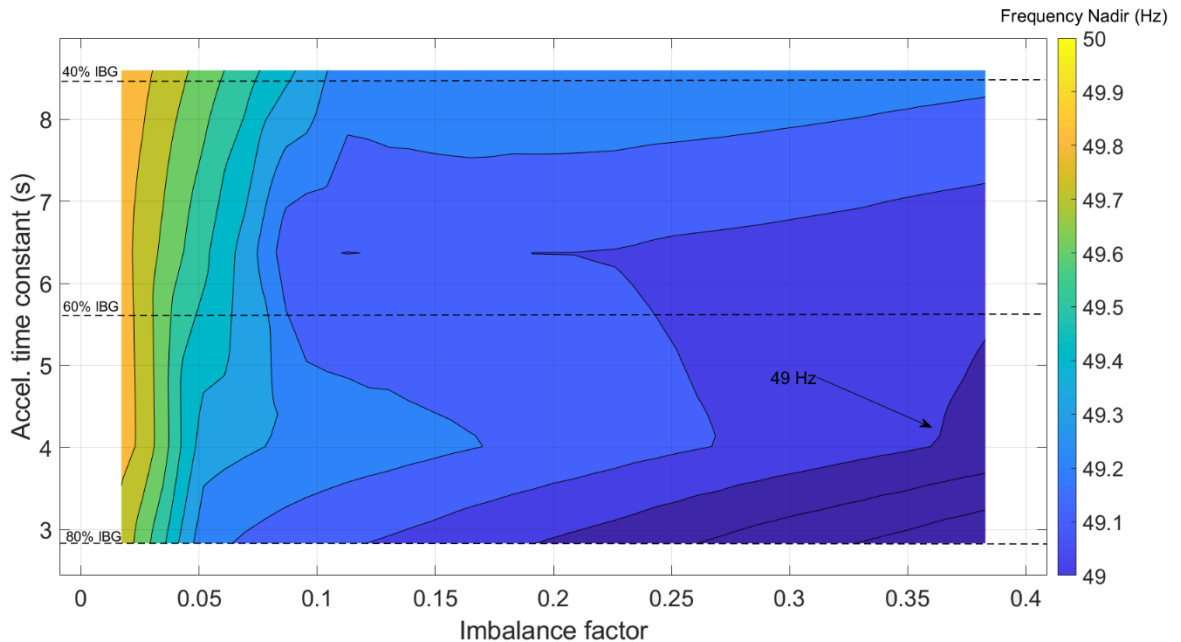


**Figure 4-12:** Frequency nadir with IBFPR delayed 100 ms.

In the previous figures only IBFPR and synchronous reserve were considered. Although UFLS is avoided in a wide range of combinations, stability is not assure when time delay is not taken into account when the ramping response is calculated.

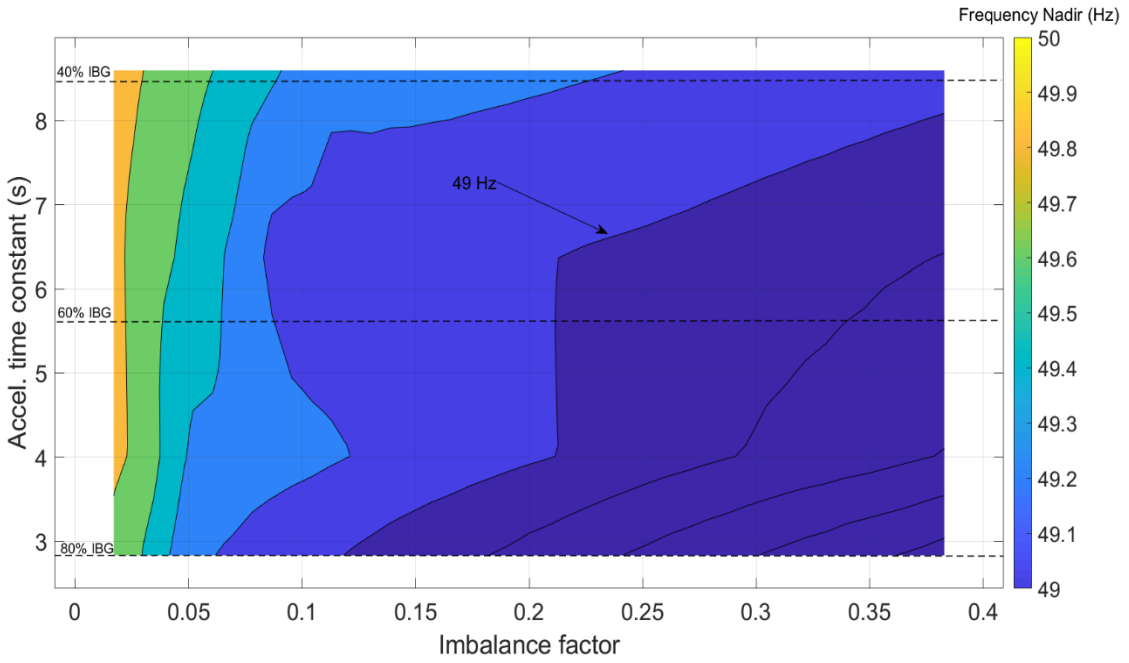


*Figure 4-13: Frequency nadir with IBFPR delayed 200 ms.*

**Figure 4-14** shows in more detail the critical imbalances of the cases with the delay incorporated.

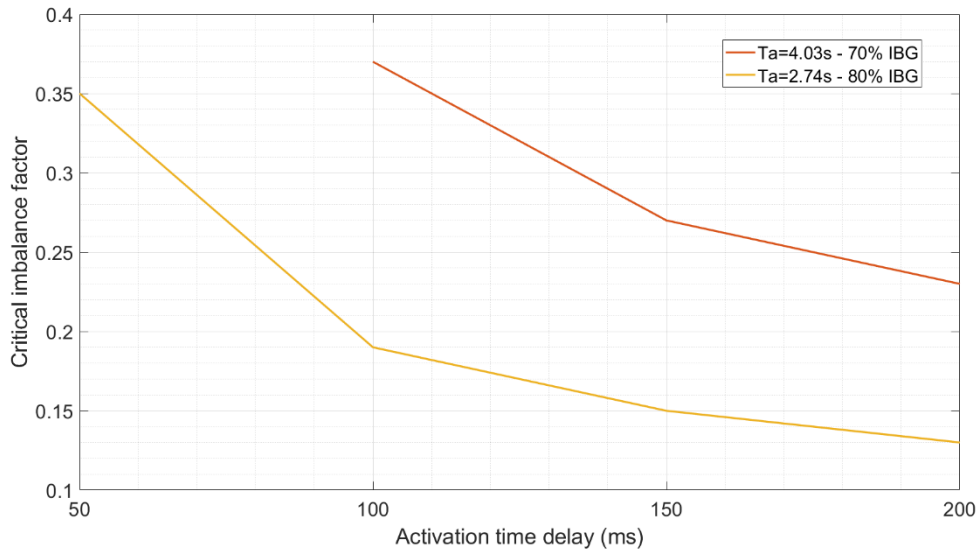


*Figure 4-14: Critical imbalances as function of delay in IBFPR activation.*

When a delay of 100 ms is considered, the UFLS would occur with 20% load imbalance when an acceleration time constant of 2.74 s governs the system. Nevertheless, underfrequency load shedding is avoided for inertia cases higher than 5.6 s (60% IBG).

## Simplified IEEE 9 bus Model

If a delay of 200 ms is introduced to the system, UFLS would start with load imbalances bigger than 12% and acceleration constants 2.74 s (80% inverter based generation). Only scenarios with inertia higher than 8.69 s (40% IBG) would not reach UFLS.

### Over-frequency case

Whenever generation surplus is the source of the power imbalance, an over-frequency event will take place. **Figure 4-15** demonstrates how the same values for critical time, nadir time and therefore power reserve applies also to the overfrequency cases as long as the same deviation from nominal is considered as the threshold as for the under-frequency case (1 Hz).

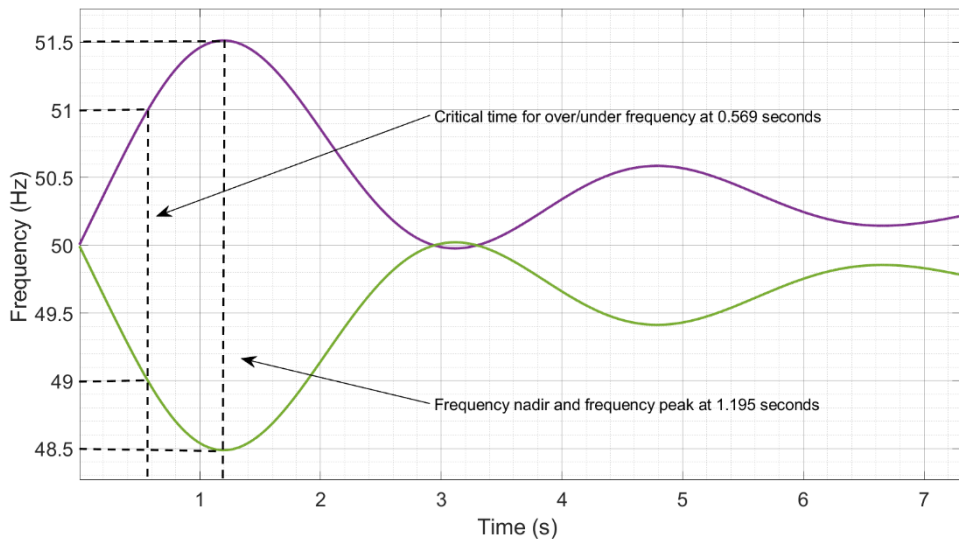


*Figure 4-15: Symmetry in critical time for over and under-frequency events.*

## 4.2 Extended IEEE 9 bus model

### Determination of Critical time and IBFPR Implementation

In the Extended model all the dynamics of the machines were considered as well as the characteristics of transmission lines and transformers. **Figure 4-16** illustrates the critical times when this model is simulated.

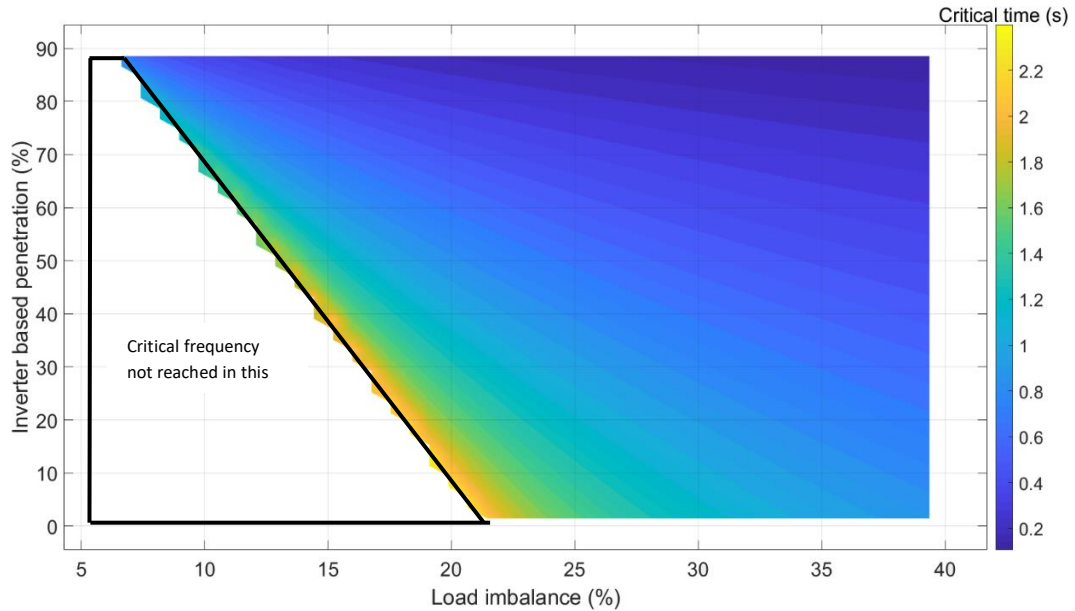


*Figure 4-16: Critical time for extended IEEE model.*

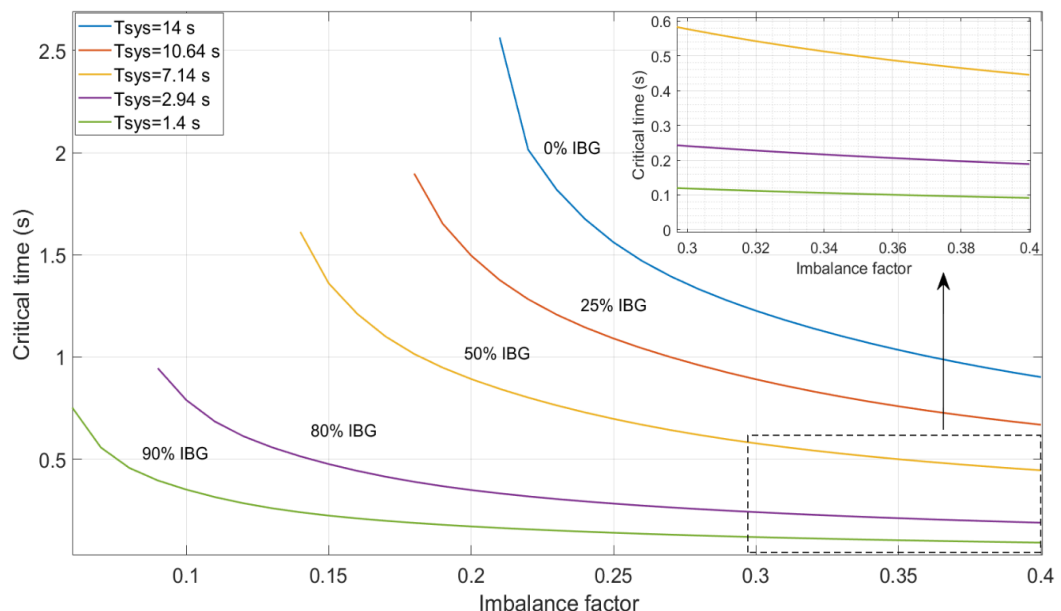


*Figure 4-17: Critical time for specific penetrations levels of IBG for extended IEEE model.*

Load shedding starts at 9% of imbalance in the 80% IBG scenario with a critical time of 0.94 seconds. When the maximum imbalance is applied, the critical time goes down to 0.189 seconds.

When the values of maximum RoCoF are related to the critical time, a regression can be performed. **Figure 4-18** depicts the relation between RoCoF and the critical time. The fit deviates from the points the most in the range between 1 and 2 Hz/s.

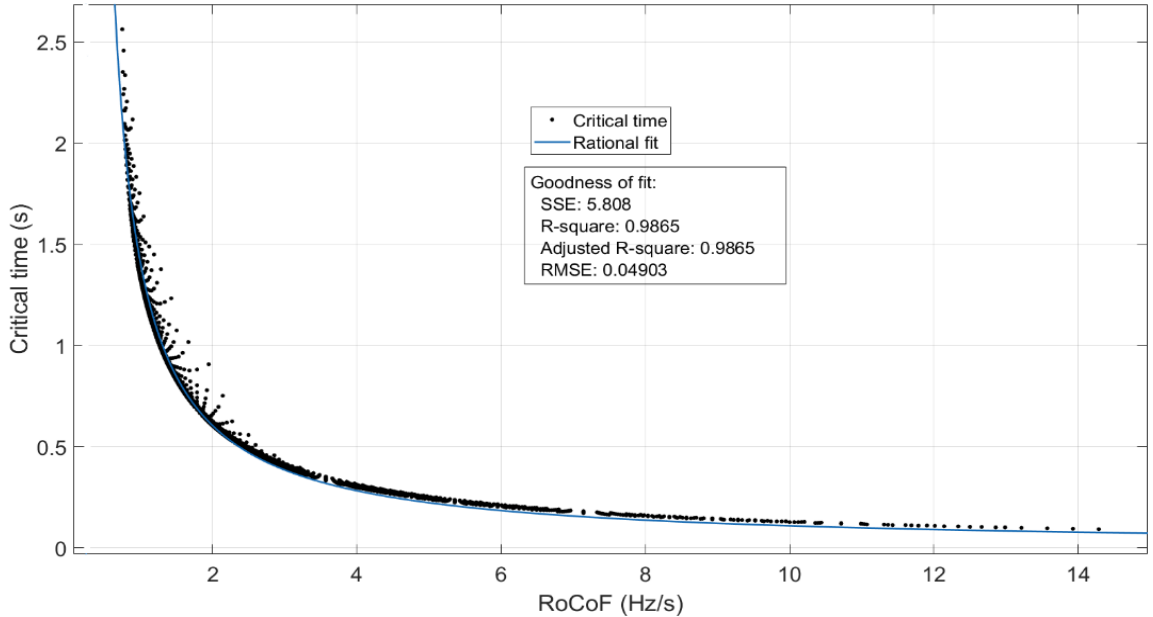


**Figure 4-18: Critical time as function of RoCoF.**

From the regression the following expression is obtained to relate RoCoF and critical time:

$$t_{cr} = \frac{1.056}{RoCoF - 0.2528} \text{ (seconds)}$$

The values for the frequency nadir of the system with no support from inverter based generation is shown in **Figure 4-20**. The shown values correspond to the lowest value of frequency reached during 30 seconds of simulation. Extreme low values are observed due to system instability of the system with big imbalances and low inertias. In the same manner as the IBFPR was implemented in the simplified approach of the IEEE 9 bus model, the IBFPR is again added to the system to evaluate frequency response. **Figure 4-19** shows the values of frequency nadir with IBFPR in operation. In all range of imbalances and inertia cases, frequency is kept within the 1 Hz deviation threshold

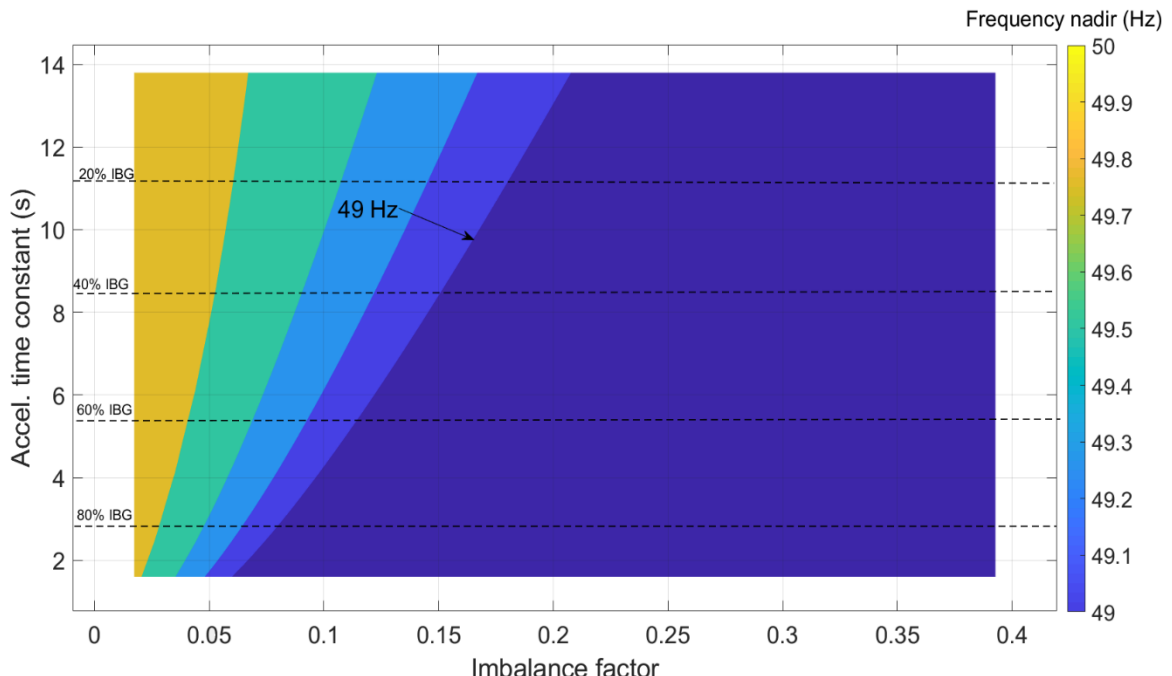


Figure 4-20: Frequency nadir with no additional frequency support

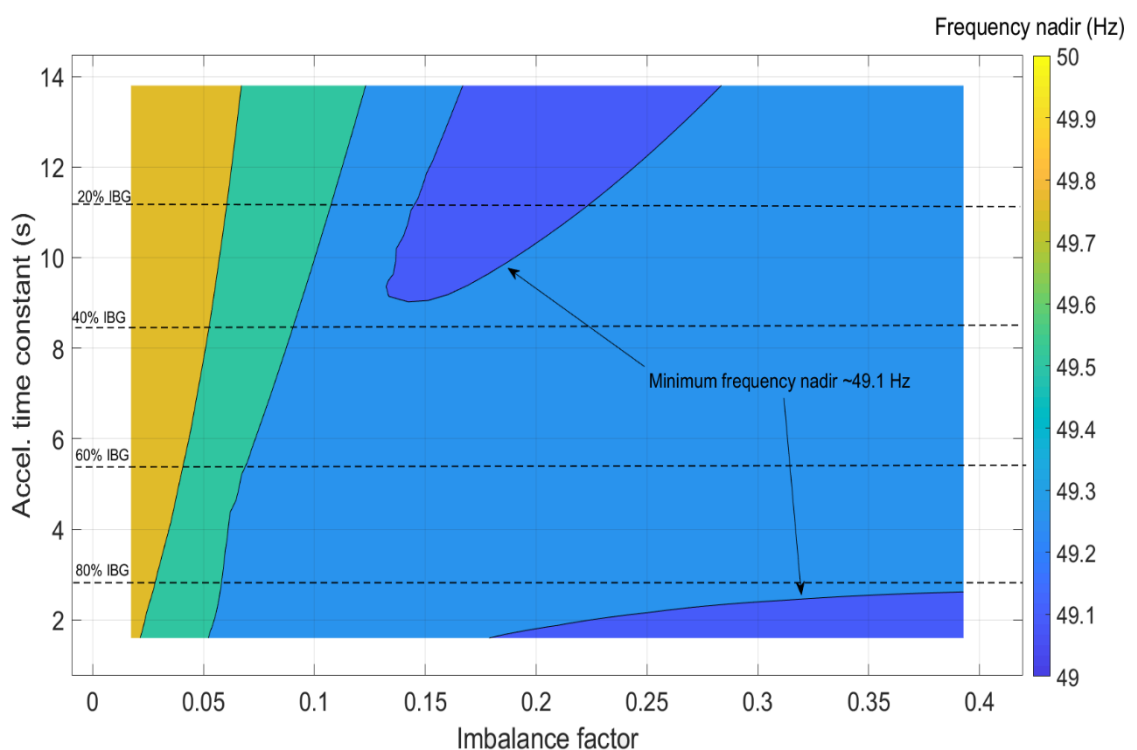
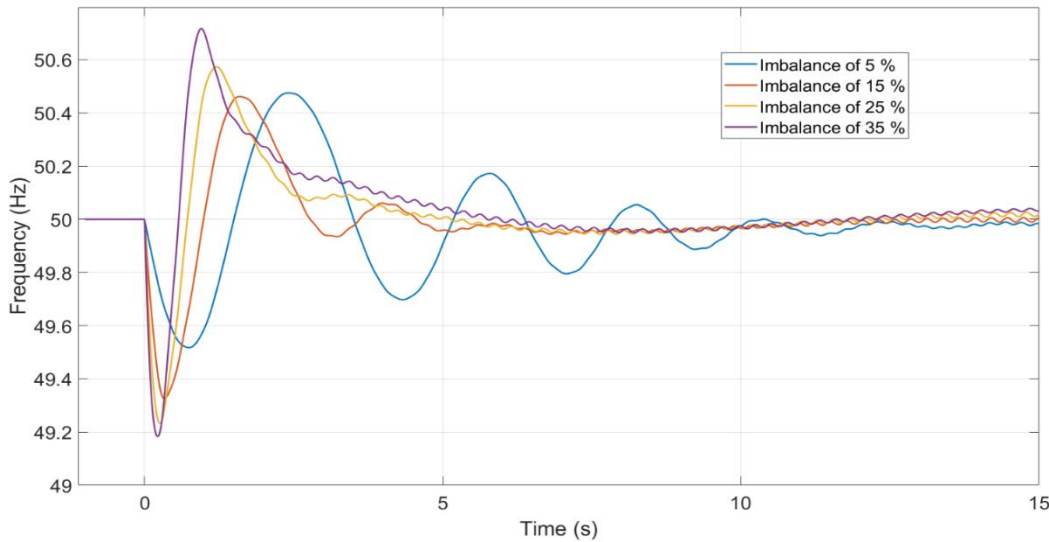


Figure 4-19: Frequency nadir with the implementation of IBFPR.

In the simulations it can be noticed how the frequency does not stabilize (assuming the frequency it is allowed to have the shown amplitud excursions) when no extra power, besides the one from synchronous machines, is injected into the system.

**Figure 4-21** shows in more detail the frequency response of the system with an acceleration constant of 2 seconds (85% of inverter based generation) when subjected to load imbalances of 5, 15, 25 and 35% and IBFPR is implemented.



*Figure 4-21: Frequency response with an accel. time constant of 2 s (85% IBG) for different levels of imbalance. IBFPR is implemented.*

### Over-frequency case

Whenever generation surplus is the source of the power imbalance, an over-frequency event will take place. With the simplified model it was demonstrated how the same values for critical time, nadir time and therefore power reserve applies also to the overfrequency cases as long as the same deviation from nominal is considered as the threshold as for the underfrequency case (1 Hz). Nevertheless in the extended model, the critical time is not exactly the same for both cases and an offset of 40 ms can be seen in **Figure 4-22**.

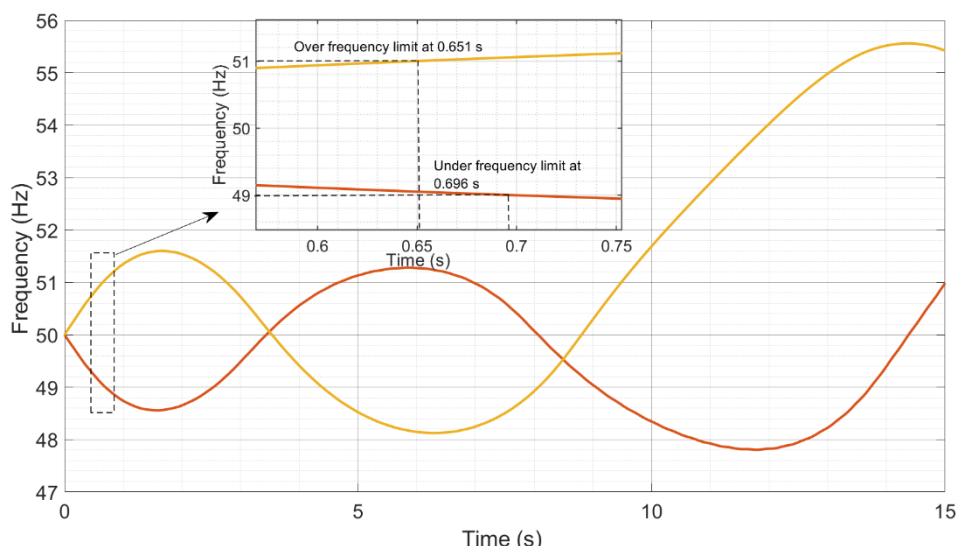


*Figure 4-22: Comparison of critical times for over and under-frequency cases.*

### 4.3 European Island Case

#### Determination of critical time

In the European island case, the system response characteristic for the interconnected scenario of ENTSOE was assumed to be the same response of each of the resulting islands after an incident leading to splitting occurs. **Figure 4-23** and **Figure 4-24** depict the critical times for IBFPR response.

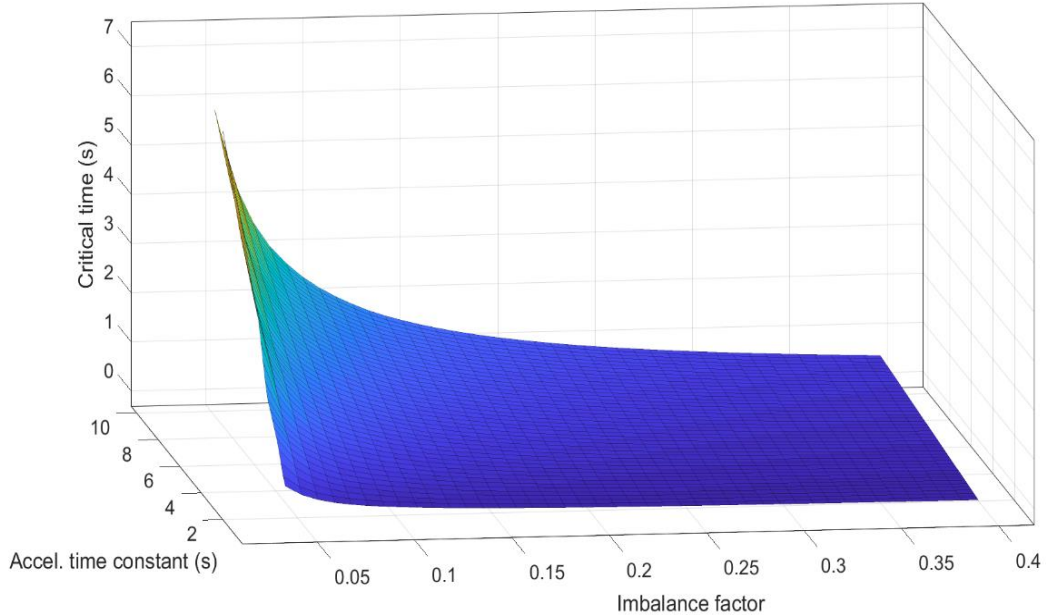


*Figure 4-23: Critical time in an electric island in the European power system.*

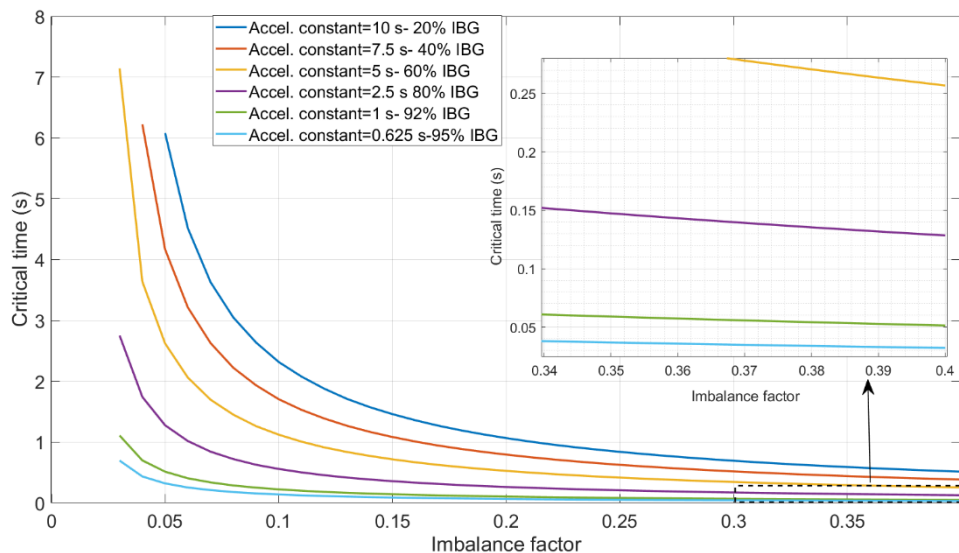


*Figure 4-24: Critical time for specific penetrations of IBG.*

## European Island Case

When 80% of inverter based generation is considered, it is noticed that allowed frequency threshold is overpassed with 3% of imbalance, this due to the slower governor reaction modeled as primary reserve. In such case, the time available to provide the fast power reserve would be 2.75 seconds. For load imbalance of 40% the system would need to react in 0.128 seconds. When shares of non-synchronous generation was considered higher than 90% reaction times in the order 50 ms would be required with imbalances of 40% as shown in **Figure 4-24**.

The relation between critical time and RoCoF is shown in **Figure 4-25**, again the best fit is for high values of RoCoF, higher residual observed below 4 Hz/s. The following fit equation describes critical time as function of RoCoF:

$$t_{cr} = \frac{1.056}{|RoCoF| - 0.2528} \text{ (seconds)}$$

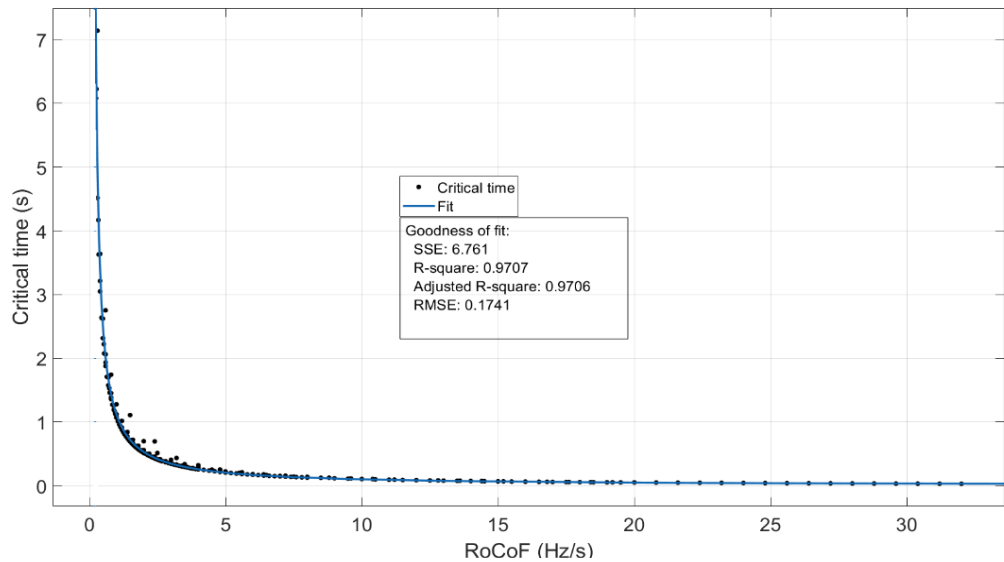


*Figure 4-25: Critical time fit as function of RoCoF*

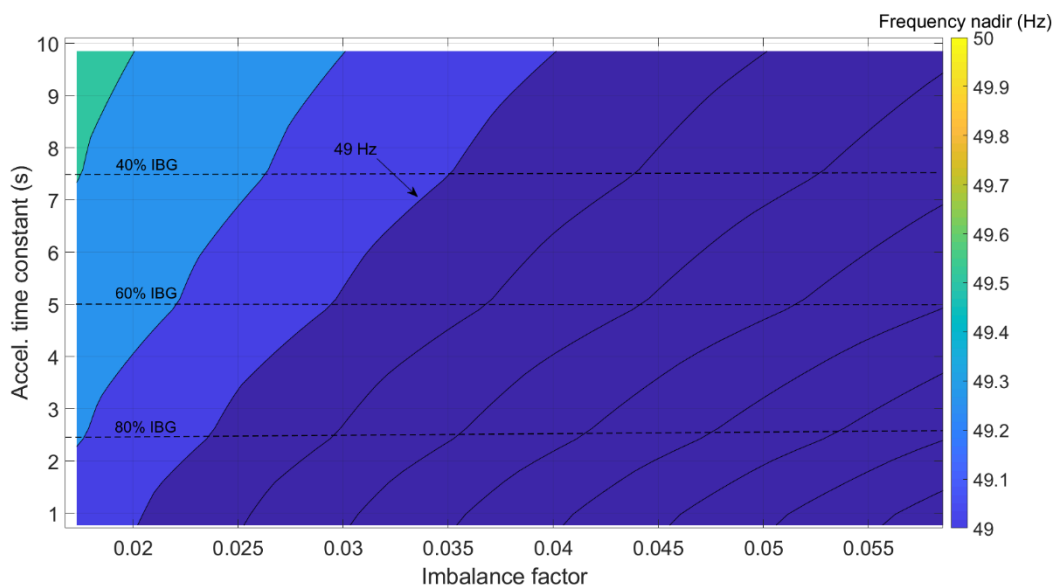


*Figure 4-26: Frequency nadir without IBFPR.*

## European Island Case

Allowing the simulation to run, even though when the values of frequency reach 49 Hz or less; the lowest value of frequency according to the inertia scenario and load imbalance is illustrated in **Figure 4-26**. At 80% (~2.5 s) of IBG frequency nadir reaches 48.73 Hz with 3% of imbalance. Values down to 30 Hz are calculated for the worst cases.

## Applying IBFPR to the system

When **Equation 3-2** is evaluated with the values of critical and nadir time for the island scenario; the values of power ramp response from the inception of the disturbance until the critical time are presented in **Figure 4-27** as function of the imbalance and system acceleration constant. In the extreme case, incredible values of ramp in the range of 1500 GW/s would be needed, due to the short available time for activation and the high imbalance factor. For an 80% IBG power ramps of 0.88 to 24.32 GW/s would be required for imbalances between 3 and 10%. For the extreme case of 40% imbalance, 457.38 GW/s are needed.

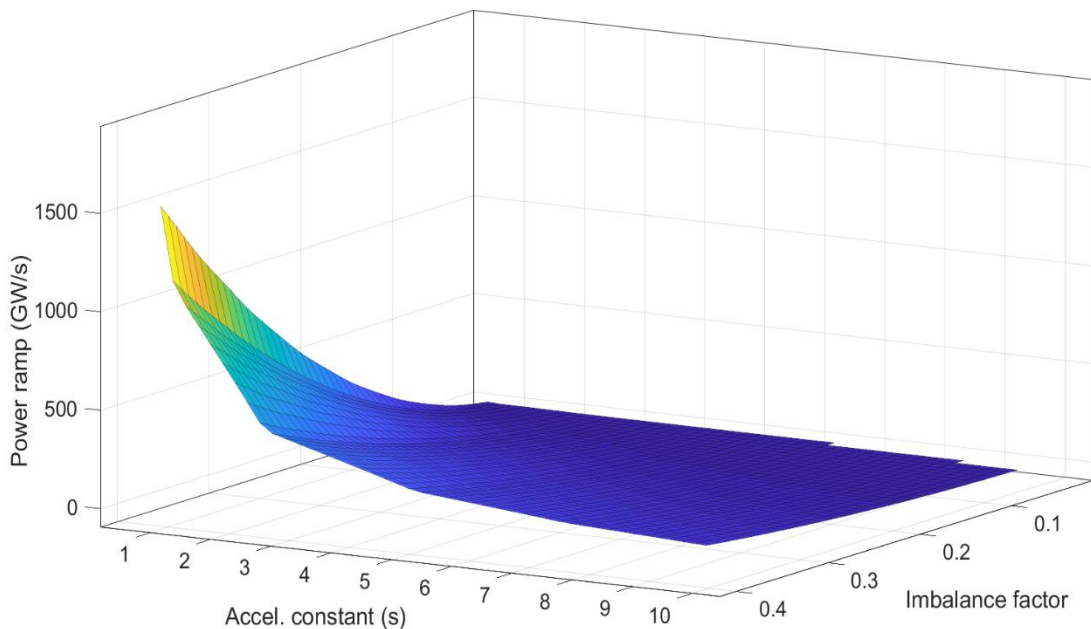
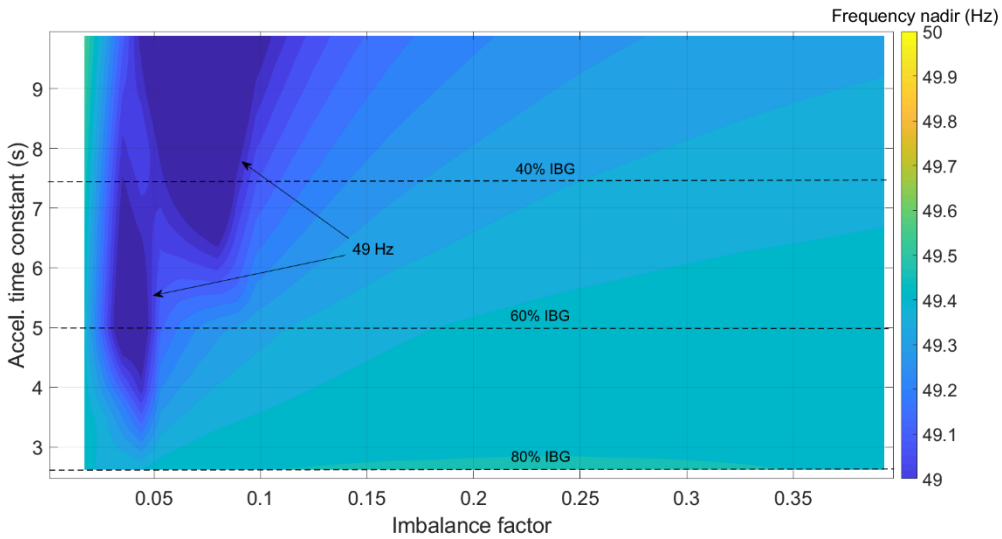


Figure 4-27: IBFPR ramp response in GW/s

After applying the IBFPR the improved frequency response depicted in **Figure 4-28** is obtained.

## European Island Case

**Figure 4-28** shows that UFLS is not avoided for all cases as in previous scenarios.



*Figure 4-28: Frequency nadir with IBFPR support; UFLS inside the indicated area.*

In general an improvement in the overall system performance is noted. Nevertheless, as shown in the indicated points by the arrows in **Figure 4-28**; the implemented algorithm is not able to avoid UFLS. The reason behind is due to the extreme offset in the calculation of the critical time from the fitting function for the low RoCoF values corresponding to that area. On the other hand, values of frequency nadir higher than 49.4 Hz are observed in the most severe combination of inertia and imbalance.

## Applying only Synthetic Inertia to the System

For the simplified IEEE 9 bus model several contributions of synthetic inertia were simulated and the results of the frequency nadir shown. Synthetic inertia was incorporated as well in the European island model and the frequency nadir values are shown in **Figure 4-29**.

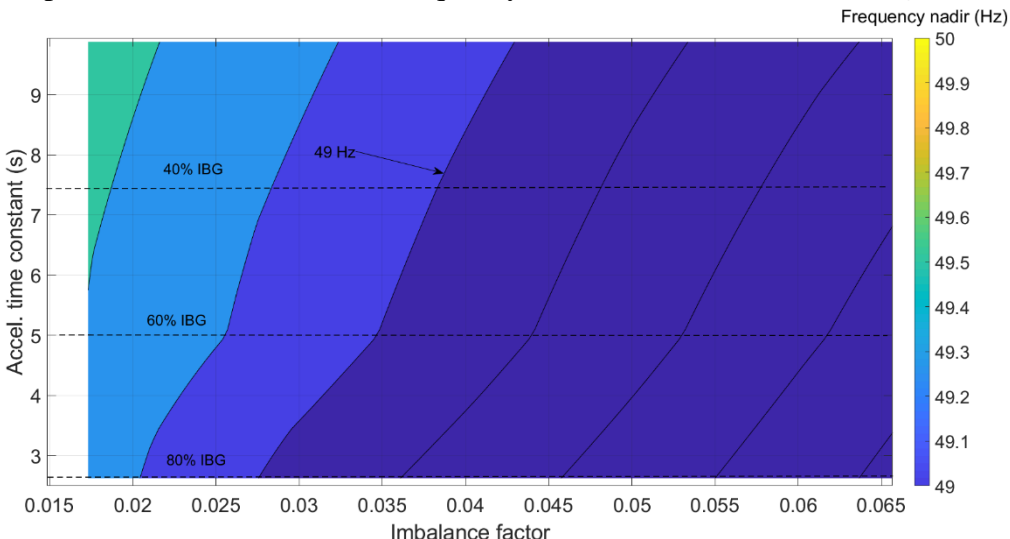


*Figure 4-29: Frequency nadir. 80% of IBG is considered to provide synthetic inertia Reference source not found..*

## European Island Case

In the same manner than in the simplified IEEE model, the synthetic inertia is not enough for withstanding severe imbalances under high penetration of inverter based generators. At 80% (~2.5 s) of IBG frequency nadir reaches 48.89 Hz with a imbalance of 3%. This does not improve not even in 1% the value obtained without frequency any support.

### Influence of the frequency measuring time delay

When the same power ramp response is maintained regardless of the inherent delay in frequency measurement, the performance of the system is affected depending on the duration of the delay. **Figure 4-** and **Figure 4-** show the corresponding nadir frequencies for delays in frequency measurement of 100 ms and 200 ms.

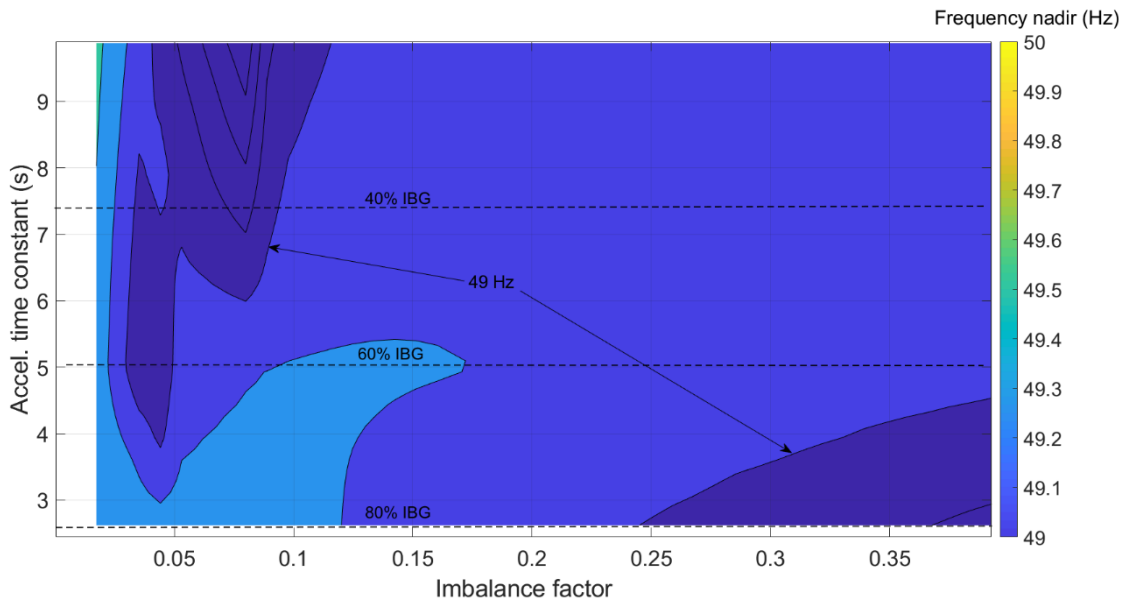


*Figure 4-32: Frequency nadir when IBFPR has a delay of 100 ms.*

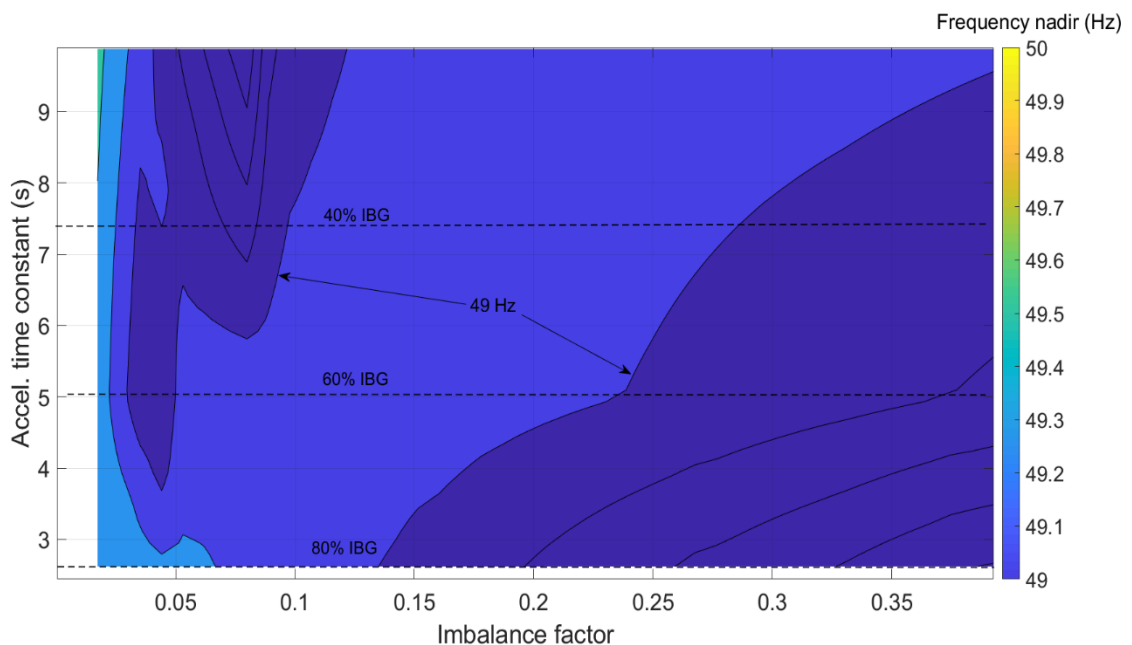


*Figure 4-33: Frequency nadir when IBFPR has a delay of 200 ms.*

## European Island Case

Similar as in **Figure 4-28**, it can be notice in **Figure 4-** and **Figure 4-**, that frequency nadir values beyond the allowed limit are found for low imbalances for almost every time constant of the system, when delay up to 200 ms is applied.

### Over-frequency case

In **Figure 4-30** it is demonstrated that the values calculated for critical time, nadir time and power responses apply equally to the over frequency case with the frequency deviation of 1 Hz from nominal.

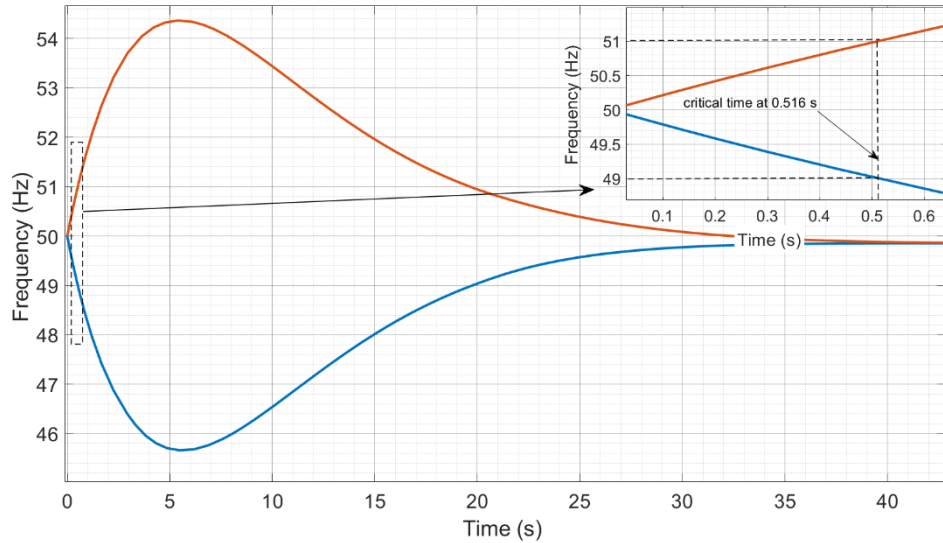


*Figure 4-30: Comparison of critical times for over and under-frequency cases.*

## 5 Analysis of the Simulation Results

---

In this section a deeper look is given to the obtained results out of the simulated cases. In order to allow understandable comparisons between each approach and models; the chapter is divided in three main sections, in which the main results of the simulations will be discussed. This chapter is divided in the following sub-sections:

- Analysis of critical time.
- Analysis of Synthetic Inertia and Fast Power Reserve
- Synchronizing effect and lack of damping torque.

### 5.1 Analysis of Critical Time

Due to the nature of the swing equation, which describes the frequency response in synchronous machines, a reduction of the available time for the inverters to react to perturbations was found as RoCoF increases.

As it was expected, the frequency response is highly dependent on the primary reserve response (governor response). When the IEEE 9 bus model is simplified to one machine and losses are disregarded; critical time deviations from the full dynamic extended model are observed to reach values up to 34%. From the fit plots it can be noticed that the highest deviations occur at high system acceleration constants and in the low range of RoCoF, allowing primary reserve to take effect. Therefore, it can be stated that the simplifications in the model have a greater influence on the results for low RoCoF and IBG penetration values; in this sense, the simplifications become less significant as the RoCoF increases in such a manner that the activated synchronous primary reserve is not relevant in frequency support.

Despite the discrepancy in the critical time between both approaches in the IEEE 9 bus model; the power ramp calculated for the simplified model and the extended model does not differ from each other in a great manner as exhibit later in **Figure 5-2**. It is then inferred that the discrepancy in critical time estimation is compensated by the factor of nadir time, which due to non-linearity characteristics considered in the Extended model, varies upon change in inertia and load imbalance (perturbation); contrary as the linear simplified model in which the nadir time is invariable for perturbations.

In the theory section, the typical frequency measurement time and technologies activation time were discussed [14]. **Figure 5-1** contrasts the critical times obtained from the models with the required time for frequency measurement and full power activation from different technologies.

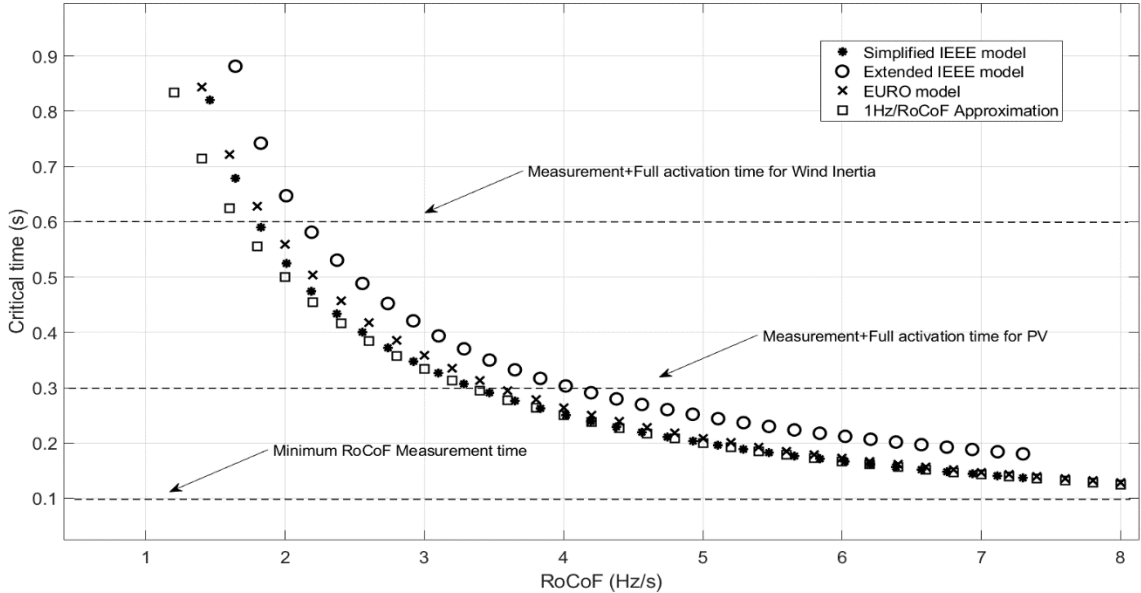


**Figure 5-1: Critical time for all scenarios at 80% IBG penetration.**

It is observed that in the range higher than 2 Hz/s; the critical time trend for the European island and the simplified IEEE model get closer each to other as RoCoF increases. In the same way the extended model but for very high values. Therefore, it is inferred that under high RoCoF conditions in any of the models, the primary reserve does not significantly counteract the frequency drop [16]. **Figure 5-1** demonstrates that primary reserve can be neglected for determination of the critical time when the combination of inverter based generation and load imbalances would lead to high values of RoCoF ( $>2$  Hz/s); as RoCoF increases, the approximation of critical time as  $1(\text{Hz})/\text{RoCoF}$  narrows the difference with the results obtained from simulations [14]. Nevertheless such simplification is applicable to the simplified IEEE model and the European island. Hence, the influence of all the dynamics and machine components, such as generator exciter and armotisour windings, seems to improve the critical time; extending up to a 34% the calculated time with the simplified approach. Damping torque in swing equation [7, 8] was not considered for the IEEE simplified model; the inclusion of such may lead to more precise times when comparing with the extended model.

Also it is then stated the need of a fast power response to avoid frequency collapse of islanded micro-grid or an electric island in the European scale. Even assuming that power reserve can immediately fully activated after RoCoF reading, the 100 ms limitation is a constraint for high unbalanced islands with high penetration of IBG in the European case as demonstrated in the result section. Additionally, the direct measurement of RoCoF in the 100 ms interval can lead to misleading readings [14]. In general, when penetration of IBG is higher than 90%; for the 40% imbalance an activation time between 30 and 50 ms would be needed to keep frequency within the allowed limits.

Due to the fact that the characteristics of the interconnected scenario provided by ENTSOE were assumed to be the same than the resulting islands after a severe event; the results for the European island can be understood as the behavior of the whole European system with bigger perturbations. The dimensioning scenario assumes a power imbalance of 3 GW, which corresponds to a 2% of the 150 GW load [1]. If in future a bigger dimensioning case is utilized, then synchronous response would not be enough to balance the system before load shedding occurs.

**Table 5-1** exhibits the required time when the dimensioning scenario is increased up to 10% for different IBG penetration.

*Table 5-1: Critical times for European case in seconds.*

IBG share (%)	Load imbalance (%)							
	3	4	5	6	7	8	9	10
20	-	-	6.081	4.517	3.629	3.050	2.638	2.316
40	-	6.226	4.169	3.215	2.628	2.222	1.934	1.705
60	7.142	3.639	2.623	2.062	1.698	1.451	1.263	1.122
80	2.753	1.744	1.277	1.018	0.843	0.722	0.628	0.559
92	1.109	0.700	0.514	0.406	0.338	0.288	0.252	0.224
95	0.697	0.436	0.322	0.254	0.211	0.179	0.157	0.140

Scenarios with higher imbalance than the reference scenario combined with high penetration of renewables will require fast power reserve as indicated in **Table 5-1**. Even though it was assumed enough synchronous reserve, this is too slow under such conditions.

## 5.2 Analysis of Synthetic Inertia and Fast Power Reserve

### Synthetic Inertia

From the results from the simplified IEEE model and the European island, it can be stated that synthetic inertia from wind turbines do not represent, by itself, a viable way to tackle with frequency transient stability for all simulated scenarios. The reason for its limited capability in contributing to very adverse system conditions is that wind turbines can be overloaded just for a short time (c.a. 10 seconds) with a limited power exceeding the rated power (also c.a. 10% of nominal power)

Since it is expected that most of the inverter based generation will come from inverters connecting wind turbines and PV inverters; it was assumed that a high share of wind power out of the total inverter based generation would successfully contend the frequency droop for light and sever perturbations in the system. Although the results from the simulated scenarios of the simplified IEEE model and the European island show that is not the case for all scenarios. When the system counts with a relative fast primary reserve, given by the governor response of the synchronous machines, as modeled in the IEEE grid. Synthetic inertia seems

to be enough to arrest frequency drops associated to imbalances up to 10% with an IBG of 80% ( $\sim 2.5$  s) for contributions from wind to IBG above 20%. As imbalance increases, contribution from wind to the IBG should increase as well to avoid UFLS. However, in the European model, under the same inertia scenario; synthetic inertia does not contribute enough to avoid UFLS. Hence, it is stated that synthetic inertia can contribute to avoid UFLS with a faster primary reserve as shown in the IEEE grid model.

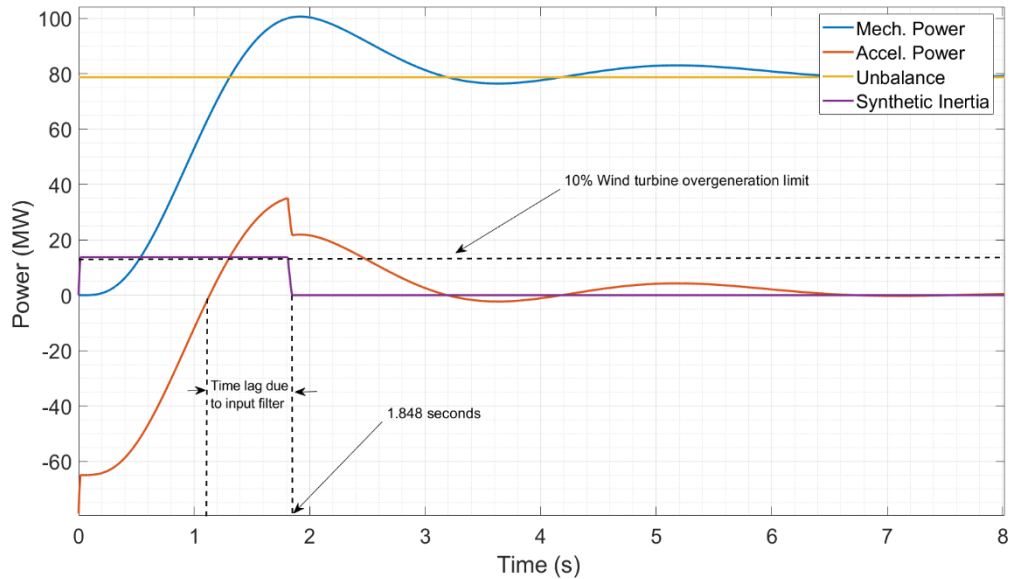


**Figure 5-2: Synthetic Inertia power response characteristics of the simplified IEEE model with 20% synthetic inertia with an imbalance of 25%. Total IBG share of 80%**

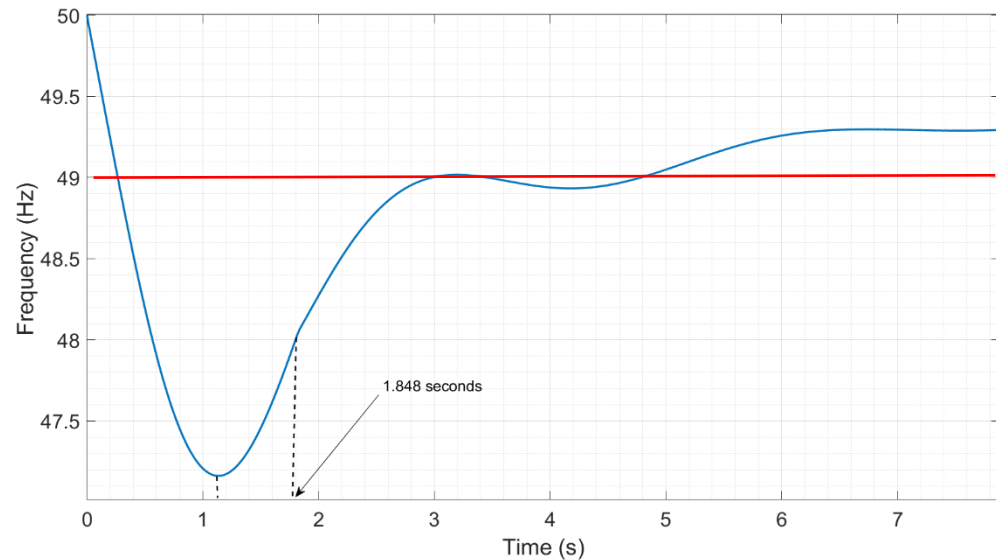


**Figure 5-3: Frequency response with 20% synthetic inertia with an imbalance of 25%. Total IBG share of 80%**

As already stated, the reasons behind the limitation for avoiding UFLS of synthetic inertia are its operation constraints. In order to illustrate this fact, the same example shown in the result section is brought again to explain how the limitations take place at what moment and circumstances. When the simplified IEEE model is considered under a load imbalance condition of 25% and wind turbine share with synthetic inertia constitutes a 20% of the

inverter based generation, which in this case is considered to be the 80% of the total generation.

The limited amount of available synthetic inertial power at the moment of inception of the perturbation causes the system frequency to droop down UFLS, as illustrated in **Figure 5-**. Since the implemented synthetic inertia model works with the derivative of frequency when a negative load imbalance occurs, meaning that the frequency derivative is negative; once the system RoCoF becomes zero (acceleration power equals zero) the inertia control deactivates. As shown in **Figure 5-** a delay is observed due to the lag imposed by the filter block in the input of the loop. Similar cases are shown in the result section for different shares of synthetic inertia out of the total inverter based share.

Another big drawback for synthetic inertia in extreme imbalance cases is “the long activation time required” in the order of 500 ms [14].

### **Fast Power Reserve: Effect of Ramp response**

When the power ramp required to meet the power load imbalance at the critical time was calculated in chapter 3; the contribution from the ramping power in diminishing system RoCoF during the inception of the perturbation until the critical time was disregarded. Therefore the fast inverter based power response values at the critical time correspond to the accelerating power at that time. Assuming an instant switching of the IBFPR at critical time, the frequency nadir would be 49 Hz (no ramping power before critical time). Nevertheless, a ramp power response was assumed instead. Therefore the calculated power ramp, when applied to the unbalanced system, commonly exhibits a frequency nadir higher than 49 Hz, due to the contribution of the ramping period. In this sense, it can be inferred that the longer the ramping period (shorter measuring time), the higher frequency nadir will be obtained. Here again the relevance of the prompt activation in time of the IBFPR. On the other hand, with the faster IBFPR activation, the ramp slope and the steady power output (Inverter based power reserve) can be diminished compromising frequency nadir.

When the activation does not takes place instantaneously, frequency nadir and therefore system stability can be compromised for some combination of system inertia and load imbalance as demonstrated in the result section. In order to assure stability a stepper ramp slope is required in order to meet the required power before critical time. That is achieved by changing equation 3-2 by the adjusted expression:

*Equation 5-1*

$$P_{IBFPR}(t) = \Delta P * \frac{\left(1 - \frac{t_{cr}}{t_{nadir}}\right)}{(t_{cr} - t_d)} * t$$

Where  $t_d$  is the time delay needed to start the activation of IBFPR.

When a comparison is established between all the calculated power ramp slopes in per unit<sup>2</sup> (pu), it is noted that with high penetration of non-synchronous power in the power system, the required power to ensure no UFLS have a consistent trend between the three models, and a close proximity in the values for RoCoF in the range of 2 to 5 Hz/s is observed between both IEEE models. Such trends can be seen in **Figure 5-2**.

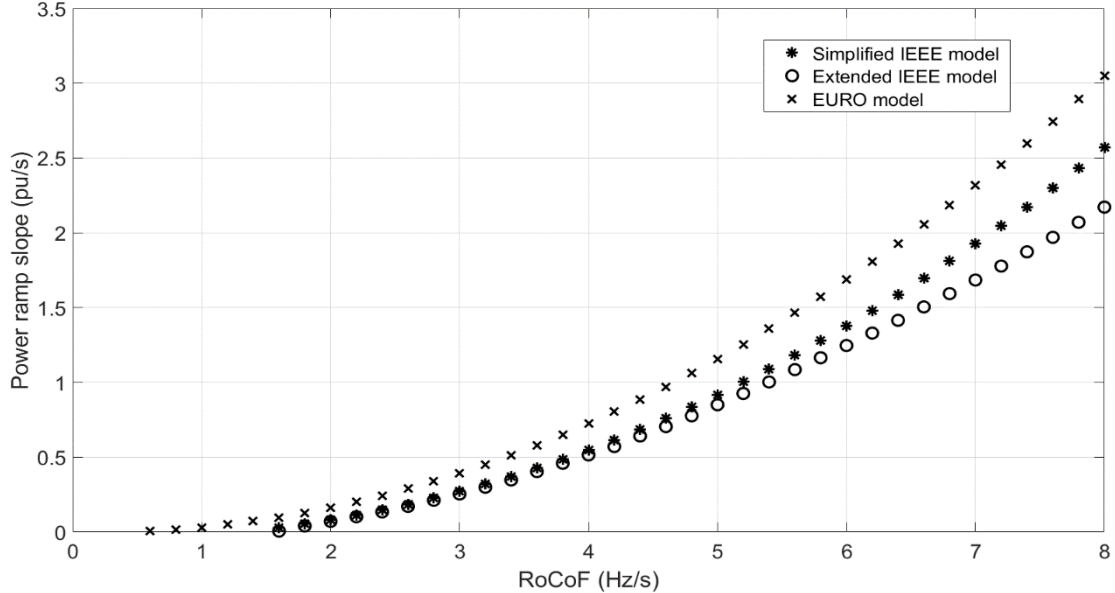


Figure 5-2: Power ramp slope with 80% of IBG penetration.

A bigger amount of power ramp slope is needed in all the range of RoCoF for the European case. After inspecting **Equation 3-2**, it is noticed that the IBFPR is affected by the factor  $(1 - t_{cr} / t_{nadir})$ , then as nadir time increases, IBFPR increases as well. The nadir time for the European case, due to the action of the self-regulation and primary reserve deployment of 30 seconds, is in the range of 3-12 seconds (6 seconds for 80% IBG penetration) whereas the nadir time for the simplified IEEE model is between 1-3 seconds. See **Appendix III** for more details in regards of nadir time.

## Fast Power Reserve

So far, the power ramp required to avoid load shedding has been found for the IEEE 9 bus model with a fast governor response and for the European island with conventional primary reserve response. Hence, the investigated inverter based fast power response at critical time which remain constant afterwards, would be accounted as the fast power reserve. Similarly as primary reserve estimations are performed considering the loss of generation at certain level; for fast power reserve the results are presented for the scenarios in which imbalance could reach even 40%

---

<sup>2</sup> Power base for each cases is given by the load power; 315 MW for the IEEE model and 150 GW for the European electric island.

**Figure 5-3** shows the results of the needed fast power reserve for each case under 80% of IBG penetration. A linear behavior is exhibit by the simplified model and the European.

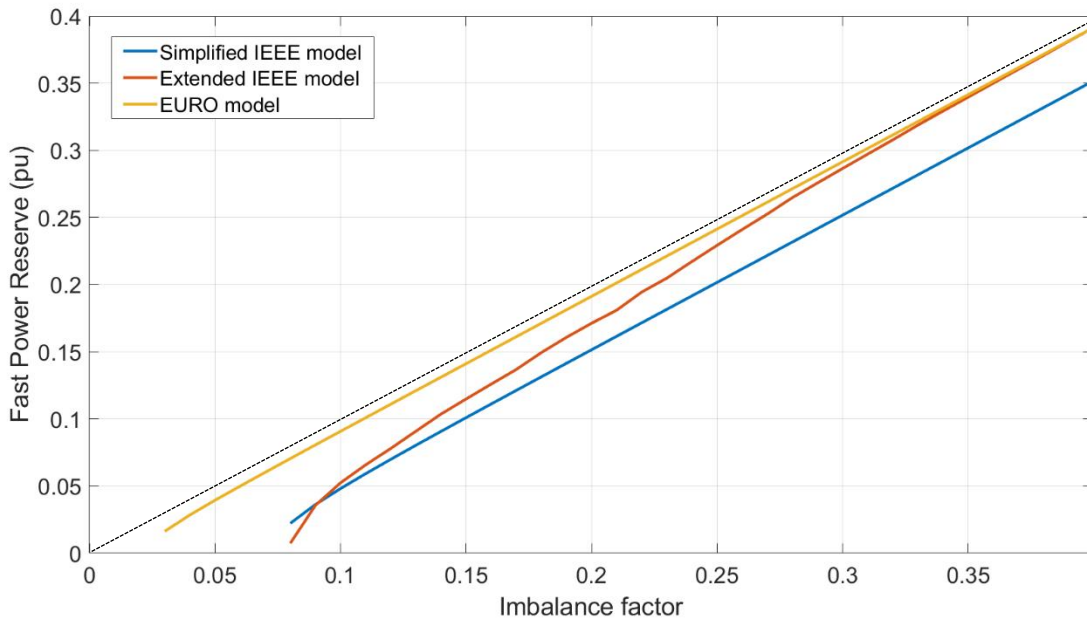


Figure 5-3: Fast power reserve at 80% of IBG.

A proportion of almost one to one is observed for the European model, this is caused by the slow primary reserve. Therefore for imbalances higher than 3% the fast power reserve has to cover all the imbalance. The observed offset from the one to one relation is due to the load reduction caused by the frequency drop (load self-regulation). The dashed line represents the one to one proportion. In the case of the IEEE grid; the simplified model exhibits a permanent offset from the dashed line of around 0.05 pu, this due to the action of a faster governor response. Therefore, it can be said that in such scenario, the conventional governor response of synchronous machines would cover 5% of the imbalances starting at 8%. Since the values for nadir time are not independent from the imbalance in the Extended model, due to the non-linearity of the model, the calculated power reserve tend to equalize the whole imbalance. As imbalance increases, the critical time decreases and the nadir time increases, this makes the reducing factor  $t_{cr}/t_{nadir}$  from **Equation 3-2** to decrease and narrows the difference between the calculated reserve and power imbalance.

Similarly as critical time was presented in **Table 5-1** the required fast power reserve in the European context is shown in **Table 5-2** for extraordinary events<sup>3</sup>

---

<sup>3</sup> Referred to an imbalance event higher than 3 GW (2% of load).

**Table 5-2: Fast power reserve in per unit for European case**

IBG share (%)	Load imbalance (%)							
	3	4	5	6	7	8	9	10
20	-	-	0.025	0.038	0.049	0.060	0.070	0.081
40	-	0.016	0.030	0.041	0.052	0.063	0.073	0.083
60	0.005	0.024	0.035	0.045	0.056	0.066	0.077	0.087
80	0.016	0.028	0.039	0.049	0.062	0.070	0.080	0.09
92	0.021	0.033	0.043	0.054	0.064	0.074	0.084	0.094
95	0.024	0.035	0.045	0.055	0.065	0.075	0.085	0.096

As IBG increases the closer to the imbalance the fast power reserve needs to be. As it was demonstrated in the result section; with a faster conventional reserve, reduction in fast power reserve can be observed.

### 5.3 Synchronizing effect, lack of damping torque and implications.

When the IEEE model was implemented using SIMULINK-SIMSCAPE blocks, in order to incorporate all system component dynamics; system instability was found for low inertia values in the system and due to high imbalances (with no IBFPR). In non-linear systems, the stability is not only determined by the equivalent transfer function but also it is dependent on the inputs or sources [7, 22]. In this sense the loss of stability due to huge load imbalances is explained by the non-linearity of the system. When the system is perturbed by a small change in one of the state variables in such a way that the system returns to its initial state or remains close to it; a linearization of the system can be performed and a so called small signal stability analysis can be performed [7].

In the simulations it was found how the extended model is unstable for imbalances above 15 % with a penetration of non-synchronous generation of 85%, corresponding to a system acceleration time constant of 2.1 seconds. The diminishing of synchronous machines, and the dependency of system frequency and voltage signal from them, lead to a very weak network, where synchronizing and damping torque, which are inherent characteristics of synchronous machines are not enough to stabilize the system (assuming that such excursion of frequency and rotor speed would be allowed to happen) [7]. Although the implementation of IBFPR contributes keeping synchronous machine on step<sup>4</sup>, low frequency oscillations in the rotor speed/frequency response are observed. This oscillations are created by the lack of damping torque which is provided mainly by the synchronous machines, through damping windings, field exciter and Power System Stabilizer (connected to the machines exciter). For the simplified IEEE model and the European island, only transfer functions describing an equivalent system governor were modeled. Hence in such approaches, the effect and

---

<sup>4</sup> Synchronized rotor speeds.

dynamics of synchronous generator's excitors and inter-machine interaction were not taken into account. The before mention factors influence greatly small signal stability [7, 8]

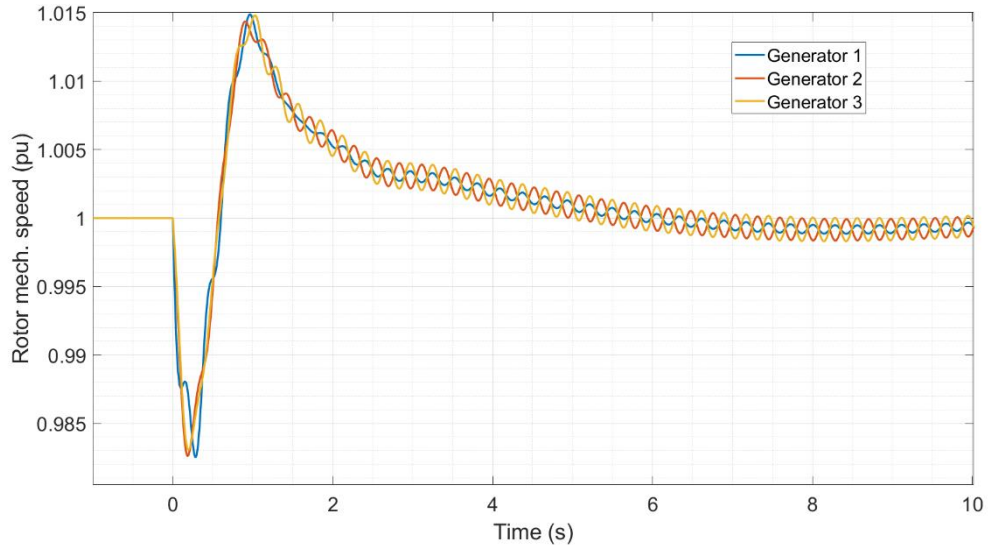


*Figure 5-4: Oscillatory effect in synchronous generators rotor speeds in the Extended IEEE model with 85% IBG and 35% load imbalance and IBFPR support.*

Even though the scope of this thesis is to analyze the power-time characteristics needed to avoid frequency collapse; oscillations associated to big perturbation were observed but they could not been addressed by the simple injection of power to the system. Also in the IEEE model, when a penetration of 95% of inverter based generation and 2% of load imbalance are considered, UFLS is not reached but the system becomes unstable as shown in **Figure 5-6** and **Figure 5-5**. From penetrations levels above 85% complete frequency stability is not ensure with the injection of fast power reserve, only UFLS on the first 10 seconds approximately. Then the system becomes unstable with increasing amplitude oscillations.

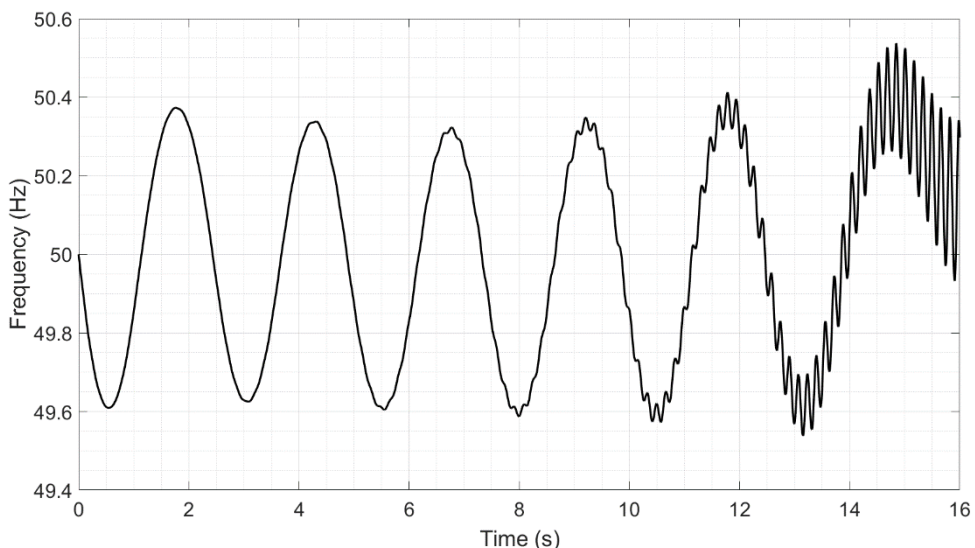


*Figure 5-5: Oscillatory behavior from extended IEEE model with 95% IBG and 2% imbalance. No IBFPR is provided.*

It is important to note that ENTSOE in its EUROPEAN interconnected scenario, determined that there is no UFLS when an unbalance of 2 % with high contribution of non-synchronous generation occurs. Nevertheless, no inter-machine interaction was considered and therefore a similar effect as the one in **Figure 5-6** could be experienced.

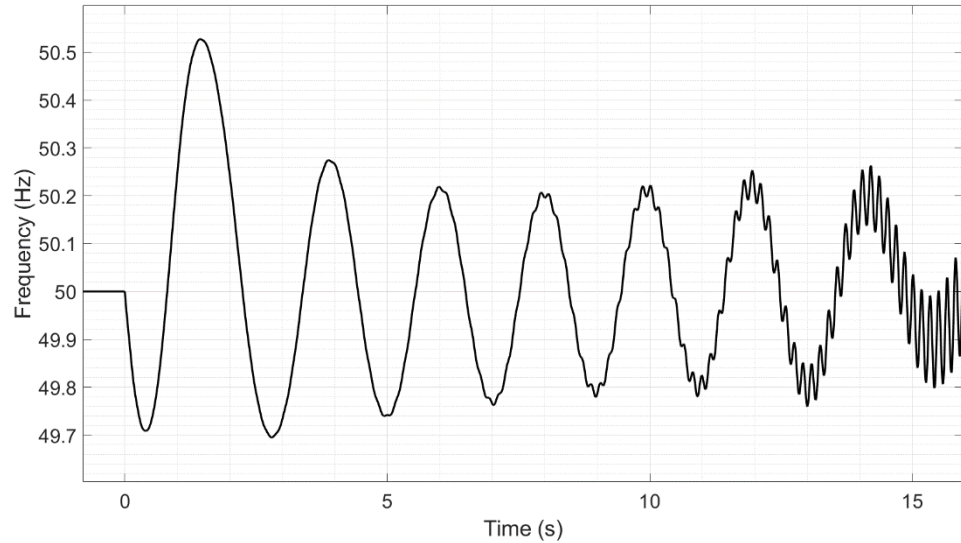


*Figure 5-6: Oscillatory behavior from extended IEEE model with 95% IBG and 2% imbalance.  
IBFPR is provided*

## 6 Conclusions

---

When a future power system dominated by distributed renewables sources is pictured, it must perform in a reliable way as today's power systems. The increasing amount of power electronic devices facing renewable power sources as PV and wind weakens the power system capability to face perturbation and ensure transient frequency stability. Due to the reduction of system inertia. The natural power output variability of renewables, increasing transmission capabilities between areas, international energy markets and increasing development of micro-grids increase the likelihood of island operation under high unbalanced conditions after a major event. In order to avoid load shedding under such conditions, inverter based generation must contribute to frequency regulation.

Conventional synchronous machines were found not to be able to ensure transient frequency stability in such conditions. The slow governor operation in the order of seconds is by far too slow to constitute the unique solution for frequency support during the transient period. Inverter based fast power reserve would be needed to be activated in an extreme short time.

To avoid load shedding in penetration scenarios above 80% of non-synchronous generation, inverter based fast power reserve must be deployed over a time in the order of 50-500 ms for load imbalances up to 40%. Nevertheless, today's full power activation time of renewable sources without storage is in the range of 200 to 600 ms. Hence with today's frequency measuring time and power deployment from renewable sources; load shedding and possible total black outs would not be avoided. In scenarios with plenty of renewables and high expected imbalances, storage would be a key factor in order to avoid de-loading and curtailment of renewables, the fast activation times (<50 ms) and promising price reduction make storage a good strategy to provide power balancing in both over and under frequency cases.

Synthetic inertia could tackle with under-frequency phenomenon. With penetrations of 80% or higher of IBG, and contribution of at least 20% of the IBG from Wind turbines with synthetic inertia controls, UFLS is avoided up to imbalances of 10% with a fast synchronous response (1-3 s in the IEEE modeled cases). For primary reserve deployment of 30 s (European model), synthetic inertia was not enough for avoiding UFLS.

An effective frequency measurement in shorter time would contribute to reduce the amount of inverter based power reserve and therefore, to diminish the de-loading factor or the storage capacity needed to provide it, up to a 10%. In order to avoid UFLS, ramping capabilities up to 3 times the base power load per second (3 pu/s) would be required from the inverter based sources; for combinations of inverter based generation above 80% and load imbalance in the order of 30% in both, micro grid and European scale islands. To achieve such response from distributed source, a continuous knowledge of the connected inertia to the system is required by the inverters since the IBFPR is based on the imbalance on the system and the critical time, which depends on system inertia. Additionally, system inertia is the linking bridge between RoCoF and power imbalance determination.

If the reference scenario for primary reserve is increased (imbalance higher than 2%) in the European context, synchronous response is not fast enough for imbalances higher than 2%. Full activation time in the range of 0.14 and 2.75 seconds would need required for the fast power reserve for penetrations of non-synchronous generation above 80 % (~2.5 s) and imbalances between 3 and 10%. Additionally, fast power reserve would be almost equivalent to the imbalance. Faster synchronous response reduces needed fast power reserve.

Although UFLS is avoided in the extended model in scenarios with penetrations of non-synchronous generation above 85% with injection of inverter based fast power reserve; total system stability is not ensured after a few seconds (~5 s), due to the presence of undamped oscillations provoked by the poor damping torque present in the system as consequence of synchronous share reduction.

Even though the approach considered throughout this work was the fast power reserve deployment to avoid under-frequency load shedding. If the same frequency deviation from nominal is considered as the critical for the over-frequency case (51 Hz); the same values would be obtained for critical time and power response. The difference lies in the power direction, in this case power should be removed from the grid or the excess converter to another form of energy, like electrochemical storage. In the case of batteries, the critical time would represent the needed time to allow charging the surplus of power available from renewables.

In general, similar behavior is exhibit from the different models and approaches, even though they differ considerably in size and complexity. Hence, simplified block representation of the power system seems to be a fair way to sketch overall system trends and responses. The difference in critical time estimation between a full grid simulation and a simplified model was calculated to differ between 20-35%, such difference could be crucial in fast power reserve studies and therefore should be considered when precise applications are implemented. A comprehensive method for estimation of the inverter based fast power reserve and critical time were developed and proved through the implementation in the two cases.

## **7 Outlook**

---

It was demonstrated the need of a fast power reserve for the reliable operation of future's grid. To do so, an accurate and fast estimation of the power grid state is fundamental in terms of frequency and connected inertia; to enable inverter based generation to play a dominant role in frequency support. Further investigation in this area is fundamental to allow flexible inverter based generation. The integration of energy storage systems are promising alternative to provide ancillary services to the grid, the diminishing trend cost and fast activation times could be optimized together with de-loading of renewable sources to provide frequency support.

Investigation of grid forming inverters connected along with synchronous machines and grid-following should be further investigated. So far, investigation and implementation of such type of inverters has been done mostly for stand-alone systems.

## 8 References

---

- [1] ENTSOE, “Frequency Stability Evaluation Criteria for the Synchronous Zone of Continental Europe,” [www.entsoe.eu](http://www.entsoe.eu), 2016.
- [2] J. Aho *et al.*, “Tutorial of Wind Turbine Control for Supporting Grid Frequency through Active Power Control: Preprint,” [www.nrel.gov](http://www.nrel.gov), 2012.
- [3] Agora Energiewende, “Energiewende: What do the new laws mean?: Ten questions and answers about EEG 2017, the Electricity Market Act, and the Digitisation Act,” [www.agora-energiewende.de](http://www.agora-energiewende.de).
- [4] A. Hoke, “Fast Grid Frequency Support from Distributed Inverter-Based Resources,” [www.nrel.gov](http://www.nrel.gov), 2018.
- [5] Andy Hoke, Mohamed Elkhatab, Austin Nelson, Jay Johnson, Jin Tan, Rasel Mahmud, Vahan Gevorgian, Jason Neely, Chris Antonio, Dean Arakawa, and Ken Fong, “The Frequency-Watt Function: Simulation and Testing for the Hawaiian Electric Companies,” <https://www.nrel.gov/docs/fy17osti/68884.pdf>.
- [6] M. Dreidy, H. Mokhlis, and S. Mekhilef, “Inertia response and frequency control techniques for renewable energy sources: A review,” *Renewable and Sustainable Energy Reviews*, vol. 69, pp. 144–155, 2017.
- [7] P. Kundur, N. J. Balu, and M. G. Lauby, *Power system stability and control*. New York, London: McGraw-Hill, 1994.
- [8] P. M. Anderson and A. A. Fouad, *Power system control and stability*, 2nd ed. New York, Chichester: Wiley, 2002.
- [9] A. D. Hansen, P. E. Sørensen, L. Zeni, and M. Altin, “Frequency control modelling - basics.,” DTU Wind, 2016.
- [10] “California ISO (CAISO),”
- [11] M. Bhuiyan and S. Dinakar, “Comparing and Evaluating Frequency Response characteristics of Conventional Power Plant with Wind Power Plant,” Master of Science in Engineering, Department of Energy & Environment, Chalmers University of Technology, Goteborg, Sweden, 2008.
- [12] Agora Energiewende, “Flexibility in Thermal Power Plants: Focus on existing coal-fired power plants,” [Online] Available: [www.agora-energiewende.de](http://www.agora-energiewende.de).
- [13] B. Kroposki *et al.*, “Achieving a 100% Renewable Grid: Operating Electric Power Systems with Extremely High Levels of Variable Renewable Energy,” *IEEE Power and Energy Mag.*, vol. 15, no. 2, pp. 61–73, 2017.
- [14] General Electric International, “Technology Capabilities for Fast Frequency Response,” 2017.
- [15] International Renewable Energy Agency (IRENA), “Electricity storage and renewables: Costs and markets to 2030,” [www.irena.org](http://www.irena.org), 2017.
- [16] Deutsche Energie-Agentur GmbH (dena) – German Energy, “dena Ancillary Services Study 2030: Security and reliability of a power supply with a high percentage of renewable energy,” German Energy Agency, Berlin, Germany, 2014. [Online] Available: [www.dena.de](http://www.dena.de).
- [17] Federal Ministry for Economic Affairs and Energy, “An electricity market for Germany's energy transition: White Paper by the Federal Ministry for Economic Affairs and Energy,”
- [18] ENTSOE, “Future System Inertia,” ENTSOE. [Online] Available: [www.entsoe.eu](http://www.entsoe.eu).
- [19] C. Hultholm, “Optimal reserve operation in Turkey – frequency control and non-spinning reserves,” Wärtsilä, 2015.
- [20] Atieh Delavari, Innocent Kamwa, and Patrice Brunelle, “Simscape Power Systems Benchmarks for Education and Research in Power Grid Dynamics and Control,”

- [21] J. J. Grainger, W. D. Stevenson, and W. D. E. o. p. s. a. Stevenson, *Power system analysis*. New York, London: McGraw-Hill, 1994.
- [22] K. Ogata, *Ingeniería de control moderna*, 3rd ed. México: Prentice-Hall, 1998.
- [23] V. Gevorgian and Y. : N. Zhang, “Wind Generation Participation in Power System Frequency Response,” [www.nrel.gov](http://www.nrel.gov), 2017.
- [24] General Electric International, “GE Wind Plant Advance Controls,” General Electric International, 2013.
- [25] B. Nesje, “The need for Inertia in the Nordic Power System,”
- [26] E. Muljadi, V. Gevorgian, and M. Singh: NREL and S. Santoso: University of Texas - Austin, “Understanding Inertial and Frequency Response of Wind Power Plants: Preprint,” 2012.
- [27] A. G. González Rodriguez, A. González Rodriguez, and M. Burgos Payán, “Estimating wind turbines mechanical constants,” *REPQJ*, vol. 1, no. 05, pp. 697–704, 2007.
- [28] L. Wu and D. G. Infield, “Towards an Assessment of Power System Frequency Support From Wind Plant—Modeling Aggregate Inertial Response,” *IEEE Trans. Power Syst.*, vol. 28, no. 3, pp. 2283–2291, 2013.
- [29] UCTE, “Final Report System Disturbance on 4 November 2006,” [Online] Available: [www.ucte.org](http://www.ucte.org).

## 9 Appendix I: Synchronous machine parameters and models

---

### IEEE- simplified model.

**Figure 9-1** shows the governor model implemented in the simplified model of the IEEE 9 bus model [8]

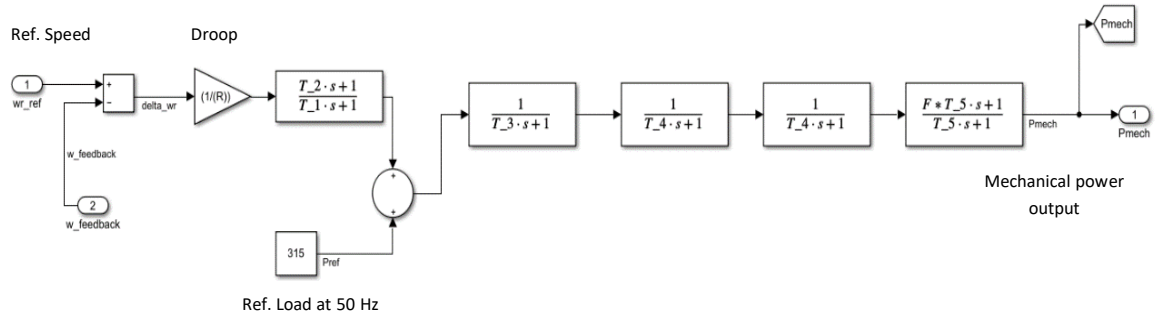


Figure 9-1: General purpose governor model

Table 9-1: Common governor parameters

Parameters	Generator Capacity (MVA)										
	911	835	590	410	384	192	100	75	51.2	35.29	25
T1 (s)	0.1	0.18	0.08	0.18	0.22	0.083	0.09	0.09	0.2	0.2	0.2
T2 (s)	0	0.03	0	0	0	0	0	0	0	0	0
T3 (s)	0.2	0.2	0.15	0.04	0.2	0.2	0.2	0.2	0.3	0.3	0.3
T4 (s)	0.1	0	0.05	0.25	0.25	0.05	0.3	0.3	0.09	0.2	0.09
T5 (s)	8.72	8	10	8	8	8	0	0	0	0	0
F	0.3	0.3	0.3	0.267	0.27	0.271	1	1	1	1	1
Kinetic Energy (MWs)	2265	2206.4	1368	1518.7	1006.5	634	498.5	464	260	154.9	125.4
H (s)	2.486	2.642	2.319	3.704	2.621	3.302	4.985	6.187	5.078	4.389	5.016
Pmax (MW)	820	766.29	553	367	360	175	105	75	53	36.1	22.5
Ta <sup>5</sup> (s)	14.381	14.009	8.686	9.643	6.390	4.025	3.165	2.946	1.651	0.983	0.796

<sup>5</sup> With a load of 315 MW

## Extended IEEE model: Governor and Exciter parameters

The following figures, show the values for the synchronous machines implemented in the Extended model [20].

Parameters	
Generator type	Tandem-compound (single mass)
Regulator gain, perm. droop, dead zone [ Kp Rp(pu) Dz(pu) ]:	[ 1 R2 0 ]
Speed relay and servo-motor time constants [ Tsr Tsm ] (s):	[ 0.001 0.15 ]
Gate opening limits [ vgmin,vgmax (pu/s) gmin,gmax (pu) ]:	[ -0.1 0.1 0 4.496 ]
Nominal speed of synchronous machine (rpm)	3600
Steam turbine time constants [ T2 T3 T4 T5 ] (s):	[ 0 10 3.3 0.5 ]
Turbine torque fractions [ F2 F3 F4 F5 ]:	[ 0 0.36 0.36 0.28 ]
Initial power Pm0 (pu):	0.85068

Figure 9-2: General settings of steam turbine model

Parameters	
Low-pass filter time constant Tr(s):	0.01
Regulator gain and time constant [ Ka() Ta(s) ]:	[ 20 0.2 ]
Exciter [ Ke() Te(s) ]:	[ 1, 0.314 ]
Transient gain reduction [ Tb(s) Tc(s) ]:	[ 10 1 ]
Damping filter gain and time constant [ Kf() Tf(s) ]:	[ 0, 0 ]
Regulator output limits and gain [ Efmin, Efmax (pu), Kp() ]:	[ -5 5 0 ]
Initial values of terminal voltage and field voltage [ Vt0 (pu) Vf0(pu) ]	[ 1.04 1.3869 ]

Figure 9-3: Exciter settings for Generator 1

Parameters

Low-pass filter time constant  $Tr(s)$ :

Regulator gain and time constant [  $Ka()$   $Ta(s)$  ]:

Exciter [  $Ke()$   $Te(s)$  ]:

Transient gain reduction [  $Tb(s)$   $Tc(s)$  ]:

Damping filter gain and time constant [  $Kf()$   $Tf(s)$  ]:

Regulator output limits and gain [  $Efmin$ ,  $Efmax$  (pu),  $Kp()$  ]:

Initial values of terminal voltage and field voltage [  $Vt0$  (pu)  $Vf0$ (pu) ]

*Figure 9-5: Exciter settings for Generator 2*

Parameters

Low-pass filter time constant  $Tr(s)$ :

Regulator gain and time constant [  $Ka()$   $Ta(s)$  ]:

Exciter [  $Ke()$   $Te(s)$  ]:

Transient gain reduction [  $Tb(s)$   $Tc(s)$  ]:

Damping filter gain and time constant [  $Kf()$   $Tf(s)$  ]:

Regulator output limits and gain [  $Efmin$ ,  $Efmax$  (pu),  $Kp()$  ]:

Initial values of terminal voltage and field voltage [  $Vt0$  (pu)  $Vf0$ (pu) ]

*Figure 9-4: Exciter settings for Generator 3*

70

## 10 Appendix II: SIMULINK models

---

### IEEE- simplified model.

**Figure 10-2 to Figure 10-3** shown the SIMULINK models employed in the simulations.

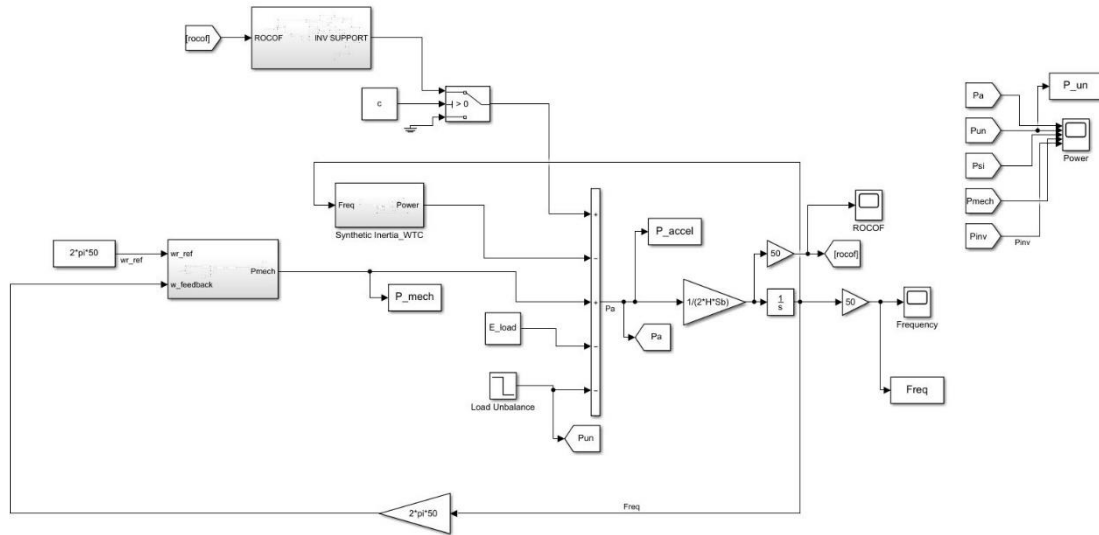


Figure 10-2: Complete simplified model, including SI and IBFPR.

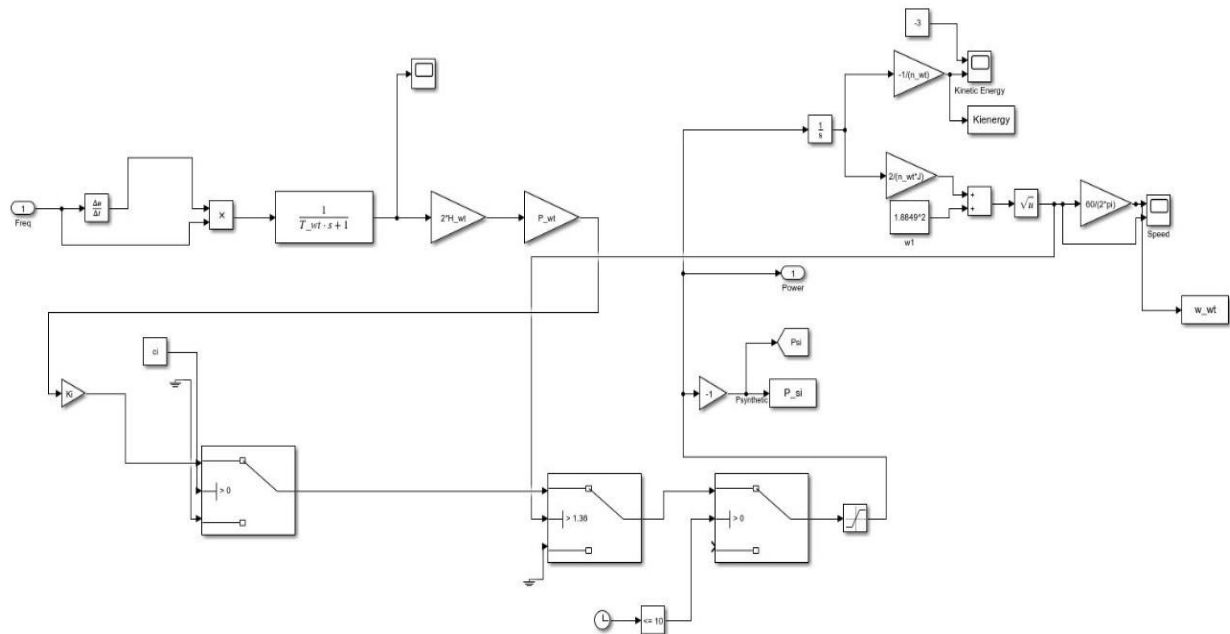


Figure 10-1: Synthetic inertia block diagram

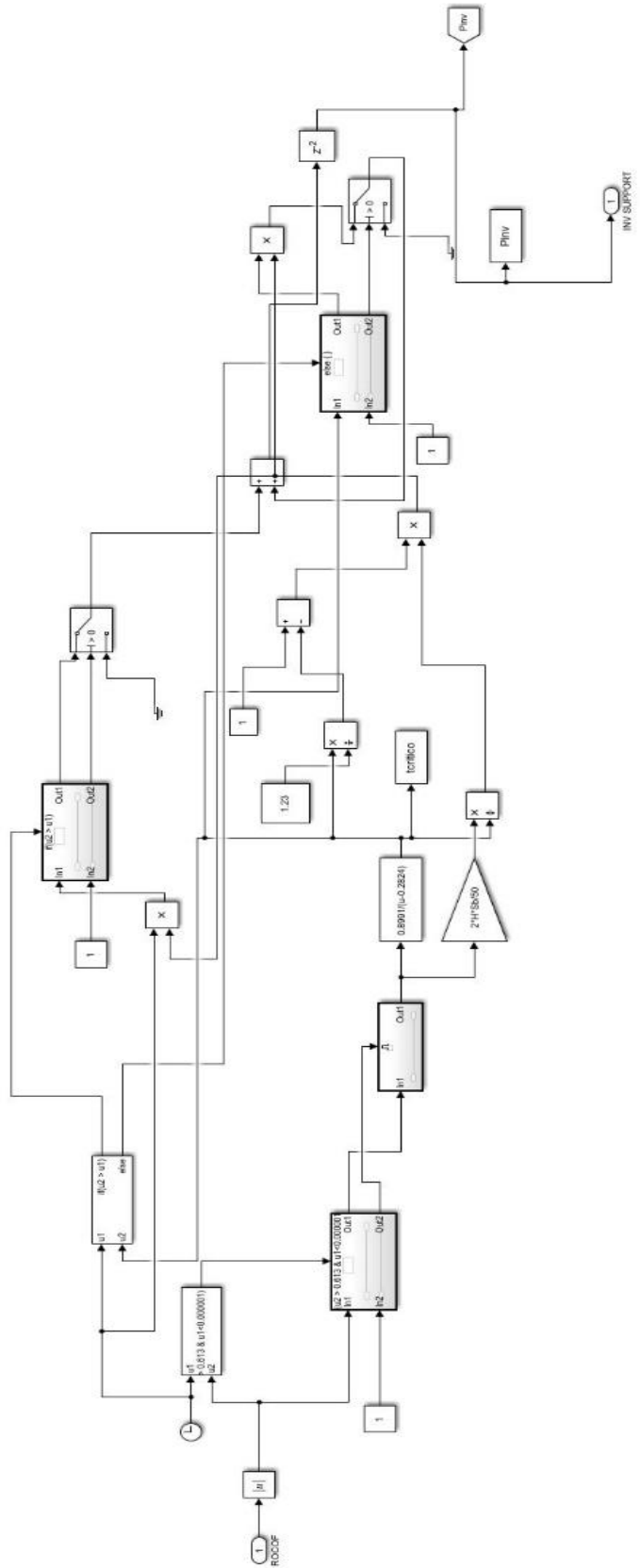


Figure 10-3: IBFPR block control block diagram

## 11 Appendix III: Nadir time.

---

### IEEE 9 bus -simplified model

Table 11-1: Nadir time for simplified IEEE model

System Accel. Constant s	Nadir time s
14	3.264
8.69	2.419
6.39	1.862
4.03	1.230
2.74	1.135

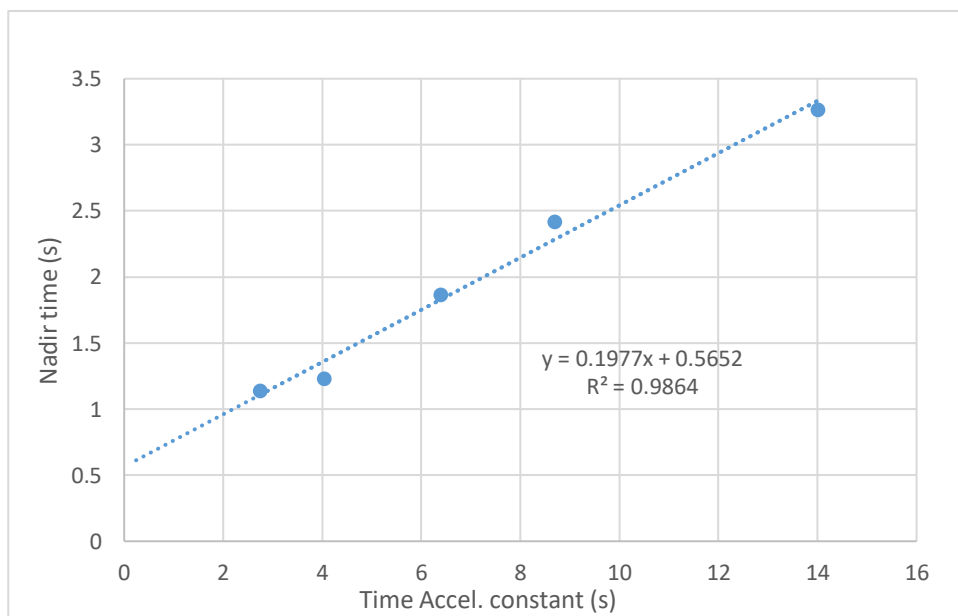
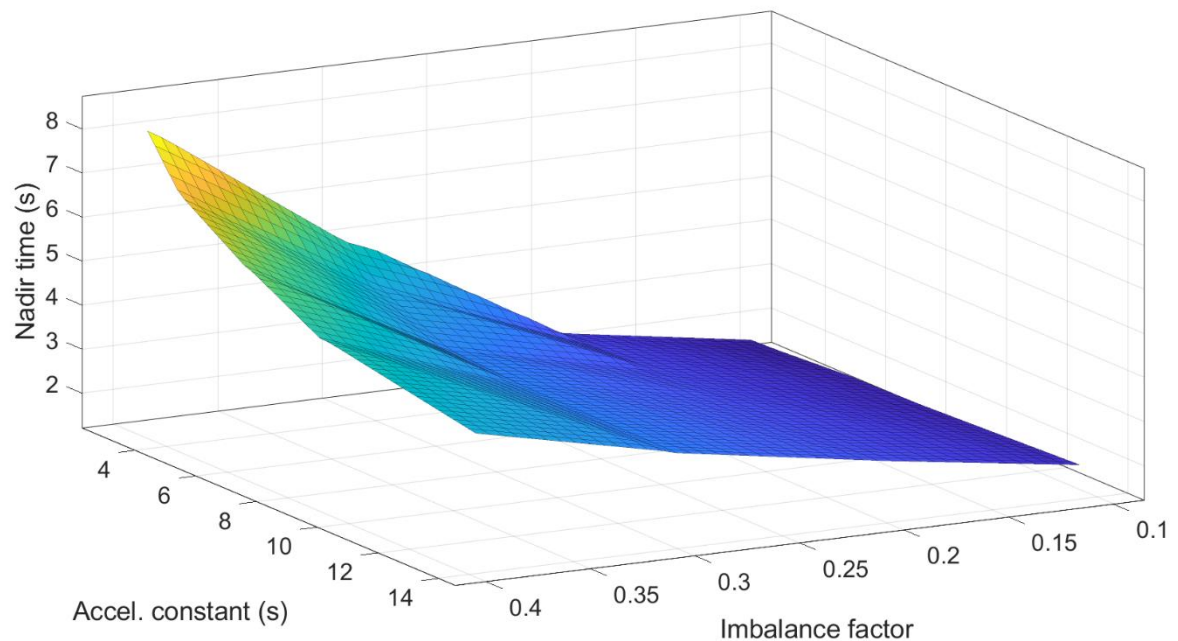


Figure 11-1: Relation between nadir time and accel. constant.

## IEEE- Extended model

**Table 11-2: Nadir time as function of imbalance and accel. constant.**

System accel. constant (s)	Imbalance factor			
	0.1	0.2	0.3	0.4
	Nadir time (s)			
14	1.892	2.575	3.342	4.375
8.68	1.725	2.516	3.392	5.092
6.3	1.692	2.451	3.508	6.008
4.06	1.592	2.392	4.235	7.058
2.8	1.558	2.308	5.098	8.397



**Figure 11-2: Relation between nadir time, accel. constant and imbalance**

## European model

Table 11-3: Nadir time for European model.

System Accel. Constant	Nadir time
s	s
10	12.37557
7.5	10.53318
5	8.828974
2.5	6.027827
1	4.138599
0.625	3.486501

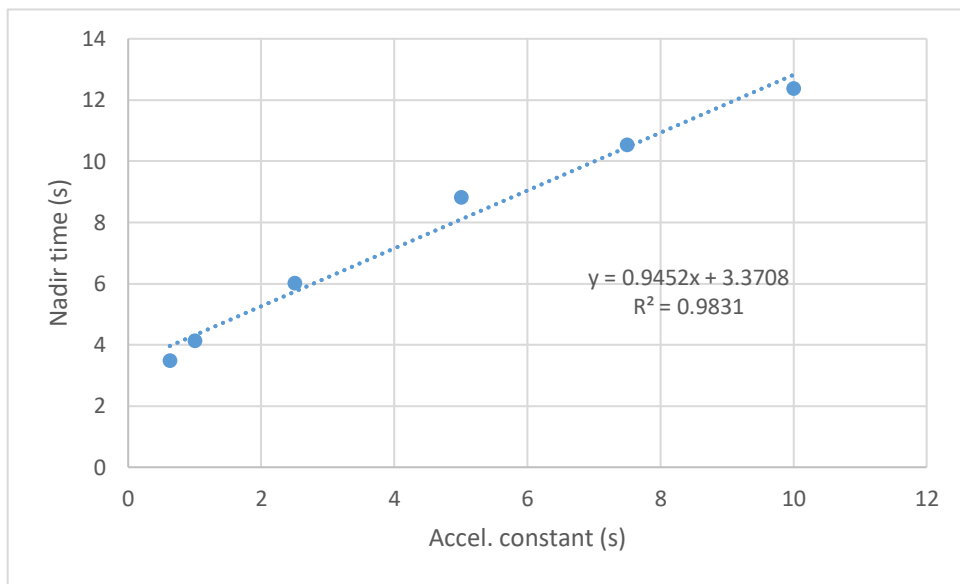


Figure 11-3: Relation between nadir time and accel. constant in the European grid representation.

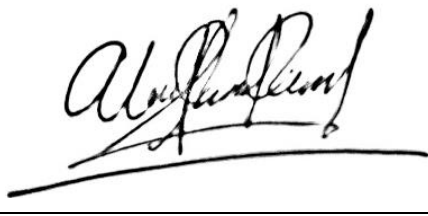
## **Acknowledgement**

I would like to give special thanks to Dr. Stefan Geißendörfer and Holger Behrends for the opportunity of carrying out this research in their research group, the constant support and help.

## DECLARATION

I hereby confirm that this thesis is entirely my own work. I confirm that no part of the document has been copied from either a book or any other source – including the internet – except where such sections are clearly shown as quotations and the sources have been correctly identified within the text or in the list of references. Moreover, I confirm that I have taken notice of the ‘Leitlinien gutter wissenschaftlicher Praxis’ of the University of Oldenburg

Oldenburg, September 23<sup>rd</sup> 2019



---